Università degli Studi di Trieste
Dipartimento di Fisica
Corso di Laurea Magistrale in Fisica

TEORIA E SIMULAZIONE NUMERICA DELLA CONDUCIBILITÀ TERMICA DELL'ACQUA

Candidato:
Paolo Pegolo
Matricola:
SM2300313

Relatore:
Prof. Stefano Baroni

Anno Accademico 2017–2018

Paolo Pegolo

Theory and numerical simulation of the thermal conductivity of water

UNIVERSITAS STUDIORUM MCMXXIV
TERGESTUM

MA PER SEGUIR VIRTUTE E CANOSCENZA

TITLEBACK
This document was written with LaTeX on Linux using ArsClassica, a reworking of the ClassicThesis style designed by André Miede, inspired to the masterpiece *The Elements of Typographic Style* by Robert Bringhurst.

CONTACTS
☞ `ppegolo@protonmail.com`

Φίλος μὲν Σοκράτης,
ἀλλὰ φιλτέρα ἀλήϑεια.

— Ἀριστοτέλης

When the beard is black, take the reasoning, ignore conclusions.
When gray, take both reasoning and conclusions.
When white, just conclusions.

— Nassim Nicholas Taleb

SOMMARIO

La conducibilità termica κ descrive come un materiale conduce il calore, ovvero come l'energia di un sistema fluisce in risposta ad un gradiente di temperatura. La computazione numerica della conducibilità termica richiede lunghe simulazioni di dinamica molecolare e grande precisione nel calcolo delle interazioni fra le particelle costituenti il sistema. MB-pol è un modello classico a molti corpi introdotto recentemente, che descrive con grande accuratezza la complicata chimica-fisica dell'acqua, dallo stato solido a quello gassoso. In questa tesi viene implementato per la prima volta il calcolo del flusso di calore del modello MB-pol per studiarne la conducibilità termica mediante la dinamica molecolare d'equilibrio e la teoria della risposta lineare di Green-Kubo. I dati vengono analizzati mediante la moderna tecnica dell'*analisi cepstrale*.

ABSTRACT

The thermal conductivity κ describes how a material conducts heat, i.e. how the energy in the system flows in response to a temperature gradient. The numerical computation of the thermal conductivity of a material requires long molecular dynamics simulations and high accuracy in the calculation of the interactions among the particles that constitute the system. MB-pol is a recently introduced many-body classical model, which describes with great accuracy the complex physical-chemistry of water, from the solid to the gaseous phase. In this thesis the calculation of the heat flux of MB-pol is implemented for the first time to study the thermal conductivity of the model via Equilibrium Molecular Dynamics and the Green-Kubo linear response theory. Data are treated via the modern technique of *cepstral analysis*.

CONTENTS

INTRODUCTION

HEAT FLOWS from hot to cold as time flows from the past to the future. This is the defining feature of the arrow of time, and a blueprint of the second law of thermodynamics. As the principle which it lays upon, heat transfer is ubiquitous in the physical sciences, from the microscopic quantum systems to planetary science. In fact, heat flow determines the internal temperature distribution of a body and the way it dissipates energy; hence, understanding heat transport sheds light on the life and death of stars and planets, the thermal stability of complex systems like living organisms, the efficiency and working conditions of electronic and mechanical tools down to the energy dissipation mechanisms in nano-scale devices that are massively developed nowadays at the industrial level.

Mechanisms of heat transfer

The three mechanisms by which heat flows are *convection*, *radiation* and *diffusion*:

- *Convection* is the transport of heat due to the movement of fluids. It only occurs in liquids and gases, in which mass can flow easily and, in geological time scales, in viscous solids such as the Earth mantle;
- *Thermal radiation* is the electromagnetic radiation generated by the thermal motion of charged particles in matter. The presence of accelerating charges and dipoles in a piece of matter produces an electromagnetic field that carries energy away from the system. Another point of view is to see the phenomenon as the transport of energy due to photons off the surface of a system, making it mostly a surface effect;
- *Diffusive conduction* is the energy transported by the collective arrangement of the elementary constituents of a physical system, i.e. atoms and, in the case of metals, conduction electrons. This form of heat transport is always present in interacting systems.

While in fluids the overall heat transport properties are due to both conduction and convection, in bulk solids conduction alone is responsible for any heat transfer. A prominent example of an area in which these issues are of great importance comes from technology: integrated electronics, where power dissipation issues limit the performance of devices of any dimension, from mobile phones that fit in the pocket to massive data centers that occupy entire portions of a city. In nano-scale electronics, for example, the aim to build smaller and smaller components and keep up with Moore's Law lead to the pursuit of well conducting materials that dissipate heat quickly. On the other hand, the industry of heat shielding or refrigeration looks for materials that do not disperse heat, i.e. that are bad conductors.

Moore's Law states that the number of transistors in integrated electronic circuits doubles every two years.

In the field of planetary science, the three effects that lead to heat transfer may coexist but, while convection is thought to be the most important mechanism in the cases of interest, the heat transfer among homogeneous convecting sectors of a physical system is completely due to thermal diffusion. Therefore, a solid grasp on the mechanism of thermal diffusion is of paramount importance both for its technological applications and from the perspective of fundamental science alone.

The origin of heat conduction

The mathematical description of heat transport originates in 1811, when Joseph Fourier proposed a phenomenological law to fit some experiments regarding the conduction of heat in common materials, whose modern formulation reads:

$$\mathbf{J}_\mathrm{q} = -\kappa \nabla T.$$

The heat flux $\mathbf{J}_\mathrm{q}$ is a vector which describes the non-convective component of the flow of energy across a surface element per unit time due to a temperature gradient ∇T. The computation of the heat flux requires a suitable definition of the energy density, i.e. a local description of how the energy behaves. The quantity κ is the thermal conductivity, and it is the fundamental property that encompasses the macroscopic phenomenon of heat conduction. The whole problem of describing and predicting the thermal properties of a material can be distilled to the issue of computing the thermal conductivity. In insulating crystalline solids well away from the melting point heat conduction is determined by the dynamics of the atomic nuclei, with the electrons following adiabatically in the ground-state. This dynamics is well described by the Boltzmann transport equation in a quasi-harmonic approximation but, when temperature increases, anharmonicities arise and break down this simplified picture.

The modern approach to the computation of heat conductivity

The simulation of thermal transport in high temperature crystals, disordered glassy systems and liquids requires a different and more general picture: the theory of hydrodynamic fluctuations, together with the Green-Kubo theory of linear response. The main result concerning heat transport theory within this approach is a formula to compute the conductivity κ from the equilibrium time-correlations of the heat flux $\mathbf{J}_\mathrm{q}$:

$$\kappa \propto \int_0^\infty \left\langle \mathbf{J}_\mathrm{q}(t) \cdot \mathbf{J}_\mathrm{q}(0) \right\rangle \mathrm{d}\, t,$$

where the angle brackets denote an ensemble average over initial conditions. Such quantities are, in principle, accessible in Molecular Dynamics simulations; since the advent of computation as a powerful tool in the hands of physicists, it has been widely used to carry out numerical experiments and predictions of the thermal conductivity of materials. Despite being intuitively easy to grasp, thermal conductivity has proven to be difficult to compute, since very long molecular dynamics trajectories are needed to collect sufficient statistics and obtain satisfying results. The Green-Kubo approach is widely used for simple classical systems, where low-computational cost inter-atomic potentials are available and it is viable to produce long simulations with many particles.

Gauge invariance and a revived enthusiasm towards heat transport theory

For *ab initio* liquids and disordered systems, the Green-Kubo method was thought to be ill-defined, due to the impossibility to decompose the total energy of a system into atomic contributions from a first-principle perspective. Recent works on the topic, e.g. Marcolongo et al., 2015, exposed that even in a classical picture the same indeterminacy is present but, nevertheless, this ill-definiteness at the microscopic level has no consequence on the macroscopic and measurable property, i.e. the thermal conductivity: there exists a *gauge invariance* on the functional form of the heat flux that does not affect κ. This remarkable result has renewed the interest in the theory of thermal transport, and stimulated the research of affordable ways to compute the conductivity from molecular dynamics simulations enhanced with Density Functional Theory (DFT), one of the most valid schemes to handle *ab initio* computation of the properties of materials. The relatively short simulations produced with these expensive techniques require appropriate care to be dealt with efficiently. The struggle to exploit the data in the most extensive manner has blossomed into the state-of-the-art of the statistical analysis of heat flux times-series: *cepstral analysis* [Ercole, Marcolongo, et al., 2017]. This approach has proven to be able to reduce considerably the cost of computing the heat conductivity using the Green-Kubo machinery.

Water: a pervasive substance that keeps surprising

A substance which is not easy to model is water. Despite having a fairly simple chemical structure, water properties are non-trivial and still nowadays not completely understood. In fact, water presents many peculiar properties that are so uncommon to be classified as *anomalies*. The most paradigmatic example is water density: in contrast with simple liquids, whose density decreases monotonically when temperature increases, water density is maximum at about 4°C and drops for smaller temperatures. When water solidifies, the hydrogen bond structure prevents the molecules from packing too closely, and density is even lower: this feature allows ice to float on liquid water instead of sinking, a necessary condition for water-based life on Earth. The other way around would make the ocean floor an immense inhospitable glacier, where microscopic primordial organisms would have never proliferated. Other distinctive departures from the usual behavior of simple liquids are the functional dependence on temperature of thermodynamic susceptibilities, for instance: specific heat, isothermal compressibility and thermal expansion coefficient. The former two increase dramatically below a specific temperature, while the latter decreases; in contrast, in a simple liquid they would increase linearly. On top of these properties, that regard the most common physical states of this substance, under extreme thermodynamics conditions water may behave in interesting ways: in giant planets' core, where pressure and temperature are huge, water is thought to be in the *superionic* phase, i.e. a ionic compound of oxygens and hydrogens that was theoretically predicted by numerical simulations and that has now some experimental evidence [Millot et al., 2018].

An intricate network of hydrogen bonds molds the structure and behavior of bulk water

The complex properties of water are mainly due to the intricate network of hydrogen bonds[1] that form between molecules. The hydrogen bond is the attraction between the electronegative oxygen atom and a hydrogen atom. It is due to the dipole-dipole interaction, but it is firmly directional like a covalent bond. This type of bond is fairly strong ($\approx 20\mathrm{kJ/mol}$), if compared to Van der Waals forces ($\approx 1\mathrm{kJ/mol}$). A hydrogen atom attached to the oxygen in another molecule is the *donor* of the bond, while the oxygen atom is the *acceptor*. A molecule can host both donor and acceptor, thus promoting the formation of hydrogen bond structures. Moreover, hydrogen bonds have a cooperative nature: when two water molecules participate in a hydrogen bond, the subsequent redistribution of charge is such that the acceptor

---

[1] This is true at sub-critical conditions, i.e. at temperatures under 647K and pressure under 218atm. Above the critical point, hydrogen bonds are less important.

becomes a better donor for another molecule. The concerted action of the water molecules driven by hydrogen bonds emerges in all its splendor in the most common form of ice: hexagonal *ice Ih*. However, even the liquid state is influenced by the incessant formation and dissolution of hydrogen bonds, whose lifetime is of $\approx 1\mathrm{ps}$ at room temperature.

The relevance of water for humanity cannot be stressed enough: it is the fundamental requirement for the existence of life as we know it. For its uttermost importance, the study of the physical properties of water has been, and currently is, a very active field of research. The will to simulate unbiasedly the properties of materials in a wide range of physical conditions, e.g. pressure and temperature, spurs to pursue the way of quantum simulations that, being first principle calculations, do not rely upon macroscopic approximations like classical potentials. Density Functional Theory, while making accessible the computation of bulk properties of material, is not the most accurate tool to simulate the correlated nature of the hydrogen bonds. Instead, Quantum Chemistry methods such as Coupled-Cluster (CC) calculations allow to obtain very precise quantum-mechanical forces among small clusters of molecules. Extended simulations with many molecules are still too expensive: the preferred route is to elaborate a classical model, whose equation of motion are of far easier resolution, that mimics the quantum behavior of desired system. This is the field of atomistic simulations, where the constituents are point atoms, molecules or ions whose interactions are described via so-called *force-fields*, i.e. the functional form and the set of parameters used to compute the potential energy of a system of interacting particles. The aim is to keep the computational costs low, while at the same time exploiting the accuracy of quantum-mechanical calculations.

Atomistic simulations are among the preferred ways to investigate complex system made of microscopic constituents

In the case of water, there have appeared a myriad of different models: from coarse grained descriptions of bare molecules, to atomically resolved rigid molecules, to sophisticated flexible models that account for polarization. Nonetheless, it is difficult to find a model able to reproduce the plethora of strange properties of water. A recently developed model called MB-pol has proven to be very accurate in the description of water properties from the gaseous to the condensed phases [Reddy et al., 2016]. While many models are designed to fit a particular property of water, or a few properties, MB-pol aspires to universality. It is one of the few models that correctly describe the density anomaly of water and other bulk properties and, at the same time, cluster structure and energies or the properties of crystalline and amorphous ice. The cost for its astounding accuracy is the great complexity of the analytical form of the potential energy, which involve many-body terms and the self-consistent computation of molecular polarization. A feature that is currently lacking in its implementation is the computation of the heat flux $\mathbf{J}_\mathrm{q}$, the fundamental ingredient to determine the thermal conductivity κ. The heat flux requires the distribution of the total energy and the forces among the atoms in the system: an easy task in weakly interacting materials, when the configurational energy is modeled through pair potentials like Lennard-Jones, but a complicated and not completely settled issue in the presence of many-body forces.

The purpose of this thesis is to compute for the first time the thermal conductivity of the MB-pol water model in the liquid state. This requires the implementation of a computer code to calculate the heat flux for this model, to perform Molecular Dynamics simulations to gather the time-series of values of the heat flux, and to analyze its fluctuations to obtain the value of κ. The ability to compute the heat flux will open the way to perform more advanced and useful calculations such as the conductivity of the various phases of ice, that are also very well described by MB-pol, and of water under extreme thermodynamic conditions.

This thesis is structured as follows:

IN THE FIRST CHAPTER the heat transport theory will be reviewed, from the hydrodynamic theory to the Green-Kubo formula of heat conductivity; the gauge invariance of thermal conductivity will be discussed.

THE SECOND CHAPTER regards how the MB-pol water model is structured.

IN THE THIRD CHAPTER, after a brief review of some topics in statistics, the main techniques used to analyze the data obtained from the numerical simulations are presented.

THE FOURTH CHAPTER covers the code implementation of the heat flux formula for the MB-pol model into the MD package `DL_POLY`.

IN THE FIFTH CHAPTER the results of the numerical simulations are presented.

THE LAST CHAPTER contains discussions, conclusions and future perspectives.

1 HEAT TRANSPORT THEORY

HEAT TRANSPORT in classical fluids is described by the theory of hydrodynamic fluctuations [Kadanoff and Martin, 1963]. The phenomenological theory of Onsager [Onsager, 1931a] provides the physical foundation, while the complete formalization of Linear Response Theory (LRT) is due to Green and Kubo [Green, 1952, 1954] [Kubo, 1957; Kubo et al., 1957]. A Green-Kubo formula relates the thermal conductivity κ, a non-equilibrium dissipative quantity, to the time integrated equilibrium autocorrelations of the heat flux $\mathbf{J}_\mathrm{q}$:

$$\kappa \propto \int_0^\infty \left\langle \mathbf{J}_\mathrm{q}(t) \cdot \mathbf{J}_\mathrm{q}(0) \right\rangle_\mathrm{eq} \mathrm{d}t. \tag{1.1}$$

1.1 HYDRODYNAMIC VARIABLES

Extensive quantities appear often in condensed matter physics. They are defined as physical properties which are additive for subsystems. An additive quantity of a system is such that its value is the sum of contributions due to the different subsystems. The additivity property allows one to express an extensive quantity as the integral of its density; for an extensive variable $A[\Omega]$ associated to a system of volume Ω, let $a(\mathbf{x})$ be the density of A, i.e.:

$$A[\Omega] = \int_\Omega a(\mathbf{x})\, \mathrm{d}^3x. \tag{1.2}$$

This statement provides the mathematical definition of extensivity: in fact, it asserts that A is the sum of small contributions $a(\mathbf{x})\, \mathrm{d}^3x$ associated to the infinitesimal subsystem of volume d^3x located at the spatial point $\mathbf{x}$.

When such a quantity is locally conserved, i.e. there are neither sources nor sinks, a *continuity equation* relates the time derivative of the density and a suitably defined current density $\mathbf{j}(\mathbf{x}, t)$:

$$\frac{\partial a(\mathbf{x}, t)}{\partial t} = -\nabla \cdot \mathbf{j}(\mathbf{x}, t). \tag{1.3}$$

The density of a locally conserved quantity will be referred to as a *conserved density*, while the current as a *conserved current*. By Fourier-transforming in space, one finds

$$\dot{\tilde{a}}(\mathbf{q}, t) = -i\mathbf{q} \cdot \tilde{\mathbf{j}}(\mathbf{q}, t), \tag{1.4}$$

where the dot indicates the time derivative, the tilde indicates the spatial Fourier-transform and $\mathbf{q}$ is a reciprocal-space vector. Since the wavelength of the Fourier mode of wave-vector $\mathbf{q}$ is

$$\lambda \propto \frac{1}{|\mathbf{q}|},$$

it is found that the longer is the wavelength, the slower is the time evolution of the conserved density. In an atomistic framework, where the properties of the system arise from the statistical behavior of a huge number of rapidly moving elementary constituents, a long enough wavelength ensures the conserved density dynamics to be adiabatically decoupled from the motion of the atoms. The *hydrodynamic variables* are defined as the long wavelength modes of conserved densities.

LOCAL THERMAL EQUILIBRIUM The adiabatic decoupling of the hydrodynamics variables with respect to the atomic motion means that, off-equilibrium, the wavelengths and timescales of the disturbances are so long that a local notion of equilibrium can be established, i.e. local intensive thermodynamic properties such as temperature, pressure and chemical potential can be defined in a small enough (but macroscopically large with respect to interatomic distances) neighborhood of the point $(\mathbf{x}, t)$. Such a construct is called *local thermal equilibrium* (LTE).

Let us suppose the system to have a number M of conserved extensive variables $\{A^l\}_{l=1}^M$, e.g. number of particles, energy, momentum etc., such that local thermal equilibrium is established. Without loss of generality, let us suppose the equilibrium values of such quantities to be zero. Thus, the associated conserved densities $\{a^l\}_{l=1}^M$ and currents $\{\mathbf{j}^l\}_{l=1}^M$ will represent the deviations from equilibrium. If the deviations from equilibrium are small enough, one can suppose the time derivative of the density to be a linear combination of the densities themselves. In both time and space Fourier domain[1] this reads:

$$-i\omega \tilde{a}^l(\mathbf{q},\omega) = \sum_j \tilde{\Lambda}^{lj}(\mathbf{q},\omega)\tilde{a}^j(\mathbf{q},\omega), \tag{1.5}$$

where $\tilde{\Lambda}^{lj}(\mathbf{q},\omega)$ are suitably defined coefficients. By combining the last equation with (1.4), the *constitutive equations* are found:

$$-i\mathbf{q}\cdot\tilde{\mathbf{j}}^l(\mathbf{q},\omega) = \sum_j \tilde{\Lambda}^{lj}(\mathbf{q},\omega)\tilde{a}^j(\mathbf{q},\omega), \tag{1.6}$$

so that, for the longitudinal component of the conserved current, it holds:

$$\tilde{\mathbf{j}}^l(\mathbf{q},\omega) = i\frac{\mathbf{q}}{q^2}\sum_j \tilde{\Lambda}^{lj}(\mathbf{q},\omega)\tilde{a}^j(\mathbf{q},\omega). \tag{1.7}$$

When a system is isotropic, i.e. its properties do not depend on the direction considered, the quantities $\tilde{\Lambda}$ are spherically symmetric in $\mathbf{q}$, and their $\mathbf{q}=\mathbf{0}$ value is zero, otherwise the long-range modes of the currents would be coupled to the density fluctuations, which conflicts with our hypothesis of local thermal equilibrium. Let us suppose that the long-wavelength, small-frequency form of such quantities is

$$\tilde{\Lambda}^{lj}(\mathbf{q},\omega) \sim q^2\lambda^{lj}. \tag{1.8}$$

---

[1] The Fourier transform of a time derivative yields a multiplicative factor of $-i\omega$:

$$\dot{\tilde{a}}(\mathbf{q},t) \overset{\text{Fourier}}{\mapsto} -i\omega\tilde{a}(\mathbf{q},\omega).$$

Then, the normalized volume-integral of the stationary (ω=0) microscopic current, i.e. the $\mathbf{q}$=$\mathbf{0}$ component of the Fourier-space current

$$\begin{aligned}\mathbf{J}^l &= \frac{1}{\Omega}\int_\Omega \mathbf{j}^l(\mathbf{x})\,\mathrm{d}^3x \\ &= \lim_{q\to 0}\tilde{\mathbf{j}}^l(\mathbf{q},\omega=0)\end{aligned} \tag{1.9}$$

is related to the density gradients $\mathbf{D}^l = \Omega^{-1}\int \nabla a^l\,\mathrm{d}^3x$:

$$\begin{aligned}\mathbf{J}^l &= \lim_{q\to 0} i\frac{\mathbf{q}}{q^2}\sum_j q^2\lambda^{lj}\tilde{a}^j(\mathbf{q},\omega=0) \\ &= \lim_{q\to 0}\sum_j \lambda^{lj} i\mathbf{q}\tilde{a}^j(\mathbf{q},\omega=0) \\ &= \sum_j \lambda^{lj}\lim_{q\to 0}\frac{1}{\Omega}\int_\Omega \nabla a^j(\mathbf{x},\omega=0)\mathrm{e}^{-i\mathbf{q}\cdot\mathbf{x}}\,\mathrm{d}^3x \\ &= \sum_j \lambda^{lj}\mathbf{D}^j.\end{aligned} \tag{1.10}$$

The macroscopic quantity $\mathbf{J}$ associated to a current density $\mathbf{j}(\mathbf{x})$, i.e. its normalized volume-integral, is called a *flux*.

The intensive thermodynamic variables conjugate to the extensive variables A^l are defined as the derivatives of the thermodynamic potential, in the microcanonical case the entropy $S(A^l)$, with respect to its arguments:

$$\zeta^l = \frac{\partial S}{\partial A^l}, \tag{1.11}$$

while the *susceptibilities* are:

$$\chi^{lj} = \frac{1}{\Omega}\frac{\partial A^l}{\partial \zeta^j}. \tag{1.12}$$

Under the hypothesis of LTE, local values of the intensive variables ζ^i can be defined, and the integrals of their gradients are called *thermodynamic forces*:

$$\mathbf{F}^l \overset{\text{def}}{=} \frac{1}{\Omega}\int_\Omega \nabla\zeta^l(\mathbf{x})\,\mathrm{d}^3x. \tag{1.13}$$

From (1.13), a relationship between the density gradients and the thermodynamic forces is found, the two quantities being coupled via the susceptibilities:

$$\mathbf{D}^l = \sum_j \chi^{lj}\mathbf{F}^j. \tag{1.14}$$

Plugging (1.14) into (1.10) yields

$$\mathbf{J}^l = \sum_j L^{lj}\mathbf{F}^j, \tag{1.15}$$

where $L^{lj} = \sum_k \lambda^{lk}\chi^{kj}$. This equation states a linear relation between the fluxes $\mathbf{J}^l$ of conserved extensive variables and the thermodynamic forces $\mathbf{F}^l$. The phenomenological coefficients L^{lj} have been found by Onsager [Onsager, 1931a,b] to fulfill a reciprocity relation

$$L^{lj} = L^{jl}.$$

1.2 LINEAR RESPONSE THEORY

Linear response theory allows to systematically evaluate the Onsager's coefficients L^{lj}. Let us consider a classical system of N atoms described by the Hamiltonian

$$H_0(\Gamma) = \sum_{i=1}^{N} \frac{P_i^2}{2M_i} + \Phi(\mathbf{R}_1, \mathbf{R}_2, \dots, \mathbf{R}_N), \tag{1.16}$$

where M_i, $\mathbf{R}_i$ and $\mathbf{P}_i$ are the mass, position and momentum of the i-th atom in the system and Φ is the inter-atomic potential energy[2]. The phase-space variables will be denoted by the short-hand notation $\Gamma = \{\mathbf{R}_i, \mathbf{P}_i\}$.

Let us suppose that a time-dependent external perturbation is linearly coupled to the conserved densities of the system:

$$\Phi'(\Gamma, t) = \sum_l \int v^l(\mathbf{x}, t) a^l(\mathbf{x}; \Gamma)\, \mathrm{d}^3 x, \tag{1.17}$$

where $\{v^l(\mathbf{x}, t)\}$ are the coupling fields, and $a^l(\mathbf{x}; \Gamma)$ is a phase-space function such that its ensemble average is a conserved density, i.e.:

$$\begin{aligned} a(\mathbf{x}) &= \langle a(\mathbf{x}; \Gamma) \rangle_{\text{eq}} \\ &= \int a(\mathbf{x}; \Gamma) \mathcal{P}_0(\Gamma) \mathrm{d}\Gamma, \end{aligned} \tag{1.18}$$

where $\mathcal{P}_0$ is the equilibrium phase-space probability distribution, i.e. the Boltzmann distribution

$$\mathcal{P}_0(\Gamma) \propto \mathrm{e}^{-H_0/k_{\mathrm{B}}T}, \tag{1.19}$$

with k_{B} the Boltzmann constant and T the system temperature. The system is assumed to be at equilibrium at $t = -\infty$, thus the coupling fields are such that $v^i(\mathbf{x}, t = -\infty) = 0\, \forall i, \mathbf{x}$. Conserved currents are also ensemble averages of phase-space dependent fields:

$$\mathbf{j}(\mathbf{x}) = \langle \mathbf{j}(\mathbf{x}; \Gamma) \rangle ,$$

and the functions $\mathbf{j}(\mathbf{x}; \Gamma)$ are called phase-space samples of the current (or of the density). A phase-space trajectory is denoted by Γ_t; the realization along a classical trajectory of a conserved density or current depends on time and on the initial conditions that uniquely determine the Hamiltonian evolution of the system. A canonical average over the initial conditions yields the time dependent expectation value of the density (or current):

$$\begin{aligned} a(\mathbf{x}, t) &= \left\langle a(\mathbf{x}; \Gamma'_t) \right\rangle_{\text{eq}} \\ &= \int a(\mathbf{x}; \Gamma'_t) \mathcal{P}_0(\Gamma_0) \mathrm{d}\Gamma_0, \end{aligned} \tag{1.20}$$

where Γ'_t indicates that the time evolution is driven by the perturbed Hamiltonian $H = H_0 + \Phi'$. The symbol Γ_t will denote the unperturbed phase-space trajectory.

---

[2] No external potential is considered.

Green-Kubo theory states that the linear response to a perturbation of the α component of a conserved current $\mathbf{j}^i$ is

$$\begin{aligned} j^l_\alpha(\mathbf{x},t) =& \frac{1}{k_\mathrm{B}T}\sum_j \int_{-\infty}^{t} \mathrm{d}t' \int \mathrm{d}^3x' \left\langle j^l_\alpha(\mathbf{x};\Gamma_t)\dot{a}^j(\mathbf{x}';\Gamma_{t'})\right\rangle_\mathrm{eq} v^j(\mathbf{x}',t') \\ =& -\frac{1}{k_\mathrm{B}T}\sum_j\sum_\beta \int_{-\infty}^{t} \mathrm{d}t' \int \mathrm{d}^3x' \left\langle j^l_\alpha(\mathbf{x};\Gamma_t)\frac{\partial j^j_\beta}{\partial x'_\beta}(\mathbf{x}';\Gamma_{t'})\right\rangle_\mathrm{eq} v^j(\mathbf{x}',t') \\ =& \frac{1}{k_\mathrm{B}T}\sum_j\sum_\beta \int_{-\infty}^{t} \mathrm{d}t' \int \mathrm{d}^3x' \left\langle j^l_\alpha(\mathbf{x};\Gamma_t) j^j_\beta(\mathbf{x}';\Gamma_{t'})\right\rangle_\mathrm{eq} \frac{\partial v^j(\mathbf{x}',t')}{\partial x'_\beta}, \end{aligned} \tag{1.21}$$

where x_β is the β Cartesian component of the position vector $\mathbf{x}$, and where the continuity equation and integration by parts have been used.

Last equation can be averaged to recover the macroscopic flux as in eq. (1.9), i.e. by Fourier-transforming the space-time dependent current and letting both q and ω go to zero. Under the assumption of space and time homogeneity, the equilibrium average in eq. (1.21) can be written as

$$G^{lj}_{\alpha\beta}(\mathbf{x}-\mathbf{x}';t-t') = \left\langle j^l_\alpha(\mathbf{x};\Gamma_t) j^j_\beta(\mathbf{x}';\Gamma_{t'})\right\rangle_\mathrm{eq}; \tag{1.22}$$

then, both the space and time integrals are convolutions. By the convolution theorem, the Fourier transform of a convolution of two functions is the product of their Fourier transforms. This allows the factorization of the volume integral in eq. (1.21) into two integrals, and one obtains eq. (1.15), with

$$J^l_\alpha(\Gamma) = \frac{1}{\Omega}\int j^l_\alpha(\mathbf{x},\Gamma)\,\mathrm{d}^3x, \tag{1.23}$$

$$F^l_\alpha = \frac{1}{\Omega T}\iint \frac{\partial}{\partial x_\alpha} v^l(\mathbf{x},t)\,\mathrm{d}^3x\mathrm{d}t, \tag{1.24}$$

$$L^{lj}_{\alpha\beta} = \frac{\Omega}{k_\mathrm{B}}\int_0^\infty \left\langle J^l_\alpha(\Gamma_t) J^j_\beta(\Gamma_0)\right\rangle_\mathrm{eq} \mathrm{d}t. \tag{1.25}$$

Last equation, known as a Green-Kubo formula, relates a non-equilibrium property, the expectation value of a quantity whose evolution is driven by a perturbed Hamiltonian, to its fluctuations at equilibrium: this connection between fluctuations and dissipation[3] allows us to compute the transport coefficient in eq. (1.1) from the equilibrium correlations of the volume integral of suitably defined conserved currents.

1.3 HEAT TRANSPORT

The phenomenology of heat transport is described by the Fourier's law of heat conduction [Fourier, 1822]:

$$\mathbf{J}_\mathrm{q} = -\kappa\nabla T, \tag{1.26}$$

---

[3] This is, in fact, tightly related to the so called Fluctuation-Dissipation Theorem.

i.e. it is due to an effective temperature gradient. Here the macroscopic heat flux $\mathbf{J}_\mathrm{q}$ is the volume integral of the microscopic heat flux

$$\mathbf{J}_\mathrm{q} = \frac{1}{\Omega} \int \mathbf{j}_\mathrm{q}(\mathbf{x})\, \mathrm{d}^3 x. \tag{1.27}$$

The theory of section 1.2 allows one to compute the linear response coefficient to a mechanical perturbation, but a temperature gradient is not due to any mechanical perturbation. Anyway, when a LTE is defined, a scalar temperature field can be defined:

$$T(\mathbf{x}) = T + \Delta T(\mathbf{x}), \text{ with } \Delta T(\mathbf{x}) \ll T. \tag{1.28}$$

This notion of local thermal equilibrium provides a way to treat the thermal disturbance as a mechanical perturbation, i.e. as a perturbation to the Hamiltonian of the form of eq. (1.17):

$$\begin{aligned} \mathcal{P}(\Gamma) &\propto \exp\left(- \int \frac{e(\mathbf{x};\Gamma)}{k_\mathrm{B} T(\mathbf{x})}\, \mathrm{d}^3 x \right) \\ &\equiv \exp\left(- \frac{H_0(\Gamma) + \Phi'(\Gamma)}{k_\mathrm{B} T} \right), \end{aligned} \tag{1.29}$$

where the *energy density* $e(\mathbf{x};\Gamma)$ is defined in such a way that

$$\int e(\mathbf{x};\Gamma)\, \mathrm{d}^3 x = H_0(\Gamma).$$

The equivalent perturbation Φ' of equation (1.17) derived from eq. (1.29) is, up to linear order in ΔT:

$$\Phi'(\Gamma) = -\frac{1}{T} \int \Delta T(\mathbf{x}) e(\mathbf{x};\Gamma)\, \mathrm{d}^3 x + \mathcal{O}(\Delta T^2). \tag{1.30}$$

Through the constitutive equation given by Fourier's law (1.26), one can express the thermal conductivity tensor[4] $\kappa_{\alpha\beta}$ as the Onsager's coefficient associated to the heat flux divided by the temperature squared:

$$\begin{aligned} \kappa_{\alpha\beta} &= \frac{L^{EE}_{\alpha\beta}}{T^2} \\ &= \frac{\Omega}{k_\mathrm{B} T^2} \int_0^\infty \left\langle J_{\mathrm{q}_\alpha}(\Gamma_t) J_{\mathrm{q}_\beta}(\Gamma_0) \right\rangle_\mathrm{eq} \mathrm{d}t. \end{aligned} \tag{1.31}$$

1.4 HEAT CURRENT DENSITY IN MOLECULAR DYNAMICS

The formula for the heat flux can be obtained, up the linear order, from equation (1.4) on page 1. In the limit of small but finite wavelength one

---

[4] In general, considering the cases in which there are inequivalent heat currents, one can speak of a conductivity tensor, instead of a scalar. This is the case, for example, of anisotropic media.

can keep the leading terms in the Taylor expansion in $\mathbf{q}$ of the continuity equation in Fourier space:

$$\dot{\tilde{e}}(\mathbf{q}=\mathbf{0},\Gamma_t) + \nabla_{\mathbf{q}}\,\dot{\tilde{e}}(\mathbf{q},\Gamma_t)\big|_{\mathbf{q}=\mathbf{0}} + i\mathbf{q}\cdot\tilde{\mathbf{j}}_{\mathrm{q}}(\mathbf{q}=\mathbf{0},\Gamma_t) + \mathcal{O}(q^2) = 0 \tag{1.32}$$

$$\begin{aligned}&\Rightarrow \frac{1}{\Omega}\frac{\mathrm{d}}{\mathrm{d}t}\int e(\mathbf{x},\Gamma_t)\,\mathrm{d}^3x + \\ &\quad - i\mathbf{q}\cdot\left[\frac{1}{\Omega}\int \mathbf{x}\dot{e}(\mathbf{x},\Gamma_t)\,\mathrm{d}^3x - \frac{1}{\Omega}\int \mathbf{j}_{\mathrm{q}}(\mathbf{x},\Gamma_t)\,\mathrm{d}^3x\right] + \mathcal{O}(q^2) = 0;\end{aligned} \tag{1.33}$$

in the thermodynamic limit, the first term is the time-derivative of the total energy which, being a constant of motion, does not vary in time. So, up to linear order in $\mathbf{q}$:

$$\begin{aligned}\mathbf{J}_{\mathrm{q}}(\Gamma_t) &= \frac{1}{\Omega}\int \mathbf{j}_{\mathrm{q}}(\mathbf{x},\Gamma_t)\,\mathrm{d}^3x \\ &= \frac{1}{\Omega}\int \mathbf{x}\dot{e}(\mathbf{x},\Gamma_t)\,\mathrm{d}^3x,\end{aligned} \tag{1.34}$$

i.e. the heat flux is the first moment of the time-derivative of the energy density. The energy density depends on time through the atomic positions and momenta, so one can use the chain rule to obtain

$$\mathbf{J}_{\mathrm{q}}(\Gamma_t) = \frac{1}{\Omega}\int\left[\sum_i \frac{\partial e(\mathbf{x};\Gamma_t)}{\partial \mathbf{R}_i}\cdot\mathbf{V}_i + \frac{\partial e(\mathbf{x};\Gamma_t)}{\partial \mathbf{P}_i}\cdot\mathbf{F}_i\right]\mathbf{x}\,\mathrm{d}^3x, \tag{1.35}$$

where $\mathbf{V}_i$ is the velocity of the i-th atom and $\mathbf{F}_i$ the total force on the i-th atom. The energy density in molecular dynamics can be defined as

$$e(\mathbf{x},\Gamma_t) = \sum_j \epsilon_j \delta(\mathbf{x}-\mathbf{R}_j), \tag{1.36}$$

i.e. the total energy is distributed among the point-like atoms in the system. While the atomic kinetic energy is a well-defined quantity

$$\epsilon_{\mathrm{kin},i} = \frac{1}{2M_i}P_i^2, \tag{1.37}$$

there is no *a priori* way to decompose the potential energy of a system of interacting particles into atomic contribution. However, let us suppose to have defined an energy decomposition[5]

$$\Phi = \sum_i \Phi_i, \tag{1.38}$$

so that the the atomic energies are given by

$$\epsilon_i = \frac{1}{2M_i}P_i^2 + \Phi_i. \tag{1.39}$$

The gradients appearing in eq. (1.35) are evaluated as

$$\frac{\partial e(\mathbf{x};\Gamma_t)}{\partial \mathbf{R}_i} = \sum_j \left[\frac{\partial \Phi_j}{\partial \mathbf{R}_i}\delta(\mathbf{x}-\mathbf{R}_j) - \delta_{ij}\epsilon_j \nabla\delta(\mathbf{x}-\mathbf{R}_j)\right] \tag{1.40}$$

$$\frac{\partial e(\mathbf{x};\Gamma_t)}{\partial \mathbf{P}_i} = \mathbf{V}_i\delta(\mathbf{x}-\mathbf{R}_i), \tag{1.41}$$

---

[5] This issue will be addressed in section 1.5.

so that the heat flux becomes

$$\mathbf{J}_{\mathrm{q}}(\Gamma_t) = \frac{1}{\Omega}\int \sum_{i,j}\left[\frac{\partial \Phi_j}{\partial \mathbf{R}_i}\cdot \mathbf{V}_i \delta(\mathbf{x}-\mathbf{R}_j) - \frac{\partial \Phi_j}{\partial \mathbf{R}_i}\cdot \mathbf{V}_i \delta(\mathbf{x}-\mathbf{R}_i) + \right. \\ \left. - \epsilon_i \mathbf{V}_i \nabla \delta(\mathbf{x}-\mathbf{R}_j)\right] \mathbf{x}\, \mathrm{d}^3 x. \quad (1.42)$$

Integrating by parts the last summand and using the properties of the Dirac-delta, one finds:

$$\mathbf{J}_{\mathrm{q}}(\Gamma_t) = \frac{1}{\Omega}\sum_i \left[\epsilon_i \mathbf{V}_i - \sum_j \frac{\partial \Phi_j}{\partial \mathbf{R}_i}\cdot \mathbf{V}_i \left(\mathbf{R}_i - \mathbf{R}_j\right)\right]. \quad (1.43)$$

This formula is well-defined in periodic boundary conditions, since it only depends on the atoms' relative positions. For this reason it is suitable for molecular dynamics simulations of bulk systems. The first term in equation (1.43) is called *kinetic heat flux* or *convective heat flux*, while the second is often called *virial heat flux*.

1.5 GAUGE INVARIANCE OF THE HEAT FLUX

The potential energy of a system of interacting particles is a global property: in general, it depends on all the atomic coordinates at once. For this reason, there is no *a priori* correct decomposition of the energy as a sum over atomic contributions. In the simplest non-trivial case, i.e. when all the forms of interaction are pair potentials, the natural choice is to split the potential energy of a pair of atoms into two equal parts, and assign half of the energy to each atom. When a particular form of interaction involves three atoms, the same prescription would suggest to divide the energy equally among the three participants. Let us show that, whatever the choice of the energy decomposition of eq. (1.38), the physics remains unchanged.

Let us suppose to choose a particular potential energy decomposition with the only constraint that the sum of the atomic energies is the total potential energy of the system, i.e. the quantity one measures[6]:

$$\Phi(\{\mathbf{R}\}) = \sum_i \Phi_i(\{\mathbf{R}\}). \quad (1.44)$$

The total potential energy is evidently invariant if one adds a quantity which is zero:

$$\begin{gathered} \Phi = \sum_i \Phi_i(\{\mathbf{R}\}) + \sum_{i,j} \xi_{ij}(\{\mathbf{R}\}), \\ \text{where } \xi_{ij}(\{\mathbf{R}\}) = -\xi_{ji}(\{\mathbf{R}\}). \end{gathered} \quad (1.45)$$

Equation (1.45) is effectively a redefinition of the atomic potential energy:

$$\Phi = \sum_i \Phi_i'(\{\mathbf{R}\}), \quad (1.46)$$

$$\Phi_i'(\{\mathbf{R}\}) = \Phi_i(\{\mathbf{R}\}) + \sum_j \xi_{ij}(\{\mathbf{R}\}). \quad (1.47)$$

---

[6] Of course even the total potential energy is defined up to a constant, i.e. its value is not absolute.

Let us see how the heat flux changes under the new definition of the potential energy per atom. The energy density e becomes

$$e'(\mathbf{x},t) = \sum_i \left(\epsilon_i + \sum_j \xi_{ij} \right) \delta(\mathbf{x} - \mathbf{R}_i(t)); \tag{1.48}$$

the same mathematical steps that led from (1.36) to (1.43) now yield:

$$\begin{aligned} \mathbf{J}_{\mathrm{q}}{}'(\Gamma_t) &= \mathbf{J}_{\mathrm{q}}(\Gamma_t) + \frac{1}{2\Omega} \sum_{j,k} \Bigg[\xi_{jk}(\{\mathbf{R}\})(\mathbf{V}_j - \mathbf{V}_k) + \\ &\qquad + \sum_i \left(\mathbf{V}_i \cdot \frac{\partial \xi_{jk}}{\partial \mathbf{R}_i} \right) (\mathbf{R}_j - \mathbf{R}_k) \Bigg] \\ &= \mathbf{J}_{\mathrm{q}}(\Gamma_t) + \frac{\mathrm{d}}{\mathrm{d}t} \left[\frac{1}{2\Omega} \sum_{j,k} \xi_{jk}(\{\mathbf{R}\})(\mathbf{R}_j - \mathbf{R}_k) \right] \\ &= \mathbf{J}_{\mathrm{q}}(\Gamma_t) + \frac{\mathrm{d}}{\mathrm{d}t} \Xi(\Gamma_t), \end{aligned} \tag{1.49}$$

$$\text{where } \Xi(\{\mathbf{R}\}) \overset{\text{def}}{=} \frac{1}{2\Omega} \sum_{j,k} \xi_{jk}(\{\mathbf{R}\})(\mathbf{R}_j - \mathbf{R}_k). \tag{1.50}$$

Under the transformation (1.47), the change in the heat flux is the total time derivative of a vector Ξ. Let us assume that Ξ is bounded from above: then a more general transformation of the energy density can be defined so that the heat flux changes by a time-derivative:

$$\begin{aligned} e(\mathbf{x},t) \mapsto e'(\mathbf{x},t) &= e(\mathbf{x},t) - \tfrac{1}{3} \nabla \cdot \boldsymbol{\xi}(\mathbf{x},t), \\ \text{where } \Xi(t) &= \frac{1}{\Omega} \int \boldsymbol{\xi}(\mathbf{x},t)\, \mathrm{d}^3 x. \end{aligned} \tag{1.51}$$

In fact, the divergence of the vector field with compact support $\boldsymbol{\xi}$ can be integrated by parts in equation (1.34) to obtain equation (1.49).

Let us now prove that the quantity measured in the laboratory, i.e. the heat conductivity κ, is invariant under the transformation (1.51). To do so, let us show that the Green-Kubo integral in equation (1.31) is insensitive of the transformation:

$$\begin{aligned} \kappa' &= \text{const} \times \int_0^\infty \left\langle \mathbf{J}_{\mathrm{q}}{}'(\Gamma_t) \cdot \mathbf{J}_{\mathrm{q}}{}'(\Gamma_0) \right\rangle_{\mathrm{eq}} \mathrm{d}t \\ &= \text{const} \times \tfrac{1}{2} \int_{-\infty}^{\infty} \left\langle \left(\mathbf{J}_{\mathrm{q}}(\Gamma_t) + \dot{\Xi}(t) \right) \cdot \left(\mathbf{J}_{\mathrm{q}}(\Gamma_0) + \dot{\Xi}(t) \right) \right\rangle_{\mathrm{eq}} \mathrm{d}t \\ &= \kappa + \text{const} \times \left[\left\langle \Xi(t) \cdot \dot{\Xi}(0) \right\rangle_{\mathrm{eq}} \Big|_{-\infty}^{\infty} + \left\langle \dot{\Xi}(t) \cdot \mathbf{J}_{\mathrm{q}}(0) \right\rangle_{\mathrm{eq}} \Big|_{-\infty}^{\infty} \right]. \end{aligned} \tag{1.52}$$

The equilibrium correlations in equation (1.52) are evaluated at large time difference, so that the mean of the product equals the product of the means. Since the equilibrium expectation of a total time-derivative vanishes, all the terms inside the square brackets are zero.

The considerations above can be fashioned into a general statement about heat trasport theory, that let us escape the unpleasant dilemma of having to decide how to distribute energy among particles [Marcolongo et al., 2015]:

GAUGE INVARIANCE OF THE HEAT FLUX The Green-Kubo heat conductivity κ of a system of interacting particles with energy density $e(\mathbf{x},t)$ is invariant under the transformation

$$e(\mathbf{x},t) \mapsto e'(\mathbf{x},t) = e(\mathbf{x},t) - \tfrac{1}{3}\nabla \cdot \boldsymbol{\xi}(\mathbf{x},t),$$

where $\boldsymbol{\xi}(\mathbf{x},t)$ is a bounded vector field. In other words, the heat fluxes $\mathbf{J}_\mathrm{q}(t)$ obtained from $e(\mathbf{x},t)$ and $\mathbf{J}_\mathrm{q}{}'(t)$ obtained from $e'(\mathbf{x},t)$ yield the same value for the heat conductivity.

1.6 MULTI-COMPONENT FLUIDS

Multi-component fluids are made of different species of particles, say M species. Each of the species has a number of particles that does not change in time; then the conserved quantities are the total energy, the total momentum and, for each species, the number of particles. The flux associated with the number of particles is proportional to the total momentum of that species, so the conserved fluxes will be the energy flux, the total momentum and the momenta per species. The conservation of total momentum imposes a linear constraint on the momenta-per-species, reducing the number of independent conserved fluxes from $M+1$ to M.

The matrix made of Onsager's coefficients, called Onsager matrix, is a $M \times M$ square matrix of entries L^{ij}. The heat flux is the non-convective contribution to the energy flux, i.e. the value of the energy flux when there is no mass transport: this condition means that all the mass fluxes must vanish. Let us write eq. (1.15) in matrix form, and order the vector of the fluxes so that the first entry is the energy flux $\mathbf{J}_\mathrm{E}$:

$$\begin{pmatrix} \mathbf{J}_\mathrm{E} \\ \mathbf{J}^2 \\ \vdots \\ \mathbf{J}^M \end{pmatrix} = \underbrace{\begin{pmatrix} L^{EE} & L^{E2} & \cdots & L^{EM} \\ L^{E2} & L^{22} & \cdots & L^{2M} \\ \vdots & \vdots & \ddots & \vdots \\ L^{EM} & L^{M2} & \cdots & L^{MM} \end{pmatrix}}_{\hat{L}} \begin{pmatrix} \nabla(1/T) \\ \nabla(\mu_2/T) \\ \vdots \\ \nabla(\mu_M/T) \end{pmatrix}, \tag{1.53}$$

where the thermodynamic forces F^i are the gradients of the chemical potentials μ_i of the different atomic species divided by the temperature T, and $\mathbf{J}^i$ are the respective mass fluxes. Heat flux is the non-convective contribution to the energy flux, i.e. what is obtained by neglecting the contribution given by transport of mass. This is the equivalent of imposing the vanishing of the mass currents in equation (1.53), i.e.:

$$\begin{pmatrix} \mathbf{J}_\mathrm{E} \\ \mathbf{J}^2 \\ \vdots \\ \mathbf{J}^M \end{pmatrix} \mapsto \begin{pmatrix} \mathbf{J}_\mathrm{q} \\ \mathbf{0} \\ \vdots \\ \mathbf{0} \end{pmatrix}. \tag{1.54}$$

Inspection of the first equation of the linear system (1.53) under condition (1.54) yields

$$\mathbf{J}_\mathrm{q} = L^{EE}\nabla(1/T) + \sum_{i=2}^{M} L^{Ei}\nabla(\mu_i/T). \tag{1.55}$$

Being κ the proportionality factor between $\mathbf{J}_\mathrm{q}$ and ∇T, one would like to get rid of the $\nabla(\mu_i/T)$'s by expressing them with respect of other known quantities. This means to solve the linear system (1.53) with respect to the F^i's. Let us apply Cramer's rule:

$$\begin{aligned} F^i &= \frac{\det(\hat{L}_i)}{\det(\hat{L})} \\ &= \det\begin{pmatrix} L^{EE} & \cdots & \overset{(i\text{-th})}{\mathbf{J}_\mathrm{q}} & \cdots & L^{EM} \\ L^{E2} & \cdots & 0 & \cdots & L^{2M} \\ \vdots & \vdots & \vdots & \ddots & \vdots \\ L^{EM} & \cdots & 0 & \cdots & L^{MM} \end{pmatrix} \Bigg/ \det(\hat{L}) \ , \end{aligned} \tag{1.56}$$

where $\hat{L}_i$ is the matrix formed by replacing the i-th column with the vector of fluxes. The determinant $\det(\hat{L}_i)$ is easily computed with respect to the i-th column: it is sufficient to multiply $(-1)^{i+1}\mathbf{J}_\mathrm{q}$ by the $(1,i)$-minor $\left[\hat{L}\right]_{Ei}$ of the matrix $\hat{L}$, i.e. the determinant of the matrix obtained deleting the first row and the i-th column from $\hat{L}$. The expression of F^i becomes:

$$F^i = \frac{(-1)^{i+1}\mathbf{J}_\mathrm{q}\left[\hat{L}\right]_{Ei}}{\det(\hat{L})}. \tag{1.57}$$

Replacing the above result in eq. (1.55), one finds:

$$\mathbf{J}_\mathrm{q}\left(\det(\hat{L}) - \sum_{i=2}^{M}(-1)^{i+1}L^{Ei}\left[\hat{L}\right]_{Ei}\right) = \det(\hat{L})L^{EE}\nabla\left(\frac{1}{T}\right). \tag{1.58}$$

By expanding the determinant of the Onsager matrix with respect to the first row, the above expression simplifies:

$$\begin{aligned} \det(\hat{L}) =& \sum_{i=1}^{M}(-1)^{i+1}L^{Ei}\left[\hat{L}\right]_{Ei} \\ =& L^{EE}\left[\hat{L}\right]_{EE} + \sum_{i=2}^{M}(-1)^{i+1}L^{Ei}\left[\hat{L}\right]_{Ei}, \end{aligned} \tag{1.59}$$

$$\mathbf{J}_\mathrm{q}L^{EE}\left[\hat{L}\right]_{EE} = L^{EE}\det(\hat{L})\nabla\left(\frac{1}{T}\right), \tag{1.60}$$

that means:

$$\mathbf{J}_\mathrm{q} = \frac{\det(\hat{L})}{\left[\hat{L}\right]_{EE}}\nabla\left(\frac{1}{T}\right). \tag{1.61}$$

From the definition of inverse matrix, i.e.

$$(\hat{L}^{-1})^{ij} = \frac{(-1)^{i+j}\left[\hat{L}\right]_{ji}}{\det\hat{L}},$$

we obtain the final result:

$$\mathbf{J}_\mathrm{q} = \frac{1}{\left(\hat{L}^{-1}\right)^{EE}} \nabla \left(\frac{1}{T}\right) = -\frac{1}{T^2 \left(\hat{L}^{-1}\right)^{EE}} \nabla T, \tag{1.62}$$

$$\kappa = \frac{1}{T^2 \left(\hat{L}^{-1}\right)^{EE}} \tag{1.63}$$

In the simplest case, i.e. $M = 2$, eq. (1.63) reads:

$$\begin{aligned} \mathbf{J}_\mathrm{q} &= \left(L^{EE} - \frac{(L^{E2})^2}{L^{22}}\right) \nabla \left(\frac{1}{T}\right) \\ &= -\frac{1}{T^2} \left(L^{EE} - \frac{(L^{E2})^2}{L^{22}}\right) \nabla T. \end{aligned} \tag{1.64}$$

The last equation expresses the thermal conductivity κ in terms of the Onsager's coefficients in the case of a two-components fluid.

1.6.1 Molecular fluids

Water is a one-component molecular fluid, i.e. a multi-component fluid in which the different atomic species are bound together in a definite way[7]. This property imposes some constraints in the way the mass fluxes and the energy flux interact. Let us define, for each atomic species X (in this case $X =$H, O) in a molecule of chemical formula $A_{N_A} B_{N_B}$, a normalized number flux as

$$\mathbf{J}_X = \frac{1}{N_X} \sum_{n \in X} \mathbf{V}_n. \tag{1.65}$$

The conservation of total momentum in the center-of-mass reference frame leads to the condition

$$\sum_X M_X N_X \mathbf{J}_X = \mathbf{0}, \tag{1.66}$$

where M_X is the atomic mass of species X.

Another flux can be defined as the difference between a pair of normalized number fluxes:

$$\mathbf{J}_{XY} = \mathbf{J}_X - \mathbf{J}_Y \tag{1.67}$$

---

[7] Of course, in nature molecules can dissociate. In such a case, there is a net contribution to the thermal diffusivity due to the mass current, and the fluid is genuinely multi-component. In this section, molecular dissociation will not be considered.

which, for molecular fluids, is the total time-derivative of a bounded vector:

$$\begin{aligned}
\mathbf{J}_{XY} =& \frac{1}{N_X}\sum_{n\in X}\mathbf{V}_n - \frac{1}{N_Y}\sum_{m\in Y}\mathbf{V}_m \\
=& \sum_{i=1}^{N_{mol}}\left(\frac{\mathbf{V}_{X,i}}{N_X} - \frac{\mathbf{V}_{Y,i}}{N_Y}\right) \\
=& \sum_{i=1}^{N_{\mathrm{mol}}}\left(\langle\mathbf{V}_{X,i}\rangle - \langle\mathbf{V}_{Y,i}\rangle\right) \\
=& \frac{\mathrm{d}}{\mathrm{d}t}\sum_{i=1}^{N_{\mathrm{mol}}}\left(\langle\mathbf{R}_{X,i}\rangle - \langle\mathbf{R}_{Y,i}\rangle\right),
\end{aligned} \tag{1.68}$$

where, in this case, the angle brackets indicate the arithmetic average. The flux inside the time derivative is obviously bounded because the molecules do not dissociate, hence the distance between every pair of atoms within the same molecule remain finite. This implies that $\mathbf{J}_{XY}$ is of the form of Ξ in equation (1.51), i.e. it does not contribute to the thermal conductivity: its Onsager's coefficients are zero. Let us call these fluxes *non-diffusive*. Any flux $\mathbf{J}_X$ can be written as a linear combination of non-diffusive fluxes of the form $\mathbf{J}_{XY}$ and the total momentum. For this reason, all the $\mathbf{J}_X$ are non-diffusive as well. Thus, the only flux that contributes to heat conductivity is the energy flux, and the description made in section 1.3 leads to the correct result.

This digression has not been purposeless: despite being theoretically correct, the one-component procedure lays on the hypothesis that the time integrals appearing in equations (1.25) are calculated up to infinity. In a molecular dynamics simulation this is obviously unfeasible: the finiteness of the computation always introduces cutoff errors of some sort. Collecting a sufficiently long trajectory up to the so-called *convergence* means to reduce the cutoff error below the limit of detectability. The convergence time, i.e. the simulation time after which the cutoff error is negligible and the value of the conductivity calculated via the integration of the time-correlation of the heat flux remains unchanged, depends strongly on the system under exam. As a rule of thumb, the more complex is the interaction, the larger is the convergence time.

To avoid wasting computation time to wait for convergence, one could treat the non-diffusive fluxes as if they were diffusive and include them in the Onsager analysis as in equation (1.53). In fact, the Onsager coefficient of a non-diffusive flux is zero in the infinite time limit but, in general, it is greater than zero when the time-integral is calculated up to a finite time. The multi-component analysis allows to discard the other interacting fluxes and achieve convergence faster. Moreover, this cannot lead to overestimation of the thermal conductivity: from formula (1.64) it is evident that the second summand in the right-hand side is necessarily positive. The global positivity of κ completes the argument. The experimental verification of these claims will be shown in chapter 5.

2 THE MODEL

The accurate description of intermolecular interactions in water requires computationally heavy calculations with *ab initio* methods. This is mainly due to the presence of an hydrogen-bond network formed by the molecules, in which bonds form and break continuously with variable strength. The variability of the hydrogen-bonds is the result of the interplay between entropic and energetic effects, as well as the important presence of nuclear quantum effects. The high computational cost of the fully *ab initio* methods, i.e. techniques that use a quantum mechanical description of the system under study, prevents from computing the properties of large systems or to make long *ab initio* molecular dynamics (AIMD) simulations. These practical problems led to the development of many classical[1] water models with a spectrum of levels of sophistication, ranging from coarse-grained description with no atomistic resolution, to flexible and polarizable models with a sufficiently good level of accuracy. However, despite the great effort in finding a compromise between accuracy and computational cost, none of the models is able to reproduce the experimental results from the gaseous to the condensed phases at the same time.

The MB-pol (**M**any **B**ody-**pol**arization) water model [Babin, Leforestier, et al., 2013; Babin, Medders, et al., 2014; Medders et al., 2014] addresses the problem of the description of a collection of water molecules by splitting the total energy calculation into different many-body contributions. Let us consider a system of N water molecules; the energy of the system can be written as a sum of n-body terms, where $n \leq N$, i.e.:

$$\begin{aligned} E(x_1, \ldots, x_N) = \sum_{a=1}^{N} V^{(1B)}(x_a) + \sum_{a>b} V^{(2B)}(x_a, x_b) + \\ + \sum_{a>b>c} V^{(3B)}(x_a, x_b, x_c) + \ldots + V^{(NB)}(x_1, \ldots, x_N), \end{aligned} \quad (2.1)$$

where x_i are collective variables used as a shorthand notation to refer to a whole water molecule (they include e.g. the atomic coordinates).

For water, this many-body expansion has been found to rapidly converge, so that one can keep only few body terms and still obtain results that are in good agreement with the experimental data available.

---

[1] In this context *classical* means that the dynamics is given by the Newton's equation, rather than Schrödinger's equation. However, the form of the interactions may be derived from quantum mechanical considerations and rendered as an effective classical interaction.

2.1 THE FORM OF THE POTENTIAL

In the MB-pol potential there are explicit n-body terms up to order three, while the rest of the interactions are taken into account through a many-body term. The form of the potential is:

$$
\begin{aligned}
E_N(x_1,\dots,x_N) = \sum_{a=1}^{N} V^{(1\mathrm{B})}(x_a) + \sum_{a>b} V^{(2\mathrm{B})}(x_a,x_b) + \\
+ \sum_{a>b>c} V^{(3\mathrm{B})}(x_a,x_b,x_c) + V^{(\mathrm{MB})}(x_1,\dots,x_N),
\end{aligned}
\tag{2.2}
$$

where the caption "MB" stands for "Many Body". In the following sections we will describe in detail every term in equation (2.2).

2.2 ONE-BODY TERM

The monomer term $V^{(1\mathrm{B})}(x)$ is the energy associated to the intra-molecular distortions of each water molecule. It is represented by the Potential Energy Surface (PES) developed by Partridge and Schwenke, 1997. The PES is constructed by an *ab initio* term modified empirically to fit the experimental data.

2.2.1 Analytic form of the PES

In this model, the *ab initio* form of the energy of an isolated water molecule is:

$$
\begin{aligned}
V^{5\mathrm{Z}}(r_{\mathrm{OH}_1}, r_{\mathrm{OH}_2}, \theta) = V^a(r_{\mathrm{OH}_1}) + V^a(r_{\mathrm{OH}_2}) + \\
+ V^b(r_{\mathrm{HH}}) + V^c(r_{\mathrm{OH}_1}, r_{\mathrm{OH}_2}, \theta),
\end{aligned}
\tag{2.3}
$$

where the r_{OH_i} are the OH bond lengths, θ is the HOH angle, and the functional form of the terms in the sum is given by:

$$
V^a(r) = D\left[\mathrm{e}^{-2a(r-r_0)} - 2\mathrm{e}^{-a(r-r_0)}\right], \tag{2.4a}
$$

$$
V^b(r) = A\mathrm{e}^{-br}, \tag{2.4b}
$$

with r_{HH} the HH distance, and

$$
\begin{aligned}
V^c(r_{\mathrm{OH}_1}, r_{\mathrm{OH}_2}, \theta) = c_{000} + \mathrm{e}^{-\beta\left[(r_{\mathrm{OH}_1}-r_e)^2+(r_{\mathrm{OH}_2}-r_e)^2\right]} \times \\
\times \sum_{ijk} c_{ijk} \left[(r_{\mathrm{OH}_1}-r_e)/r_e\right]^i \left[(r_{\mathrm{OH}_2}-r_e)/r_e\right]^j \times \\
\times \left[\cos(\theta) - \cos(\theta_e)\right]^k.
\end{aligned}
\tag{2.5}
$$

The other quantities are parameters, either obtained by fitting the function to experimental data or preliminarily fixed.

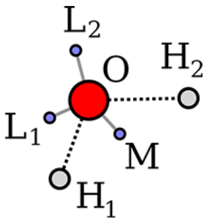

Figure 2.1: Water molecule with the additional M and L sites.

2.2.2 Empirical corrections

The fit to *ab initio* data is not practically feasible in its entirety, so this PES does not perfectly agree with experiments. In addition to that, *ab initio* data used are not exact, because of the approximations made to obtain them; relativistic corrections are not taken into account, as well as mass polarization, radiative and diagonal adiabatic modifications to the Born-Oppenheimer approximation; non-adiabatic effects and experimental errors lead to more inaccuracy. Empirical corrections are made in attempt to get better results. Thus, a new PES called V^{emp} is defined:

$$\begin{aligned}V^{\text{emp}} = {} & c^{5\text{Z}} V^{5\text{Z}}(r_{\text{OH}_1}, r_{\text{OH}_2}, \theta) + c^{\text{core}} \Delta V^{\text{core}}(r_{\text{OH}_1}, r_{\text{OH}_2}, \theta) + \\ & + c^{\text{basis}} \Delta V^{\text{basis}}(r_{\text{OH}_1}, r_{\text{OH}_2}, \theta) + \Delta V^{\text{rest}}(r_{\text{OH}_1}, r_{\text{OH}_2}, \theta),\end{aligned} \tag{2.6}$$

where $\Delta V^{\text{rest}} = V^c$ of eq. (2.5), and new parameters c have been introduced.

2.3 TWO-BODY TERM

The two-body term in the many-body expansion takes into account the interaction of two water molecules whose coordinates are labeled x_a and x_b. The different physical origin of the interaction at different separations suggests to split the potential into short- and long-range contributions:

$$V^{(2\text{B})}(x_a, x_b) = V^{(2\text{B})}_{\text{short}}(x_a, x_b) + V^{(2\text{B})}_{\text{long}}(x_a, x_b). \tag{2.7}$$

2.3.1 Long-range

The long-range term is dominated by the electrostatic interaction between permanent and induced dipole moments associated with the charge distribution of the molecules. In addition, there is a dispersion term. The chosen form is such that:

$$V^{(2\text{B})}_{\text{long}}(x_a, x_b) = V^{(2\text{B})}_{\text{TTM,elec}}(x_a, x_b) + V^{(2\text{B})}_{\text{TTM,ind}}(x_a, x_b) + V^{(2\text{B})}_{6}(x_a, x_b), \tag{2.8}$$

where each term is described as follows. For a more detailed description of the electrostatic interaction, see the appendix A at page 73:

THE PERMANENT DIPOLES are modeled through point charges placed on the two H atoms and in the M site, placed near the middle of the segment joining the hydrogens in such a way to optimize the quadrupole moment of an isolated molecule (see fig. 2.1). The effective contribution is only a charge-charge term. The functional form of the interaction is the TTM4-F model:

$$V^{(2B)}_{\text{TTM,elec}}(x_a, x_b) = \tfrac{1}{2} \sum_{a \neq b} q_a q_b A^{-1}_{ab} \lambda_1(u_{ab}), \tag{2.9}$$

where q_a are the charges, $u_{ab} = r_{ab}/A_{ab}$, $r_{ab} = |\mathbf{r}_a - \mathbf{r}_b|$ is the distance between interaction sites a and b, $A_{ab} = (\alpha_a \alpha_b)^{1/6}$ and α_n are the dipole polarizabilities. Functions $\lambda_n(u)$ implement the screened interactions by assuming a particular density in place of the point charges. They are defined recursively as:

$$\lambda_{n+2}(u) = -\frac{1}{un}\frac{\partial}{\partial u}\lambda_n(u), \tag{2.10}$$

$$\lambda_1(u) = \frac{1}{u}(1 - \mathrm{e}^{-au^m}) + a^{1/m}\Gamma\left[1 - \tfrac{1}{m}, au^m\right], \tag{2.11}$$

where $\Gamma(a, x)$ is defined as:

$$\Gamma(a, x) = \int_x^\infty \mathrm{d}t\, t^{a-1}\mathrm{e}^{-t}, \tag{2.12}$$

and $m = 4$ in the TTM4-F model.

THE INDUCED DIPOLES are described by point dipoles placed on the oxygen (O) and on the hydrogens (H). An additive damping factor between the hydrogen within the same molecule has been included. The functional form of the interaction is:

$$V^{(2B)}_{\text{TTM,ind}}(x_a, x_b) = -\tfrac{1}{2} \sum_a \boldsymbol{\mu}_a \cdot \mathbf{E}_a, \tag{2.13}$$

where $\boldsymbol{\mu}_a$ is the induced dipole moment at the interaction site a and $\mathbf{E}_a$ is the Thole-smeared electric field at site a due to the charges and the dipoles.

THE LONG-RANGE DISPERSION contribution is represented by damped r^{-6} terms associated to all pairs of atoms:

$$V^{(2B)}_6(x_a, x_b) = -\sum_{i \in a, j \in b} f_6(\delta^{(ij)}_6 r_{ij}) C^{(ij)}_6 \frac{1}{r^6_{ij}}, \tag{2.14}$$

where i and j in the sums run over all atoms belonging to molecules a and b, r_{ij} denotes the distance between atom i and atom j and $f_n(\xi)$ are the Tang-Toennies damping functions:

$$f_n(\xi) = 1 - \mathrm{e}^{-\xi} \sum_{k=0}^{n} \frac{\xi^k}{k!}, \tag{2.15}$$

and the quantities δ and C are parameters.

2.3.2 Short-range

The short range part of the interaction represents a quantum correction to the classical interaction described above, due to the overlap of the monomer electron densities. It is represented by a permutationally invariant polynomial that smoothly switches to zero when the separation between water molecules exceeds a cutoff value:

$$V^{(2\mathrm{B})}_{\mathrm{short}}(x_a, x_b) = s\left(\frac{r_{\mathrm{OO}} - \rho_i}{\rho_o - \rho_i}\right) V_{2\mathrm{S}}, \tag{2.16}$$

with

$$s(x) = \begin{cases} 1 & \text{if } x < 0 \\ \cos^2\left(\frac{\pi}{2}x\right) & \text{if } 0 \le x \le 1 \\ 0 & \text{if } \le x \end{cases} \tag{2.17}$$

and $\rho_{i,o}$, the inner and outer radii of the switching function, are set to 4.5Å and 6.5Å respectively. This provides a good compromise between accuracy and computational efficiency. In eq. (2.17), $V_{2\mathrm{S}}$ is a polynomial in functions of the distances between all pair of atoms and two additional sites, L_1 and L_2, placed symmetrically along the oxygen lone-pair direction (see fig. 2.1). Such positions are:

$$\mathbf{r}_L^{(\pm)} = \mathbf{r}_\mathrm{O} + \tfrac{1}{2}\gamma_{\|}(\mathbf{r}_{\mathrm{OH}_1} + \mathbf{r}_{\mathrm{OH}_2}) \pm \gamma_{\perp}\left(\mathbf{r}_{\mathrm{OH}_1} \times \mathbf{r}_{\mathrm{OH}_2}\right), \tag{2.18}$$

where $\gamma_{\|}$ and $\gamma_{\perp}$ are fitting parameters that optimize the location of the L sites, and $\mathbf{r}_{\mathrm{OH}_{1,2}}$ are vectors joining O and H atoms within the same molecule of H_2O. There are 31 possible distances between all types of sites described; these distances $d_{m=1-31}$ are used to form the same number of negative exponential variables in the distances, divided into three groups: 6 intramolecular variables $\xi_{i=1-6}$, 9 intermolecular Coulomb-like variables $\xi_{i=7-16}$ and 16 intermolecular variables involving L sites $\xi_{i=17-31}$. With these definitions, $V_{2\mathrm{S}}$ is constructed as a permutationally invariant polynomial in ξ_i. Such a polynomial is a sum of 1153 symmetrized monomials η_l:

$$V_{2\mathrm{S}} = \sum_{l=1}^{1153} c_l \eta_l, \tag{2.19}$$

where c_i are linear fitting parameters.

2.4 THREE-BODY TERM

Like the two-body term, the three-body interaction can be split into two parts:

$$V^{(3\mathrm{B})}(x_a, x_b, x_c) = V^{(3\mathrm{B})}_{\mathrm{short}}(x_a, x_b, x_c) + V^{(3\mathrm{B})}_{\mathrm{TTM,ind}}(x_a, x_b, x_c), \tag{2.20}$$

where $V^{(3\mathrm{B})}_{\mathrm{TTM,ind}}$ is the TTM 3-body induction energy, analog to the one introduced in section 2.3.1, while $V^{(3\mathrm{B})}_{\mathrm{short}}$ is again a quantum correction that takes into account the electronic overlap. Its form is:

$$\begin{aligned} V^{(3\mathrm{B})}_{\mathrm{short}}(x_a, x_b, x_c) = {} & [s(t_{ab})s(t_{ac}) + s(t_{ab})s(t_{bc}) + \\ & + s(t_{ac})s(t_{bc})]\, V^{(3\mathrm{B})}_{\mathrm{poly}}(x_a, x_b, x_c), \end{aligned} \tag{2.21}$$

where the sum in the square brackets represents a function that smoothly goes to zero as one of the three water molecules a, b or c moves apart from the other two. The function s is the same as in equation (2.17), and $t_{mn} = R_{mn}^{(\mathrm{O})}/\rho_{\mathrm{cut}}^{(3\mathrm{B})}$, where $R_{mn}^{(\mathrm{O})}$ is the distance between the oxygen atoms of water molecules m and n, and $\rho_{\mathrm{cut}}^{(3\mathrm{B})} = 4.5\text{Å}$ is the three-body cutoff distance. The value has been chosen to optimize both accuracy and computational efficiency.

The $V_{\mathrm{poly}}^{(3\mathrm{B})}$ term in equation (2.21) is a permutationally invariant polynomial in exponentials of the inter-atomic distances $d_{m=1-36}$ discussed above. From these distances one can define variables ξ_i in a similar manner as discussed for the 2-body term.

2.5 MANY-BODY TERM

All the contributions to the interaction with $n \geq 4$ are included as a TTM induction correction, i.e. only the induced dipole interaction is taken into account. The high accuracy of the MB-pol potential has been demonstrated in the literature, e.g. [Babin, Medders, et al., 2014; Paesani, 2016].

3 DATA ANALYSIS

In a molecular dynamics simulation what one measures is the time series of the heat flux (1.43). In the following, we will review some results in the field of time-series analysis that will be useful in the following chapters. Let us fix some notations:

- The expectation value of a random variable will be denoted by $\mathbb{E}\left[\cdot\right]$ or by the angle brackets $\langle\cdot\rangle$;
- The variance of a random variable will be denoted by $\mathrm{Var}\left[\cdot\right]$;
- The symbol "$\sim$" will mean *is distributed as*.

3.1 A BRIEF REMINDER OF STATISTICS

DEFINITION 1 (STOCHASTIC PROCESS): A stochastic process $\{X_t\,:\,t\in\mathcal{T}\}$ is a collection of random variables X_t labeled by a (possibly continuous) index t belonging to a set of indexes $\mathcal{T}$ which, in our case, will be thought of as time. The values assumed by X_t will be indicated by $x(t)$.

In the case of a numerical simulation, the process will be discrete and correspond to the instantaneous value of an observable of the system. However, the underlying physics is built upon a continuous time parameter so, when necessary, the definitions and the examples will regard the X_t's as continuous random variables. The time-series of the realizations of the process will often be referred to as *signal* or *time-series*.

DEFINITION 2 (WIDE-SENSE STATIONARY PROCESS): A stochastic process $\{X_t\}$ is said to be *wide-sense stationary* if its expectation value do not vary with respect to time, and its autocorrelation function only depends on time differences, i.e.:

$$m_X(t) \overset{\text{def}}{=} \mathbb{E}\left[X_t\right] = m_X(t+\tau)\ \forall \tau\in\mathbb{R}, \tag{3.1}$$

$$C_X(t_1,t_2) \overset{\text{def}}{=} \mathbb{E}\left[\left(X_{t_1}-m_X(t_1)\right)\left(X_{t_2}-m_X(t_2)\right)\right] = C_X(t_1-t_2,0), \tag{3.2}$$

A stronger notion of stationarity would require the cumulative distribution function of the whole process to be insensitive of time translations; however, for our purposes such a restriction is not required.

An important tool that will be useful to analyze the data is the power spectral density:

DEFINITION 3 (POWER SPECTRAL DENSITY): Given a stochastic process $\{X_t\}$, its *truncated power spectral density* $S_{\mathcal{T}}$ is defined as the expectation value of the modulus squared of its truncated Fourier transform divided by the width of the truncation window:

$$S_{\mathcal{T}}(f) \overset{\text{def}}{=} \frac{1}{\mathcal{T}} \left\langle \left| \int_{-\mathcal{T}/2}^{\mathcal{T}/2} \mathrm{e}^{2\pi i f t} x(t)\,\mathrm{d}t \right|^2 \right\rangle = \frac{1}{\mathcal{T}} \left\langle |\tilde{x}_{\mathcal{T}}(f)|^2 \right\rangle, \tag{3.3}$$

where the truncated Fourier transform $\tilde{x}_{\mathcal{T}}(f)$ has been defined in the last equality. The *power spectral density* or *power spectrum* of the process is defined as the limit for large $\mathcal{T}$ of the truncated power spectral density[1]:

$$S(f) \overset{\text{def}}{=} \lim_{\mathcal{T}\to\infty} S_{\mathcal{T}}(f) = \lim_{\mathcal{T}\to\infty} \frac{1}{\mathcal{T}} \left\langle |\tilde{x}_{\mathcal{T}}(f)|^2 \right\rangle. \tag{3.4}$$

The power spectrum turns out to be useful in the analysis of the heat flux time series because of the following theorem:

THEOREM 1 (WIENER-KINTCHINE): Let X_t be a stochastic process whose realizations will be denoted by the signal $x(t)$, and let $C(\tau) = \langle x(t)x(t+\tau)\rangle$ be its autocorrelation function. Then, when the Fourier transform of $C(\tau)$ is well defined, it is equal to the power spectrum $S(f)$ of the signal, i.e.:

$$S(f) = \int_{-\infty}^{\infty} C(\tau)\mathrm{e}^{2\pi i f \tau}\,\mathrm{d}\tau \tag{3.5}$$

Proof. Let us write explicitly the expectation value of the modulus squared of the truncated Fourier transform of the process:

$$\begin{aligned} \left\langle |\tilde{x}_{\mathcal{T}}(f)|^2 \right\rangle &= \int_{-\mathcal{T}/2}^{\mathcal{T}/2} \int_{-\mathcal{T}/2}^{\mathcal{T}/2} \langle x(t)x(s)\rangle\, \mathrm{e}^{2\pi i (t-s) f}\,\mathrm{d}t\mathrm{d}s \\ &= \int_{-\mathcal{T}/2}^{\mathcal{T}/2} \int_{-\mathcal{T}/2}^{\mathcal{T}/2} C(t-s)\mathrm{e}^{2\pi i (t-s) f}\,\mathrm{d}t\mathrm{d}s. \end{aligned} \tag{3.6}$$

The integral can be simplified using the simple lemma:

LEMMA 1: The following formula holds:

$$\int_{-\mathcal{T}/2}^{\mathcal{T}/2} \int_{-\mathcal{T}/2}^{\mathcal{T}/2} f(t-s)\,\mathrm{d}t\mathrm{d}s = \int_{-\mathcal{T}}^{\mathcal{T}} f(\tau)(\mathcal{T} - |\tau|) \tag{3.7}$$

Proof. The proof is simply a matter of calculus:

$$\begin{aligned} I \equiv & \int_{-\mathcal{T}/2}^{\mathcal{T}/2} \int_{-\mathcal{T}/2}^{\mathcal{T}/2} f(t-s)\,\mathrm{d}t\mathrm{d}s = \int_{-\mathcal{T}/2}^{\mathcal{T}/2} \int_{-\mathcal{T}/2-t}^{\mathcal{T}/2-t} f(\tau)\,\mathrm{d}\tau\mathrm{d}t \\ = & \int_{-\mathcal{T}/2}^{\mathcal{T}/2} \left[\int_{-\mathcal{T}}^{\mathcal{T}} f(\tau)\,\mathrm{d}\tau - \int_{-\mathcal{T}}^{-\mathcal{T}/2-t} f(\tau)\,\mathrm{d}\tau - \int_{\mathcal{T}/2-t}^{\mathcal{T}} f(\tau)\,\mathrm{d}\tau \right] \mathrm{d}t \\ = & \mathcal{T} \int_{-\mathcal{T}}^{\mathcal{T}} f(\tau)\,\mathrm{d}\tau - \int_{-\mathcal{T}}^{0} f(\tau) \int_{-\mathcal{T}/2}^{-\mathcal{T}/2-\tau} \mathrm{d}t\mathrm{d}\tau - \int_{0}^{\mathcal{T}} f(\tau) \int_{\mathcal{T}/2-\tau}^{\mathcal{T}/2} \mathrm{d}t\mathrm{d}\tau \\ = & \mathcal{T} \int_{-\mathcal{T}}^{\mathcal{T}} f(\tau)\,\mathrm{d}\tau - \int_{-\mathcal{T}}^{0} f(\tau)(-\tau)\,\mathrm{d}\tau - \int_{0}^{\mathcal{T}} f(\tau)\tau\,\mathrm{d}\tau \\ = & \int_{-\mathcal{T}}^{\mathcal{T}} f(\tau)(\mathcal{T} - |\tau|)\,\mathrm{d}\tau. \end{aligned} \tag{3.8}$$

□

---

[1] The limit may not exist. However, for weakly stationary processes such as the ones we are interested in, it happens to exist.

Let us apply the formula to $f(\tau) = C(\tau)\mathrm{e}^{2\pi i\tau f}$:

$$\left\langle |\tilde{x}_{\mathcal{T}}(f)|^2 \right\rangle = \int_{-\mathcal{T}}^{\mathcal{T}} C(\tau)\mathrm{e}^{2\pi i\tau f}(\mathcal{T} - |\tau|)\,\mathrm{d}\tau. \tag{3.9}$$

Dividing by $\mathcal{T}$ and letting $\mathcal{T}$ go to infinity one gets:

$$\begin{aligned} S(f) &= \lim_{\mathcal{T}\to\infty} \frac{1}{\mathcal{T}} \left\langle |\tilde{x}_{\mathcal{T}}(f)|^2 \right\rangle = \int_{-\mathcal{T}}^{\mathcal{T}} C(\tau)\mathrm{e}^{2\pi i\tau f}\left(1 - \frac{|\tau|}{\mathcal{T}}\right)\mathrm{d}\tau \\ &= \lim_{\mathcal{T}\to\infty} \int_{-\infty}^{\infty} C(\tau)\mathrm{e}^{2\pi i\tau f} + \mathcal{O}\left(\frac{1}{\mathcal{T}}\right). \end{aligned} \tag{3.10}$$

☐

When the autocorrelation function is even in time, as in the case of the processes we are interested in, the integral can be rewritten as

$$S(f) = 2\int_{0}^{\infty} C(\tau)\mathrm{e}^{2\pi i\tau f}. \tag{3.11}$$

The Wiener-Kintchine theorem allows to express the Green-Kubo thermal conductivity as the zero-frequency value of the power spectrum of the heat flux:

$$\kappa = \frac{\Omega}{k_{\mathrm{B}}T^2}\int_0^{\infty} C_{J_{\mathrm{q}}J_{\mathrm{q}}}(t)\mathrm{d}t \tag{3.12}$$

$$= \frac{\Omega}{2k_{\mathrm{B}}T^2} S(f=0), \tag{3.13}$$

where Ω is the volume of the system, k_{B} is the Boltzmann constant and T is the temperature.

Eventually, a concept in statistics that allows to infer the value of an unknown parameter is the *estimator*:

DEFINITION 4 (ESTIMATOR): An *estimator* $\hat{\theta}(X_t)$ of a parameter θ is a function of the sample space designed to compute an estimate of the desired parameter, given the available data. An estimator is said to be *consistent* if it converges in probability to the to the quantity being estimated as sample size (i.e. time) grows[2]. It is said to be *unbiased* when its expectation value equals the real value of the quantity of interest.

After this brief reminder of some useful statistical tools, let us get into how the signal obtained from the MD simulations will be analyzed.

3.2 EINSTEIN-HELFAND APPROACH

The estimate of the Onsager's coefficients via direct integration of the correlation functions is usually tricky. After the correlation time, in fact, the correlation functions are dominated by noise, and their integral behaves like a random walk. Thus, the evaluation of the transport coefficients requires the averaging of the correlation functions over multiple trajectories, possibly many segments of the same long trajectory. The error estimate has to be

---

[2] This is like saying that its variance should go to zero as the number of observations grows.

carried out as a function of both the number of trajectories and the upper limit of time-integration. This procedure is neither efficient nor satisfactory, since it often leads to a poor estimate of the desired conductivity, in particular when the signal is inherently oscillatory because of the high frequency molecular motion of the constituents of the system.

A slightly better approach that, however, does not resolve the issue of the error estimate, is a generalization of the Einstein relation to compute the diffusion coefficient in its explanation of the Brownian motion [Einstein, 1905]. Let us and consider the zero-frequency value of the function in eq. (3.10) before evaluating the limit:

$$S_{\mathcal{T}}(0) = \int_{-\mathcal{T}}^{\mathcal{T}} \langle x(t)x(0)\rangle \,\mathrm{d}t - \frac{1}{\mathcal{T}} \int_{-\mathcal{T}}^{\mathcal{T}} \langle x(t)x(0)\rangle \, t\,\mathrm{d}t. \tag{3.14}$$

The parity of $\langle x(t)x(0)\rangle$ allows to write

$$S_{\mathcal{T}}(0) = 2\int_{0}^{\mathcal{T}} \langle x(t)x(0)\rangle \,\mathrm{d}t - \frac{2}{\mathcal{T}} \int_{0}^{\mathcal{T}} \langle x(t)x(0)\rangle \, t\,\mathrm{d}t, \tag{3.15}$$

which is the zero-frequency value of the truncated power spectral density.

The usual way to estimate the thermal conductivity from the heat flux time-series computed in a molecular dynamics simulation is to wait for the convergence of a discretized version of eq. (3.15) with respect to the simulation time $\mathcal{T}$. In fact, since the second integral in the above equation is finite for all $\mathcal{T}$, in the large $\mathcal{T}$ limit its value divided by $\mathcal{T}$ tends to zero. This is known as the Einstein-Helfand method [Helfand, 1960]. When the time-series of interest is the velocity of a particle in a fluid, the large $\mathcal{T}$ limit of equation (3.15) is proportional to the diffusivity of that fluid. When the heat flux time-series is considered, that limit becomes proportional to the thermal conductivity of the system. The value of the thermal conductivity is found as:

$$\kappa = \frac{\Omega}{3k_\mathrm{B}T^2} \lim_{\mathcal{T}\to\infty} \frac{\left\langle \mathcal{D}_\epsilon^2(\mathcal{T})\right\rangle}{\mathcal{T}}, \tag{3.16}$$

where the *energy displacement* $\mathcal{D}_\epsilon$ is defined as

$$\mathcal{D}_\epsilon(\mathcal{T}) = \int_0^{\mathcal{T}} \mathbf{J}_\mathrm{q}(t)\,\mathrm{d}t.$$

As it will be clear in the next section, the idea behind cepstral analysis is to focus on estimating the low frequency spectrum of the desired time-series, instead that on the zero-frequency value only as in the Einstein-Helfand method. From the analytical properties of the power spectrum, in fact, one can gather more information and reduce the error on the estimate of the desired transport coefficient.

3.3 CEPSTRAL ANALYSIS

Let us indicate the (scalar) time series of the heat flux as

$$J_n = {J_\mathrm{q}}^\alpha(t = n\varepsilon), \quad n = 0, \dots, N-1, \tag{3.17}$$

where ε is the sampling time, ${J_{\mathrm{q}}}^{\alpha}$ is one of the Cartesian components of the heat flux $\mathbf{J}_{\mathrm{q}}$ and N is the length of the time-series. As stated above, according to the Wiener-Kintchine theorem 1 it is possible to write κ as:

$$\kappa = \frac{\Omega}{2k_{\mathrm{B}}T^2} S(f=0). \tag{3.18}$$

Since the signal, i.e. the time-series, is a discrete stochastic process, let us define the convention used for discrete Fourier transforms as:

$$\tilde{J}_k = \sum_{n=0}^{N-1} J_n \mathrm{e}^{2\pi i k n/N}, \quad k = 0, \ldots, N-1. \tag{3.19}$$

An unbiased estimator of the power spectral density is given by the *periodogram* $\hat{S}_k$:

$$\hat{S}_k \overset{\text{def}}{=} \frac{\varepsilon}{N} \left| \tilde{J}_k \right|^2 . \tag{3.20}$$

For a real-valued signal as J_n, the discrete Fourier transform has the symmetry property

$$\tilde{J}_k = \tilde{J}^*_{N-k}, \tag{3.21}$$

so that

$$\hat{S}_k = \hat{S}_{N-k}; \tag{3.22}$$

then one can simply report half of the periodogram.

The heat flux is the volume integral of the heat current; the space autocorrelations of the latter are usually short ranged: therefore, in the thermodynamic limit, the fluxes can be thought of as a sum of almost independent identically distributed stochastic variables. The Central Limit Theorem then ensures the distribution of the heat flux to be Gaussian. For this reason its discrete Fourier transform is also a zero-mean Gaussian variable, and from the definition (3.20) of periodogram the variance can be obtained as:

$$\begin{aligned} \operatorname{Var}\left[\tilde{J}_k\right] =& \mathbb{E}\left[\left|\tilde{J}_k\right|^2\right] \\ =& \mathbb{E}\left[(\mathfrak{Re}\tilde{J}_k)^2 + (\mathfrak{Im}\tilde{J}_k)^2\right] \\ =& \mathbb{E}\left[(\mathfrak{Re}\tilde{J}_k)^2\right] + \mathbb{E}\left[(\mathfrak{Im}\tilde{J}_k)^2\right] \\ =& \frac{N}{\varepsilon}\left\langle \hat{S}_k \right\rangle = \frac{N}{\varepsilon} S(f_k), \end{aligned} \tag{3.23}$$

where $f_k = k/N$ and the fact that the real and imaginary part of $\tilde{J}_k$ are uncorrelated has been used. The last step follows from the fact that the periodogram is an unbiased estimator of the true power spectrum. With this result, one can say that the real and imaginary part of $\tilde{J}_k$ (or simply $\tilde{J}_k$, when it is real) are distributed as

$$k = 0, \frac{N}{2}: \qquad \tilde{J}_k \in \mathbb{R}, \tilde{J}_k \sim \mathcal{N}\left(0, \frac{N}{\varepsilon} S(f_k)\right) \tag{3.24}$$

$$k \neq 0, \frac{N}{2}: \qquad \mathfrak{Re}\tilde{J}_k, \mathfrak{Im}\tilde{J}_k \sim \mathcal{N}\left(0, \frac{N}{2\varepsilon} S(f_k)\right), \tag{3.25}$$

where $\mathcal{N}(\mu,\sigma^2)$ represents a Gaussian random variable with expectation value μ and variance σ^2. To understand how $\left|\widetilde{J}_k\right|^2$ is distributed let us multiply and divide it by its variance in the case $k \neq \{0, N/2\}$:

$$\begin{aligned}\left|\widetilde{J}_k\right|^2 &=(\mathfrak{Re}\widetilde{J}_k)^2 + (\mathfrak{Im}\widetilde{J}_k)^2 \\ &=\frac{N}{2\varepsilon}S(f_k)\left[\mathcal{N}_1^2 + \mathcal{N}_2^2\right] \\ &\equiv\frac{N}{\varepsilon}S(f_k)\hat{\xi}_k,\end{aligned} \tag{3.26}$$

where both $\mathcal{N}_1$ and $\mathcal{N}_2$ are standard Gaussian variables. The distribution of the sum of the squares of two standard Gaussian variables is the chi-squared distribution with two degrees of freedom, i.e. the variables $\hat{\xi}_k$ introduced above are distributed as

$$\hat{\xi}_k \sim \frac{1}{2}\chi^2_2, \quad k \neq 0, \frac{N}{2}; \qquad \hat{\xi}_k \sim \chi^2_1, \quad k = 0, \frac{N}{2}. \tag{3.27}$$

The result for $k = \{0, N/2\}$ follows straightforwardly from equation (3.26) in the case $\widetilde{J}_k \in \mathbb{R}$. Since N is large and the distribution is χ^2_1 only in two cases, we will assume that the distribution is $\frac{1}{2}\chi^2_2 \forall k$, thus introducing an error of order $\mathcal{O}(1/N)$ that vanishes in the limit of $N \to \infty$.

The final result is that the periodogram can be expressed as

$$\hat{S}_k = S(f_k)\hat{\xi}_k, \tag{3.28}$$

with $\hat{\xi}_k$ distributed as in (3.27). All of this is valid for a single, scalar valued time-series. Being the heat flux a vector valued quantity, every MD simulation gives three independent time-series J_{q_α}, $\alpha = \{1, 2, 3\}$. In the general case, let us suppose there are ℓ different realizations of the same process. A mean periodogram can be defined as the arithmetic mean of the ℓ periodograms obtained from the different time-series:

$$\begin{aligned}{}^\ell\hat{S}_k &\overset{\text{def}}{=} \frac{\varepsilon}{\ell N}\sum_{p=1}^{\ell}\left|{}^p\widetilde{J}_k\right|^2 \\ &=S(f_k)\,{}^\ell\hat{\xi}_k,\end{aligned} \tag{3.29}$$

where ${}^\ell\hat{\xi}_k$ are distributed as ${}^\ell\hat{\xi}_k \sim \frac{1}{2\ell}\chi^2_{2\ell}$. The mean periodogram is an unbiased estimator of the power spectrum, but it is not consistent, i.e. its accuracy does not increase for increasing N. In fact:

$$\mathbb{E}\left[{}^\ell\hat{S}_k\right] = S(f_k)\mathbb{E}\left[{}^\ell\hat{\xi}_k\right] = S(f_k); \tag{3.30}$$

$$\operatorname{Var}\left[{}^\ell\hat{S}_k\right] = S(f_k)^2 \operatorname{Var}\left[{}^\ell\hat{\xi}_k\right] = \frac{1}{\ell}S(f_k)^2. \tag{3.31}$$

The factor $\hat{\xi}_k$ can be regarded as a multiplicative noise term that affects the signal ${}^\ell\hat{S}_k$. An additive noise can be filtered away more easily than a multiplicative one, so that it is better to analyze the logarithm of ${}^\ell\hat{S}_k$, instead of the quantity itself. Let us define the log-mean-periodogram as

$$\begin{aligned}{}^\ell\hat{L}_k &= \log\left({}^\ell\hat{S}_k\right) \\ &= \log(S(f_k)) + \log({}^\ell\hat{\xi}_k).\end{aligned} \tag{3.32}$$

The logarithm of ${}^{\ell}\hat{\xi}_k$ has mean and variance given by

$$\mathbb{E}\left[\log\left({}^{\ell}\hat{\xi}_k\right)\right] = \psi(\ell) - \log(\ell); \tag{3.33}$$

$$\operatorname{Var}\left[\log\left({}^{\ell}\hat{\xi}_k\right)\right] = \psi'(\ell), \tag{3.34}$$

where ψ is the digamma function, i.e. the logarithmic derivative of the Euler Gamma-function:

$$\psi(z) = \frac{\partial \log \Gamma(z)}{\partial z}. \tag{3.35}$$

The additive noise can be redefined to be the zero mean random variable ${}^{\ell}\hat{\lambda}_k$ such that

$$\mathbb{E}\left[{}^{\ell}\hat{\lambda}_k\right] = 0,\ \operatorname{Var}\left[{}^{\ell}\hat{\lambda}_k\right] = \psi'(\ell), \tag{3.36}$$

so the log-mean-periodogram becomes

$${}^{\ell}\hat{L}_k = \log(S(f_k)) + {}^{\ell}\Lambda + {}^{\ell}\hat{\lambda}_k, \tag{3.37}$$

where ${}^{\ell}\Lambda = \psi(\ell) - \log(\ell)$ is a constant added to the true log-power spectrum.

The whole problem of estimating the zero frequency value of the power spectrum to obtain the heat conductivity has been recast into the issue of denoising the low-frequency part of the log-periodogram of the heat flux time-series. Such a signal happens to have a rather smooth behavior at large scales (i.e. small frequencies[3]), while at small scales the noise dominates and the details are indiscernible.

The idea behind the so called *cepstral analysis* [Ercole, Marcolongo, et al., 2017] is to find a way to keep the Fourier components of ${}^{\ell}\hat{L}_k$ associated to the large scale behavior, while discarding the high frequency oscillations due to the noise. One can define the *cepstrum* of the time-series J_n as the inverse Fourier-transform of the log-mean-periodogram:

$${}^{\ell}\hat{C}_n \overset{\text{def}}{=} \frac{1}{N}\sum_{k=0}^{N-1} {}^{\ell}\hat{L}_k \mathrm{e}^{-2\pi i k n/N}. \tag{3.38}$$

In the large N limit a generalized form of the Central Limit Theorem applies [Peligrad and Wu, 2010], so that these random variables are almost surely[4] independent identically distributed zero mean Gaussian variables:

$${}^{\ell}\hat{C}_n = \delta_{n,0}{}^{\ell}\Lambda + C_n + {}^{\ell}\mu_n, \tag{3.39}$$

where ${}^{\ell}\mu_n$ are zero-mean normal variables with variance given by

$$\left\langle {}^{\ell}\mu_{\ell}^2 \right\rangle = \frac{\psi'(\ell)}{N} \text{ for } n \notin \{0, N/2\}$$

and

$$\left\langle {}^{\ell}\mu_{\ell}^2 \right\rangle = 2\frac{\psi'(\ell)}{N} \text{ otherwise,}$$

---

[3] Here the word *frequency* indicates the frequency of oscillation of the new signal ${}^{\ell}\hat{L}_k$, not the physical frequency associated to the oscillations of the time-series of the heat flux.

[4] Here *almost surely* means that the probability of the event not happening is zero.

and the C_n are

$$C_n = \frac{1}{N}\sum_{k=0}^{N-1} \log\left(S(f_k)\right) \mathrm{e}^{2\pi i k n/N}. \tag{3.40}$$

To discard the high-frequency part of the signal ${}^{\ell}\hat{L}_k$ means to keep only the cepstral coefficients that are significantly different from zero, i.e. to choose an integer P^* such that the $f = 0$ component of the log-spectrum can be estimated from

$$\begin{aligned}{}^{\ell}\hat{L}_0^* &= {}^{\ell}\hat{C}_0 + 2\sum_{n=1}^{P^*-1} {}^{\ell}\hat{C}_n \\ &= {}^{\ell}\Lambda + \log(S(f=0)) + {}^{\ell}\mu_0 + 2\sum_{n=1}^{P^*-1} {}^{\ell}\mu_n.\end{aligned} \tag{3.41}$$

From the properties of ${}^{\ell}\mu_n$ it follows that ${}^{\ell}\hat{L}_0^*$ is normal with mean and variance given by

$$\mathbb{E}\left[{}^{\ell}\hat{L}_0^*\right] = \log(S(f=0)) + {}^{\ell}\Lambda; \tag{3.42}$$

$$\mathrm{Var}\left[{}^{\ell}\hat{L}_0^*\right] = \psi'(\ell)\frac{4P^*-2}{N}. \tag{3.43}$$

The quality of the signal's feature extraction depends on how the number of significant coefficients P^* is chosen. Ercole, Marcolongo, et al., 2017 suggested to use Akaike's Information Criterion [Akaike, 1974] to estimate the number of coefficients to retain. Given a statistical model, the AIC is a sample statistic defined as:

$$\mathrm{AIC}(P) = -2\max_{\boldsymbol{\theta}} \log \mathscr{L}(\theta, P) + 2P, \tag{3.44}$$

where $\mathscr{L}(\boldsymbol{\theta}, P)$ is the likelihood function of the set of P parameters upon which the chosen models depends, $\boldsymbol{\theta} = \{\theta_1, \theta_2, , \dots, \theta_P\}$.

The optimal number of parameters is the one that minimizes the AIC function, i.e.:

$$P^* = \arg\min_P \mathrm{AIC}(P). \tag{3.45}$$

In our case, the parameters are the cepstral coefficients C_n of eq. (3.40). The log-likelihood of these parameters is

$$\begin{aligned}2\log\mathscr{L}(C,P) = -&\frac{N}{2\sigma_\ell^2}(C_0 + \Lambda_\ell - \hat{C}_0)^2 + \\ &-\frac{N}{\sigma_\ell^2}\sum_{n=1}^{P-1}(C_n - \hat{C}_n)^2 - \frac{N}{\sigma_\ell^2}\sum_{n=P}^{N/2}\hat{C}_n^2.\end{aligned} \tag{3.46}$$

Since finding the argument that maximizes a function is equivalent to finding the argument that minimizes the negative of that function, the AIC of this model can be written as:

$$\begin{aligned}\mathrm{AIC}(P) = \min_C \Bigg[&\frac{N}{2\sigma_\ell^2}(C_0 + \Lambda_\ell - \hat{C}_0)^2 + \\ &+\frac{N}{\sigma_\ell^2}\sum_{n=1}^{P-1}(C_n - \hat{C}_n)^2 - \frac{N}{\sigma_\ell^2}\sum_{n=P}^{N/2}\hat{C}_n^2\Bigg] + 2P.\end{aligned} \tag{3.47}$$

The minimum of the negative log-likelihood is readily found by nullifying the squares in the above equation. Then, the AIC function becomes:

$$\mathrm{AIC}(P) = \frac{N}{\sigma_\ell^2} \sum_{n=P}^{N/2} \hat{C}_n^2 + 2P. \tag{3.48}$$

The final step is to choose P^* as the one that minimizes the above function i.e., by explicitly referring to the value of σ_ℓ^2:

$$\mathrm{AIC}(P) = \frac{N}{\psi'(\ell)} \sum_{n=P}^{N/2} \hat{C}_n^2 + 2P. \tag{3.49}$$

3.3.1 Multi-component cepstral analysis

In the general case, say a system admits M interacting conserved fluxes, the first being the energy flux. A *cross-spectrum* can be defined as a straightforward generalization of the power-spectrum [Bertossa et al., 2018]:

$$S^{ij}(\omega) = \int_{-\infty}^{\infty} \left\langle J^i(t) J^j(0) \right\rangle \mathrm{e}^{i\omega t} \mathrm{d}\, t. \tag{3.50}$$

In analogy to eq. (3.18), the Onsager matrix elements L^{ij} are proportional to the zero frequency value of the associated cross-spectrum:

$$L^{ij} = \frac{\Omega}{2k_\mathrm{B}} S_0^{ij}, \tag{3.51}$$

where $S_0^{ij} = S^{ij}(0)$.

When all the fluxes but the energy flux vanish, the thermal conductivity can be expressed as

$$\kappa = \frac{1}{T^2 (\hat{L}^{-1})^{EE}} = \frac{\Omega}{2k_\mathrm{B} T^2} S'_0, \tag{3.52}$$

$$S'(\omega) = 1/(\hat{S}^{-1})^{EE}\,. \tag{3.53}$$

The function $S'(\omega)$ takes the name of *multi-component power spectrum*. An equilibrium MD simulation allows to sample M stationary stochastic processes, one for each conserved flux. It is useful to think of each flux as a component of a multivariate stochastic process. As in (3.29), let us assume there are ℓ independent samples of this multivariate random process, and let us denote its realization as

$$\{{}^pJ : n^i\},\ p = 1, \dots, \ell;\ i = 1, \dots, M;\ n = 0, \dots, N-1, \tag{3.54}$$

where the independent samples can be e.g. the cartesian components of the fluxes in an isotropic medium or different segments of a long trajectory. The asymptotically unbiased estimator of the cross-spectrum in this case is the *cross-periodogram*:

$${}^{\ell M}\hat{S}_k^{ij} \overset{\text{def}}{=} \frac{\varepsilon}{\ell N} \sum_{p=1}^{\ell} \left({}^p\tilde{J}_k^i\right)^* {}^p\tilde{J}_k^j, \tag{3.55}$$

$$\left\langle {}^{\ell M}\hat{S}_k^{ij} \right\rangle = S^{ij}(\omega_k). \tag{3.56}$$

In the large N limit the real and the imaginary part of ${}^{p}\widetilde{J}^{i}_{k}$ are normal random variable uncorrelated for different k. Arranging the (i,j) components of the cross-periodogram in a square $M \times M$ matrix gives a realization of the random process associated to the covariance matrix of a complex zero mean normal deviate: the random distribution of such a process is called Complex Wishart distribution:

$$ {}^{\ell M}\hat{S}_k \sim \mathcal{CW}_M\left(S(\omega_k), \ell\right). \tag{3.57}$$

The parameter ℓ is the number of degrees of freedom, i.e. the number of independent samples of the normal processes. M is the rank of the matrix, while S is its expectation value. A matrix drawn from a Complex Wishart distribution admits a Bartlett decomposition of the form:

$$ {}^{\ell M}\hat{S}_k = \frac{1}{\ell}\mathcal{C}(\omega_k)\mathcal{R}\mathcal{R}^{\top}\mathcal{C}^{\dagger}(\omega_k), \tag{3.58}$$

where $\mathcal{C}(\omega_k)$ is the complex upper-triangular matrix known as the Cholesky factor of $S(\omega_k)$, with the property

$$ S(\omega_k) = \mathcal{C}(\omega_k)\mathcal{C}^{\dagger}(\omega_k) \tag{3.59}$$

and $\mathcal{R}$ is a lower-triangular random matrix of the form

$$ \mathcal{R} = \begin{pmatrix} c_1 & 0 & 0 & \cdots & 0 \\ n_{21} & c_2 & 0 & \cdots & 0 \\ n_{31} & n_{32} & c_3 & \cdots & 0 \\ \vdots & \vdots & \vdots & \ddots & \vdots \\ n_{M1} & n_{M2} & n_{M3} & \cdots & c_M \end{pmatrix}, \tag{3.60}$$

where $c_i^2 \sim \chi^2_{2(\ell-i+1)}$ and $n_{ij} \sim \mathcal{N}(0,1)$. The matrix $\mathcal{R}$ is independent of $S(\omega_k)$, as it depends only on ℓ and M. Hence, it is independent of the ordering of the fluxes J^i.

We are interested in the EE, i.e. $(1,1)$, matrix element of the inverse cross-periodogram, since it is related to the thermal conductivity. It can be expressed ad the ratio between the $(1,1)$-minor of ${}^{\ell M}\hat{S}_k$ and the full determinant of the same matrix, i.e.:

$$ \left({}^{\ell M}\hat{S}_k^{-1}\right)^{EE} = \frac{\det\left(\left[{}^{\ell M}\hat{S}_k\right]_{11}\right)}{\det\left({}^{\ell M}\hat{S}_k^{-1}\right)}, \tag{3.61}$$

where $\left[{}^{\ell M}\hat{S}_k\right]_{11}$ has been used as a short-hand notation for the $(1,1)$-minor of ${}^{\ell M}\hat{S}_k$. The determinant of the cross periodogram can be calculated thanks to the properties of its Bartlett decomposition:

$$ \begin{aligned} \det\left({}^{\ell M}\hat{S}_k^{-1}\right) &= \det\left(\frac{1}{\ell}\mathcal{C}(\omega_k)\mathcal{R}\mathcal{R}^{\top}\mathcal{C}^{\dagger}(\omega_k)\right) \\ &= \frac{1}{\ell^M}\det\left(\mathcal{R}\right)\det\left(\mathcal{R}^{\top}\right)\det\left(\mathcal{C}(\omega_k)\mathcal{C}^{\dagger}(\omega_k)\right) \\ &= \frac{1}{\ell^M}\det\left(\mathcal{R}\right)\det\left(\mathcal{R}^{\top}\right)\det\left(S(\omega_k)\right), \end{aligned} \tag{3.62}$$

where equation (3.59) has been used.

The determinant of a triangular matrix is the product of its diagonal elements, thus:

$$\det\left({}^{\ell M}\hat{S}_k^{-1}\right) = \frac{1}{\ell^M}\det\left(S(\omega_k)\right) c_1^2 c_2^2 \cdots c_M^2. \tag{3.63}$$

An analogous computation yields the value of the minor determinant:

$$\det\left(\left[{}^{\ell M}\hat{S}_k\right]_{11}\right) = \frac{1}{\ell^{M-1}}\det\left(\left[S(\omega_k)\right]_{11}\right) c_1^2 \cdots c_{M-1}^2. \tag{3.64}$$

The ratio turns out to be:

$$\begin{aligned}\left({}^{\ell M}\hat{S}_k^{-1}\right)^{EE} &= \ell\frac{\det\left(\left[S(\omega_k)\right]_{11}\right)}{\det\left(S(\omega_k)\right)}\frac{1}{c_1^2} \\ &= \frac{\ell}{c_M^2}\left(S^{-1}(\omega_k)\right)^{EE}\end{aligned} \tag{3.65}$$

so, rearranging the terms one gets:

$$\frac{1}{\left({}^{\ell M}\hat{S}^{-1}\right)^{EE}} = \frac{c_M^2}{\ell\left(S^{-1}(\omega_k)\right)^{EE}}. \tag{3.66}$$

Taking the expectation value of both sides yields:

$$\begin{aligned}\mathbb{E}\left[\frac{1}{\left({}^{\ell M}\hat{S}^{-1}\right)^{EE}}\right] &= \frac{\mathbb{E}\left[c_M^2\right]}{\ell\left(S^{-1}(\omega_k)\right)^{EE}} \\ &= \frac{2(\ell - M + 1)}{\ell\left(S^{-1}(\omega_k)\right)^{EE}} \\ &= \frac{2(\ell - M + 1)}{\ell} S'(\omega_k).\end{aligned} \tag{3.67}$$

This means that an unbiased estimator of the multi-component power spectrum is:

$$\begin{aligned}{}^{\ell M}\hat{S}'_k &= \frac{\ell}{2(\ell - M + 1)}\frac{1}{\left({}^{\ell M}\hat{S}_k^{-1}\right)^{EE}} \\ &\stackrel{\text{def}}{=} S'(\omega_k)\,{}^{\ell M}\hat{\xi}_k,\end{aligned} \tag{3.68}$$

where ${}^{\ell M}\hat{\xi}_k$ are random variables independent for each k and distributed as

$${}^{\ell M}\hat{\xi}_k \sim \frac{1}{2(\ell - M + 1)}\chi^2_{2(\ell - M + 1)}. \tag{3.69}$$

This is the direct generalization of equation (3.29). It can be easily verified that the case $M = 1$ reduces consistently to the one-component procedure outlined in section 3.3.

The definition (3.38) of the cepstrum follows straightforwardly from the one-component case:

$${}^{\ell M}\hat{C}_n \stackrel{\text{def}}{=} \frac{1}{N}\sum_{k=0}^{N-1}\log\left({}^{\ell M}\hat{S}'_k\right) \mathrm{e}^{-2\pi i \frac{kn}{N}}, \tag{3.70}$$

and the subsequent analysis yields

$$\log\left(S_0'\right) = -\overline{\Lambda} + \sum_{n=-P^*+1}^{P^*-1} {}^{\ell M}\hat{C}_n \pm \overline{\sigma}^*, \tag{3.71}$$

$$\overline{\sigma}^*(P^*, N)^2 = \overline{\sigma}^2 \frac{4P^*-2}{N}, \tag{3.72}$$

where $\overline{\Lambda} = \psi(\ell - M + 1) - \log(\ell - M + 1)$ and $\overline{\sigma}^2 = \psi'(\ell - M + 1)$. The estimate of the thermal conductivity becomes, using equations (3.52) and (3.71):

$$\kappa = \frac{\Omega}{2k_\mathrm{B}T^2} \exp\left[\sum_{n=-P^*+1}^{P^*-1} {}^{\ell M}\hat{C}_n - \psi(\ell - M + 1) - \log(\ell - M + 1)\right], \tag{3.73}$$

while its statistical error:

$$\varepsilon_\kappa = \kappa \sqrt{\psi'(\ell - M + 1)\frac{4P^*-2}{N}}. \tag{3.74}$$

Both the one-component and the multi-component cepstral analysis techniques are implemented in the `thermocepstrum` open-source code [Ercole and Bertossa, 2018].

4 IMPLEMENTATION OF THE HEAT FLUX CALCULATION

The implementation of the heat flux formula (1.43) in the MD package `DL_POLY` requires to choose a way to distribute the total potential energy into atomic contributions and to calculate the derivatives of the atomic energies with respect to the coordinates of the other atoms. Once the atomic energies and the respective derivatives are computed, the heat flux can be calculated and written in a file at each simulation step. The many contributions to the total energy of the MB-pol force-field request particular care in doing this operation: in the next sections each term that will enter the heat flux formula will be analyzed and explained.

4.1 ENERGY DISTRIBUTION

The convective contribution to the heat flux is

$$\mathbf{J}_{\text{conv}} = \frac{1}{\Omega} \sum_i \epsilon_i \mathbf{V}_i, \tag{4.1}$$

i.e. the first sum in equation (1.43). Each paragraph in this section will contribute a term in equation (4.1). This section addresses the potential energy distribution among atoms: for each type of interaction, a contribution to ϵ_i (and, consequently, to eq. (4.1)) will be defined.

4.1.1 Water monomer energy

In this section we will review how the Partridge-Schwenke monomer energy model [Partridge and Schwenke, 1997] is implemented in `DL_POLY`, and how each contribution to the monomer energy enters the heat flux formula.

Bond term

The subroutine `bndfrc` calculates the bond contribution to the monomer energy, i.e. the pairwise interaction between atoms within a given water molecule. Such contribution is the Morse-like term given in (2.4). The interaction is pairwise, so the natural choice is to distribute equally the bond energy between the two atoms involved. If $\Phi^{\text{bond}}_{i_a j_a}$ is the potential energy of the bond between two atoms i_a and j_a within the same molecule a, the energy associated to each atom is $\frac{1}{2}\Phi^{\text{bond}}_{i_a j_a}$ and the contribution to the convective heat flux is

$$\mathbf{J}^{\text{bond}}_{\text{conv}} = \frac{1}{\Omega} \sum_{a=1}^{N_{\text{mol}}} \sum_{i_a=1}^{3} \sum_{j_a(\neq i_a)} \tfrac{1}{2}\Phi^{\text{bond}}_{i_a j_a} \mathbf{V}_{i_a}. \tag{4.2}$$

Angular term

The subroutine `angfrc` calculates the angular constraints acting on the atoms within a given water molecule so that it tends to keep the HOH angle at a fixed value. The analytic form of such contribution is given in eq. (2.5). This contribution involves three atoms at the same time, so it is not a pair potential, but a three-body term. The angular energy Φ_a^{ang} of the three atoms in the a-th water molecule is distributed equally among them:

$$\Phi_{i_a}^{\text{ang}} = \tfrac{1}{3}\Phi_a^{\text{ang}}, \tag{4.3}$$

where $i_a = 1, 2, 3$ is the atomic label that runs among the three atoms in the a-th molecule. The contribution to the convective heat flux is:

$$\mathbf{J}_{\text{conv}}^{\text{ang}} = \frac{1}{\Omega} \sum_{a=1}^{N_{\text{mol}}} \sum_{i_a=1}^{3} \tfrac{1}{3}\Phi_a^{\text{ang}} \mathbf{V}_{i_l}, \tag{4.4}$$

where N_{mol} is the number of water molecules.

4.1.2 Water dimer energy

The computation of the dimer terms, whose mathematical form is given in section 2.3 at page 17, is handled by the module `mbpol` and the subroutine `srfrce2`.

Short range term

The short range part of the interaction is computed by the subroutine `do_dimer`. Although being presented as a two-body term, it is actually a six-body potential, because each of the three atoms in each molecule interacts with the other five. The total energy $\Phi_{ab}^{(2B)}$ of the dimer made of molecules a and b is distributed equally among the six atoms:

$$\Phi_{i_a j_b}^{(2B)} = \tfrac{1}{6}\Phi_{ab}^{(2B)}, \tag{4.5}$$

so that the contribution to the convective heat flux is:

$$\mathbf{J}_{\text{conv}}^{(2B)} = \frac{1}{\Omega} \sum_{a<b}^{N_{\text{mol}}} \left[\sum_{i_a=1}^{3} \tfrac{1}{6}\Phi_{ab}^{(2B)} \mathbf{V}_{i_a} + \sum_{j_b=1}^{3} \tfrac{1}{6}\Phi_{ab}^{(2B)} \mathbf{V}_{j_b} \right] \tag{4.6}$$

Dispersion term

The Van der Waals-like dispersion energy is computed in the subroutine `srfrce2`. Its expression is given in equation (2.14). The dispersion energy is represented by a pair potential, so this contribution to the dimer energy, say $\Phi_{i_a j_b}^{\text{VdW}}$, is distributed equally between the two atoms i_a in molecule a and j_b in molecule b. The term to be added to the convective heat flux is

$$\mathbf{J}_{\text{conv}}^{\text{VdW}} = \frac{1}{\Omega} \sum_{a<b}^{N_{\text{mol}}} \sum_{i_a=1}^{3} \sum_{j_b=1}^{3} \left[\tfrac{1}{2}\Phi_{i_a j_b}^{\text{VdW}} \mathbf{V}_{i_a} + \tfrac{1}{2}\Phi_{i_a j_b}^{\text{VdW}} \mathbf{V}_{j_b} \right]. \tag{4.7}$$

4.1.3 Water trimer energy

The trimer term, i.e. the contribution to the total energy which involves explicitly triplets of water molecules, is computed in the subroutine `do_trimer` in the module `mbpol`. Its mathematical form is given by eq. (2.21).

Analogously to the dimer short-range term, the trimer energy is actually a nine-body term, being nine (three per molecule) the total number of atoms involved in the interaction. Since none of the three molecules is privileged in any way, the total energy should be distributed equally among the three molecules. Then, one third of the energy of a single molecules has been assigned to each atom in it. So the total energy $\Phi^{(3B)}_{abc}$ of the trimer made of molecules a, b, and c is equally distributed among the nine interacting atoms. The contribution to the convective heat flux is:

$$\mathbf{J}^{(3B)}_{\text{conv}} = \frac{1}{\Omega} \sum_{a<b<c}^{N_{\text{mol}}} \left[\sum_{i_a=1}^{3} \tfrac{1}{9} \Phi^{(3B)}_{abc} \mathbf{V}_{i_a} + \sum_{j_b=1}^{3} \tfrac{1}{9} \Phi^{(3B)}_{abc} \mathbf{V}_{j_b} + \sum_{k_c=1}^{3} \tfrac{1}{9} \Phi^{(3B)}_{abc} \mathbf{V}_{k_c} \right] . \quad (4.8)$$

4.1.4 Electrostatic energy

As shown in equation (A.15) in appendix A, only an effective charge-charge electrostatic contribution and the polarization energy survives[1]:

$$U_{\text{elec,tot}} = \tfrac{1}{2} \sum_{i,j} \frac{q_i q_j}{R_{ij}} + \sum_{i} \frac{\boldsymbol{\mu}_i \cdot \boldsymbol{\mu}_i}{2\alpha_i} . \quad (4.9)$$

The long range nature of the charge-charge interaction requires the Ewald summation approach [de Leeuw et al., 1980] to reduce the computational cost when there are periodic boundary conditions. A neutralizing Gaussian charge distribution is added to the original set of point charges, so that the range of the interaction becomes shorter and converges quicker; another Gaussian charge distribution of opposite sign is also added, to compensate for the additional charge previously put in the system. The computation of the energy is then split into three terms:

- A direct-space part, i.e. the rapidly converging computation of the interaction energy among the point-charges plus the neutralizing density contribution;
- A reciprocal-space part, i.e. the computation of the interaction between the point charges and the compensating charge distributions. Also this term converges rapidly if calculated in Fourier domain, hence the name of "reciprocal" term;
- A self-interaction correction part, which corrects for the self-interaction contribution included in the previous term.

---

[1] The Thole-smearing functions are not shown here for ease of notation. The calculation of the energy terms in the presence of those functions proceeds in the same way and the result is in eq. (A.22).

Direct space term

The direct-space term is calculated in the subroutine `ewald2p`. It is due to the interaction of the neutralized charges. The Gaussian charge distribution at site i has the form:

$$\rho_i(\mathbf{x}) = \frac{\eta^3}{\pi^{3/2}} q_i \mathrm{e}^{-\eta^2|\mathbf{x}-\mathbf{R}_i|^2}, \tag{4.10}$$

where η is a parameter that controls the width of the Gaussian. The interaction energy between the charges and the charge densities above becomes:

$$\begin{aligned} U^{(\mathrm{CC})}_{\mathrm{dir}} &= \tfrac{1}{2} \sum_{\mathbf{m}\in\mathbb{Z}^3}{}' \sum_{i,j} q_i q_j \frac{\operatorname{erfc}(\eta\,|\mathbf{R}_{ij}+\mathbf{m}L|)}{|\mathbf{R}_{ij}+\mathbf{m}L|} \\ &\overset{\mathrm{def}}{=} \sum_i U^{(\mathrm{CC})}_{\mathrm{dir,i}}, \end{aligned} \tag{4.11}$$

where $\operatorname{erfc}(x) = 1 - \operatorname{erf}(x)$ is the complementary error function, and the primed summation means that, when $\mathbf{m}{=}\mathbf{0}$, the $i{=}j$ self-interaction should be excluded. L is the linear dimension of the simulation box. Equation (4.11) yields a natural way to distribute the energy among the atoms, with $U^{(\mathrm{CC})}_{\mathrm{dir,i}}$ the energy associated to atom i. The convective heat flux associated to this type of interaction is

$$\mathbf{J}^{(\mathrm{CC})\mathrm{dir}}_{\mathrm{conv}} = \frac{1}{\Omega} \sum_{i=1}^{N} U^{(\mathrm{CC})}_{\mathrm{dir,i}} \mathbf{V}_i. \tag{4.12}$$

Reciprocal space term

The reciprocal space term is calculated in the subroutine `ewald1p`. It is the contribution due to the interaction of charges q_i in the i-th site with the all the periodic images of the Ewald charge densities in the other sites, plus their own images in all the periodic cells except for the central one, where the charge is placed. The charge q_i interacts with the electrostatic potential due to all the sources listed above. The Ewald approach consists in Fourier-transforming the total charge density of the sources, calculating the electrostatic potential in reciprocal space and then Fourier-transforming back to real space to compute the electrostatic interaction energy between the charge and the potential.

The total charge density of the sources is:

$$\rho(\mathbf{x}) = \sum_j \sum_{\mathbf{m}\in\mathbb{Z}^3} \frac{\eta^3}{\pi^{3/2}} q_j \mathrm{e}^{-\eta^2|\mathbf{x}-\mathbf{R}_j+\mathbf{m}L|^2}, \tag{4.13}$$

where $\mathbf{m}$ points at the center of one of the periodic cells and L is the length of a side of the cell. Its Fourier-transform is:

$$\begin{aligned} \widetilde{\rho}(\mathbf{k}) =& \frac{1}{\Omega} \int_\Omega \mathrm{d}^3x \rho(\mathbf{x}) \mathrm{e}^{-i\mathbf{k}\cdot\mathbf{x}} \\ =& \frac{1}{\Omega} \int_\Omega \mathrm{d}^3x \sum_j \sum_{\mathbf{m}\in\mathbb{Z}^3} \frac{\eta^3}{\pi^{3/2}} q_j \mathrm{e}^{-\eta^2|\mathbf{x}-\mathbf{R}_j+\mathbf{m}L|^2} \mathrm{e}^{-i\mathbf{k}\cdot\mathbf{x}} \\ =& \sum_j \frac{q_j}{\Omega} \int_{\mathbb{R}^3} \mathrm{d}^3x \mathrm{e}^{-i\mathbf{k}\cdot\mathbf{x}} \frac{\eta^3}{\pi^{3/2}} \mathrm{e}^{-\eta^2|\mathbf{x}-\mathbf{R}_j|^2}, \end{aligned} \tag{4.14}$$

where additivity of the integral has been exploited, and Ω is the volume of the simulation cell. By a change of variable $\mathbf{x} \mapsto \mathbf{x} + \mathbf{R}_j$ one obtains:

$$\begin{aligned}\widetilde{\rho}(\mathbf{k}) =& \sum_j \frac{q_j}{\Omega} \int_{\mathbb{R}^3} \mathrm{d}^3x \mathrm{e}^{-\eta^2 x^2 - i\mathbf{k}\cdot\mathbf{x}} \frac{\eta^3}{\pi^{3/2}} \\ =& \sum_j \frac{q_j}{\Omega} \mathrm{e}^{-k^2/4\eta^2} \\ =& \frac{1}{\Omega} \mathrm{e}^{-k^2/4\eta^2} S(\mathbf{k}),\end{aligned} \tag{4.15}$$

where the structure factor $S(\mathbf{k})$ has been defined.

Poisson's equation in reciprocal space reads:

$$k^2 \widetilde{\phi}_c(\mathbf{k}) = 4\pi \widetilde{\rho}(\mathbf{k}), \tag{4.16}$$

so that

$$\begin{aligned}\widetilde{\phi}_c(\mathbf{k}) =& \frac{4\pi}{k^2} \widetilde{\rho}(\mathbf{k}) \\ =& \frac{4\pi}{k^2} \sum_j \frac{q_j}{\Omega} \mathrm{e}^{-k^2/4\eta^2}.\end{aligned} \tag{4.17}$$

Let us anti-Fourier-transform eq. (4.17) to get the direct-space electrostatic potential due to the reciprocal term in Ewald's summation:

$$\begin{aligned}\phi_c(\mathbf{x}) =& \sum_{\mathbf{k}\neq\mathbf{0}} \widetilde{\phi}_c(\mathbf{k}) \mathrm{e}^{i\mathbf{k}\cdot\mathbf{x}} \\ =& \sum_{\mathbf{k}\neq\mathbf{0}} \frac{4\pi}{\Omega} \frac{\mathrm{e}^{-k^2/4\eta^2}}{k^2} \sum_j q_j \mathrm{e}^{i\mathbf{k}\cdot(\mathbf{x}-\mathbf{R}_j)}.\end{aligned} \tag{4.18}$$

The total interaction energy between the charges and the potential is:

$$\begin{aligned}U_{\text{rec}}^{(\text{CC})} =& \frac{1}{2} \sum_i q_i \phi_c(\mathbf{R}_i), \\ =& \frac{1}{2} \sum_{i,j} q_i q_j \frac{4\pi}{\Omega} \sum_{\mathbf{k}\neq\mathbf{0}} \frac{\mathrm{e}^{-k^2/4\eta^2}}{k^2} \mathrm{e}^{i\mathbf{k}\cdot\mathbf{R}_{ij}}.\end{aligned} \tag{4.19}$$

Such expression is apparently complex (i.e. it belongs to $\mathbb{C}$) but, since $\mathrm{e}^{it} = \cos(t) + i\sin(t)$ and since the sum over $\mathbf{k}$ is spherical[2], only the even term survives:

$$\begin{aligned}U_{\text{rec}}^{(\text{CC})} =& \sum_{i,j} q_i q_j \frac{2\pi}{\Omega} \sum_{\mathbf{k}\neq\mathbf{0}} \frac{\mathrm{e}^{-k^2/4\eta^2}}{k^2} \cos(\mathbf{k}\cdot\mathbf{R}_{ij}) \\ =& \sum_i \frac{2\pi}{\Omega} \sum_{\mathbf{k}\neq\mathbf{0}} \sum_j q_i q_j \frac{\mathrm{e}^{-k^2/4\eta^2}}{k^2} \cos(\mathbf{k}\cdot\mathbf{R}_{ij}).\end{aligned} \tag{4.20}$$

A natural way to define the atomic energy is, then:

$$U_{\text{rec,i}}^{(\text{CC})} = q_i \phi_c(\mathbf{R}_i) = \frac{2\pi}{\Omega} \sum_{\mathbf{k}\neq\mathbf{0}} \frac{\mathrm{e}^{-k^2/4\eta^2}}{k^2} q_i \sum_j q_j \cos(\mathbf{k}\cdot\mathbf{R}_{ij}), \tag{4.21}$$

---

[2] "Spherical" here means that for every $\mathbf{k}$ in the sum, there is also its opposite $-\mathbf{k}$.

which is the contribution given by each atom to the interaction energy appearing in the sum in equation (4.19). The contribution to the convective heat flux of the reciprocal Ewald summation is

$$\mathbf{J}_{\text{conv}}^{\text{(CC)rec}} = \frac{1}{\Omega}\sum_{i=1}^{N} U_{\text{rec,i}}^{\text{(CC)}}\mathbf{V}_i. \tag{4.22}$$

Self-interaction term

A self-interaction term must be included to correct for the spurious contribution to the reciprocal space energy. It is calculated in the subroutine `ewald3p`. Its expression can be obtained from Poisson's equation for eq. (4.18) in spherical coordinates[3]:

$$\begin{aligned} -\frac{1}{r}\frac{\partial^2 r\phi_c(r)}{\partial r^2} =& 4\pi\rho(r) \\ =& 4\pi\frac{\eta^3}{\pi^{3/2}}q_i \mathrm{e}^{-\eta^2 r^2}. \end{aligned} \tag{4.23}$$

Integration with respect to r on both sides yields:

$$\begin{aligned} -\frac{\partial r\phi_c(r)}{\partial r} =& 4\pi\int_{\infty}^{r} \mathrm{d}r\, r\rho(r') \\ =& 4\pi\int_{\infty}^{r} \mathrm{d}r\, r\frac{\eta^3}{\pi^{3/2}}q_i \mathrm{e}^{-\eta^2 r^2} \\ =& -\frac{2q_i\eta \mathrm{e}^{-\eta^2 r^2}}{\sqrt{\pi}}. \end{aligned} \tag{4.24}$$

A second partial integration gives the result for $\phi_c(r)$:

$$\phi_c(r) = \frac{2q_i\eta\,\mathrm{erf}(\eta r)}{\sqrt{\pi}}. \tag{4.25}$$

The self-interaction term is the interaction between the point charges and this electrostatic potential at $r = 0$, with the minus sign since it is a correction:

$$U_{\text{self}} = \sum_i q_i\phi_c(0) \tag{4.26}$$

$$= -\frac{\eta}{\sqrt{\pi}}\sum_i q_i^2. \tag{4.27}$$

It is already expressed as a sum over particles, so the atomic contribution is simply:

$$U_{\text{self},i} = -\frac{\eta}{\sqrt{\pi}}q_i^2. \tag{4.28}$$

The convective heat flux associated to the self-interaction correction is

$$\mathbf{J}_{\text{conv}}^{\text{self}} = \frac{1}{\Omega}\sum_{i=1}^{N} U_{\text{self},i}\mathbf{V}_i. \tag{4.29}$$

---

[3] The Gaussian charge density in the right-hand side of the Poisson's equation is spherical, and so must be the electrostatic potential in the left-hand side.

Polarization energy

The polarization energy is the energy required to induce the dipoles. Its expression is:

$$U_{\text{pol}} = \sum_i \frac{\boldsymbol{\mu}_i \cdot \boldsymbol{\mu}_i}{2\alpha_i}, \tag{4.30}$$

where α_i is the polarizability of the i-th site. An immediate way to distribute the energy over the atoms is to define:

$$U_{\text{pol},i} = \frac{\boldsymbol{\mu}_i \cdot \boldsymbol{\mu}_i}{2\alpha_i}. \tag{4.31}$$

The contribution to the convective heat flux is

$$\mathbf{J}^{\text{pol}}_{\text{conv}} = \frac{1}{\Omega} \sum_{i=1}^{N} U_{\text{pol},i} \mathbf{V}_i. \tag{4.32}$$

4.2 FORCE DISTRIBUTION

The virial part of the heat flux is

$$\mathbf{J}_{\text{vir}} = -\frac{1}{\Omega} \sum_{i,j} \frac{\partial \Phi_j}{\partial \mathbf{R}_i} \cdot \mathbf{V}_i \left(\mathbf{R}_i - \mathbf{R}_j \right) \tag{4.33}$$

It requires a decomposition of the total force on an atom and, in particular, the calculation of expressions like

$$\sum_j - \left(\frac{\partial \Phi_j}{\partial \mathbf{R}_i} \cdot \mathbf{V}_i \right) (\mathbf{R}_i - \mathbf{R}_j), \ \forall i. \tag{4.34}$$

In the special case of a pair potential, the total force on an atom can be decomposed into pair forces that satisfy Newton's *action-reaction* law:

$$\Phi^{\text{tot}}_{\text{pair}} = \sum_i \sum_{j(\neq i)} \tfrac{1}{2} \phi_{ij}(R_{ij}), \tag{4.35}$$

$$\mathbf{F}_i = \sum_{j(\neq i)} \mathbf{F}_{ij}, \tag{4.36}$$

$$\mathbf{F}_{ij} = -\frac{\partial \Phi_{ij}}{\partial \mathbf{R}_{ij}} = -\mathbf{F}_{ji}. \tag{4.37}$$

The gradient of the j-th atomic energy with respect to the i-th atomic coordinate is

$$\frac{\partial \Phi_j}{\partial \mathbf{R}_i} = \tfrac{1}{2} \frac{\partial \phi_{ij}}{\partial \mathbf{R}_{ij}} - \tfrac{1}{2} \sum_{k(\neq j)} \delta_{ij} \frac{\partial \phi_{kj}}{\partial \mathbf{R}_{kj}}. \tag{4.38}$$

The second term in the right-hand side in the above equation does not contribute, once inserted in eq. (4.33): when $i{=}j$, $\mathbf{R}_i - \mathbf{R}_j{=}0$. $\mathbf{J}_{\mathrm{vir}}$ for a pair potential becomes

$$\begin{aligned}
\mathbf{J}_{\mathrm{vir}}^{\mathrm{pair}} &= -\frac{1}{\Omega}\sum_{i,j}\left[\frac{1}{2}\frac{\partial\phi_{ij}}{\partial\mathbf{R}_{ij}}\cdot\mathbf{V}_i\right](\mathbf{R}_i-\mathbf{R}_j)\\
&= \frac{1}{\Omega}\sum_{i,j}\left[\tfrac{1}{2}\mathbf{F}_{ij}\cdot\mathbf{V}_i\right](\mathbf{R}_i-\mathbf{R}_j)\\
&= -\frac{1}{\Omega}\sum_{i}\left[-\sum_{j}\tfrac{1}{2}(\mathbf{R}_i-\mathbf{R}_j)\otimes\mathbf{F}_{ij}\right]\cdot\mathbf{V}_i\\
&= -\sum_{i}\overset{\leftrightarrow}{\mathbf{W}}_i\cdot\mathbf{V}_i
\end{aligned} \tag{4.39}$$

where $\overset{\leftrightarrow}{\mathbf{W}}_i$ is the contribution to the potential *virial stress* due to the i-th atom. Let us define a slightly modified version of the atomic virial stress as:

$$\begin{aligned}
\overset{\leftrightarrow}{\mathbf{W}}_i &\overset{\mathrm{def}}{=} \frac{1}{\Omega}\sum_{j}(\mathbf{R}_i-\mathbf{R}_j)\otimes\frac{\partial\Phi_j}{\partial\mathbf{R}_i}\\
&\equiv \sum_{j}\overset{\leftrightarrow}{\boldsymbol{\sigma}}_{ij}
\end{aligned} \tag{4.40}$$

where in this case the potential energy per particle is obtained from a general many body potential, e.g. as those described in section 4.1.

In the following, the the word "stress" will refer to what is defined in equation (4.40) so that, when the interaction is pairwise, the expression reduces to the one in (4.39). It is worth noting that the actual atomic virial stress tensor for a many-body potential is not necessarily the one defined in (4.40); however, the expression required by the heat flux formula (1.43) is the one in equation (4.40).

In the following sections, each contribution to the virial heat flux will be described.

4.3 WATER MONOMER STRESS

Let us analyze how the intra-molecular stress can be distributed to the three atoms in a water molecule.

4.3.1 Bond term

The subroutine `bndfrc` calculates the pairwise bond contribution to the stress. For each pair of interacting atoms i and j, the subroutine computes the force $\mathbf{F}_{ij}$ that one exerts on the other as the gradient of the interaction energy (2.4) between the two atoms with respect to the position of one of the atoms, i.e.:

$$\mathbf{F}_{ij}^{\mathrm{bond}} = -\frac{\partial\Phi_{i_a j_a}^{\mathrm{bond}}(|\mathbf{R}_{i_a}-\mathbf{R}_{j_a}|)}{\partial\mathbf{R}_{i_a j_a}}. \tag{4.41}$$

The stress contribution is:

$$\overset{\leftrightarrow}{\boldsymbol{\sigma}}^{\text{bond}}_{i_a j_a} = -\frac{1}{\Omega}\mathbf{R}_{i_a j_a} \otimes \tfrac{1}{2}\mathbf{F}^{\text{bond}}_{i_a j_a}, \tag{4.42}$$

The contribution to the virial heat flux is

$$\mathbf{J}^{\text{bond}}_{\text{vir}} = -\sum_{a=1}^{N_{\text{mol}}} \sum_{i_a=1}^{3} \left[\sum_{j_a(\neq i_a)}^{3} \overset{\leftrightarrow}{\boldsymbol{\sigma}}^{\text{bond}}_{i_a j_a} \right] \cdot \mathbf{V}_{i_a} \tag{4.43}$$

4.3.2 Angular term

The subroutine `angfrc` calculates the contribution to the total stress due to the angular restraints which shape the water molecules. This interaction involves the three atoms in a water molecules and its functional form depends explicitly on the hydrogen-oxygen distances and on the angle HOH:

- The force $\mathbf{F}_{\text{H1}}$ exerted by the oxygen on the first hydrogen atom is calculated;
- The force $\mathbf{F}_{\text{H2}}$ on the second hydrogen atom is calculated;
- The force on the oxygen atom is calculated via the conservation of linear momentum[4] as

$$\mathbf{F}_{\text{O}} = -\mathbf{F}_{\text{H1}} - \mathbf{F}_{\text{H2}}.$$

Here the interaction is not pairwise: the choice of the energy decomposition induces the criterion for the force decomposition. Having distributed equally the angular energy among the three atoms in the molecule yields, for the atomic angular virial stress

$$\begin{aligned} \overset{\leftrightarrow}{\boldsymbol{\sigma}}^{\text{ang}}_{i_a j_a} &= \frac{1}{\Omega}(\mathbf{R}_{i_a} - \mathbf{R}_{j_a}) \otimes \frac{\partial \Phi^{\text{ang}}_{j_a}}{\partial \mathbf{R}_{i_a}} \\ &= \frac{1}{\Omega}(\mathbf{R}_{i_a} - \mathbf{R}_{j_a}) \otimes \tfrac{1}{3}\frac{\partial \Phi^{\text{ang}}_{a}}{\partial \mathbf{R}_{i_a}}. \end{aligned} \tag{4.44}$$

The virial heat flux associated to the angular interaction is

$$\mathbf{J}^{\text{ang}}_{\text{vir}} = -\sum_{a=1}^{N_{\text{mol}}} \sum_{i_a=1}^{3} \left[\sum_{j_a(\neq i_a)}^{3} \overset{\leftrightarrow}{\boldsymbol{\sigma}}^{\text{ang}}_{i_a j_a} \right] \cdot \mathbf{V}_{i_a}. \tag{4.45}$$

4.4 WATER DIMER STRESS

In this section the contribution to the stress due to the two-molecule interactions will be treated.

---

[4] I.e., using the fact that the sum of the internal forces must be zero, being the time-derivative of the total momentum.

4.4.1 Short range

The short-range interaction between two water molecules due to the overlap of electronic orbitals is calculated by the subroutines contained in the module `mbpol`. The program calculates the force exerted by a molecule to the other via the gradient of the analytic potential (2.16). This term is a many-body contribution, since the interaction energy is a function of all the positions of the six atoms in the molecules. The energy has been distributed equally among the six atoms, so the expression of the inter-atomic stress contribution between atom i_a in molecule a and atom j_b in molecule b is

$$\overleftrightarrow{\boldsymbol{\sigma}}^{(2B)}_{i_a j_b} = \frac{1}{\Omega}(\mathbf{R}_i - \mathbf{R}_j) \otimes \tfrac{1}{6}\frac{\partial \Phi^{(2B)}_{ab}}{\partial \mathbf{R}_{i_a}}, \tag{4.46}$$

$$\overleftrightarrow{\mathbf{W}}^{(2B)}_{i_a} = \frac{1}{\Omega}\sum_{b(\neq a)}^{N_{\text{mol}}}\sum_{j_b=1}^{3}(\mathbf{R}_{i_a} - \mathbf{R}_{j_b}) \otimes \tfrac{1}{6}\frac{\partial \Phi^{(2B)}_{ab}}{\partial \mathbf{R}_{i_a}} \tag{4.47}$$

and the expression of the virial heat flux to be added to the total heat flux is

$$\mathbf{J}^{(2B)}_{\text{vir}} = -\sum_{a=1}^{N_{\text{mol}}}\sum_{i_a=1}^{3}\overleftrightarrow{\mathbf{W}}^{(2B)}_{i_a}\cdot\mathbf{V}_{i_a}. \tag{4.48}$$

4.4.2 Dispersion term

The dispersion terms are pairwise interactions calculated in the subroutines `srfrce2` and `lrcorrect`. The forces on the two atoms involved are calculated as the negative gradient of the potential, and the stress contribution is equally distributed among them as in eq. (4.42). The virial heat flux is

$$\mathbf{J}^{\text{VdW}}_{\text{vir}} = -\sum_{i=1}^{N}\overleftrightarrow{\mathbf{W}}^{\text{VdW}}_{i}\cdot\mathbf{V}_{i}. \tag{4.49}$$

4.5 WATER TRIMER STRESS

As for the dimer term, the module `mbpol` addresses the computation of the trimer energy, i.e. the explicit interaction of three water molecules constructed on highly accurate AIMD calculations. The form of the potential is given by eq. (2.21). The forces on the nine atoms constituting the trimer is calculated, and the contribution to the total stress is distributed as

$$\begin{aligned}\overleftrightarrow{\mathbf{W}}^{(3B)}_{i_a} = -\frac{1}{\Omega}\sum_{\substack{c(\neq a)\\ b<c}}^{N_{\text{mol}}}\Bigg[&\sum_{j_b=1}^{3}(\mathbf{R}_{i_a} - \mathbf{R}_{j_b}) \otimes \tfrac{1}{9}\frac{\partial \Phi^{(3B)}_{abc}}{\partial \mathbf{R}_{i_a}} + \\ &+ \sum_{k_c=1}^{3}(\mathbf{R}_{i_a} - \mathbf{R}_{k_c}) \otimes \tfrac{1}{9}\frac{\partial \Phi^{(3B)}_{abc}}{\partial \mathbf{R}_{i_a}}\Bigg],\end{aligned} \tag{4.50}$$

so that the virial heat flux due to the three-body interaction is

$$\mathbf{J}_{\text{vir}}^{(3B)} = -\sum_{a=1}^{N_{\text{mol}}} \sum_{i_a=1}^{3} \overleftrightarrow{\mathbf{W}}_{i_a}^{(3B)} \cdot \mathbf{V}_{i_a}. \tag{4.51}$$

4.6 ELECTROSTATIC STRESS TENSOR

The electrostatic stress tensor is more complicated than the other contributions explained before. Since the computation of the long-range Coulomb interaction is performed via the Ewald summation approach, even the stress tensor calculation divided into three different components: a direct-space term, a reciprocal-space term, and a self-interaction correction term. Since in MB-pol water every atom has a polarizability, in presence of an electric field an induced dipole is established; the total electrostatic energy is then reduced to a charge-charge interaction term plus a polarization term, as explained in eq. (A.17). However, to compute forces the whole expression of the interaction is required, i.e. one has to take into account the dipole-dipole and charge-dipole terms too.

4.6.1 Direct-space term

The derivation of the atomic stress tensor will be divided into the three different contributions:

- The charge-charge (CC) term;
- the charge-dipole (CD) term;
- the dipole-dipole (DD) term.

In the code, the calculation is done by the subroutine `ewald2p`.

CC term

Let us recall formula (4.11):

$$\begin{aligned} U_{\text{dir,i}}^{(\text{CC})} &= \frac{1}{2} \sum_{\mathbf{m}\in\mathbb{Z}^3}{}^{'} \sum_{j} q_i q_j \frac{\operatorname{erfc}(\eta\,|\mathbf{R}_{ij} + \mathbf{h}\,\mathbf{m}|)}{|\mathbf{R}_{ij} + \mathbf{h}\,\mathbf{m}|} \\ &= \frac{1}{2} \sum_{\mathbf{m}\in\mathbb{Z}^3}{}^{'} \sum_{j} q_i q_j \frac{\operatorname{erfc}(\eta R_{\mathbf{m}ij})}{R_{\mathbf{m}ij}}, \end{aligned} \tag{4.52}$$

where

$$\mathbf{h} = \begin{pmatrix} \mathbf{a}, & \mathbf{b}, & \mathbf{c} \end{pmatrix} \tag{4.53}$$

is the matrix of the cell (column) vectors and $\mathbf{R}_{\mathbf{m}ij} = \mathbf{R}_{ij} + \mathbf{h}\,\mathbf{m}$ has been conveniently defined as a shorthand notation. The total force on the i-th particle due to this type of interaction is given by

$$\mathbf{F}_i = -\sum_{\mathbf{n}\in\mathbb{Z}^3}{}^{'} \frac{\partial U_{\text{dir,i}}^{(\text{CC})}}{\partial \mathbf{R}_{\mathbf{n}i}}. \tag{4.54}$$

It is worth calculating the derivative of the complementary error function divided by its argument:

$$\frac{\mathrm{d}(\operatorname{erfc}(x)/x)}{\mathrm{d}x} = -\frac{2\mathrm{e}^{-x^2}}{\sqrt{\pi}x} - \frac{\operatorname{erfc}(x)}{x^2}. \tag{4.55}$$

With this result we obtain, for eq. (4.54):

$$\begin{aligned}\mathbf{F}_i &= -\tfrac{1}{2}\sum_{\mathbf{n}\in\mathbb{Z}^3}{}^{'}\sum_j q_i q_j \left[-\frac{2\mathrm{e}^{-\eta^2 R^2_{\mathbf{n}ij}}\eta R_{\mathbf{n}ij}}{\sqrt{\pi}} - \operatorname{erfc}(\eta R_{\mathbf{n}ij})\right]\frac{\mathbf{R}_{\mathbf{n}ij}}{R^3_{\mathbf{n}ij}} \\ &= \sum_{\mathbf{n}\in\mathbb{Z}^3}{}^{'}\sum_j \tfrac{1}{2} q_i q_j \left[\frac{2\mathrm{e}^{-\eta^2 R^2_{\mathbf{n}ij}}\eta R_{\mathbf{n}ij}}{\sqrt{\pi}} + \operatorname{erfc}(\eta R_{\mathbf{n}ij})\right]\frac{\mathbf{R}_{\mathbf{n}ij}}{R^3_{\mathbf{n}ij}} \\ &\equiv \sum_{\mathbf{n}\in\mathbb{Z}^3}{}^{'}\sum_j \mathbf{F}_{\mathbf{n}ij},\end{aligned} \tag{4.56}$$

where $\mathbf{F}_{\mathbf{n}ij}$ is the force exerted on particle i by the image of particle j in the image cell placed in $\mathbf{h}\,\mathbf{n}$. The stress tensor contribution is, then:

$$\begin{aligned}W^{(\mathrm{CC})}_{\mathrm{dir,i},\alpha\beta} &= -\frac{1}{\Omega}\sum_{\mathbf{n}\in\mathbb{Z}^3}{}^{'}\sum_j R_{\mathbf{n}ij,\alpha}F_{\mathbf{n}ij,\beta} \\ &= -\frac{1}{2\Omega}\sum_{\mathbf{n}\in\mathbb{Z}^3}{}^{'}\sum_j q_i q_j \left[\frac{2\mathrm{e}^{-\eta^2 R^2_{\mathbf{n}ij}}\eta R_{\mathbf{n}ij}}{\sqrt{\pi}} + \right. \\ &\qquad\qquad \left. \operatorname{erfc}(\eta R_{\mathbf{n}ij})\right]\frac{R_{\mathbf{n}ij,\alpha}R_{\mathbf{n}ij,\beta}}{R^3_{\mathbf{n}ij}}.\end{aligned} \tag{4.57}$$

CD term

The charge-dipole interaction energy in the Ewald framework has not been calculated above, since it is not explicitly computed by the program. However, it is easily obtained from (4.52) by mapping one of the two charges in the sum as

$$q_k \mapsto \boldsymbol{\mu}_k \cdot \frac{\partial}{\partial \mathbf{R}_{\mathbf{n}k}}. \tag{4.58}$$

To obtain a nice formula it is expedient to consider half of the interaction energy as due to the interaction of charges with dipoles, and half as due to the interaction of dipoles and charges:

$$\begin{aligned}
U^{(\mathrm{CD})}_{\mathrm{dir,i}} &= \tfrac{1}{4} \sum_{\mathbf{m}\in\mathbb{Z}^3}{}' \sum_j q_i \left(\boldsymbol{\mu}_j \cdot \frac{\partial}{\partial \mathbf{R}_{\mathbf{m}j}}\right) \frac{\operatorname{erfc}(\eta R_{\mathbf{m}ij})}{R_{\mathbf{m}ij}} + \\
&\quad + \tfrac{1}{4} \sum_{\mathbf{m}\in\mathbb{Z}^3}{}' \sum_j q_j \left(\boldsymbol{\mu}_i \cdot \frac{\partial}{\partial \mathbf{R}_{\mathbf{m}i}}\right) \frac{\operatorname{erfc}(\eta R_{\mathbf{m}ij})}{R_{\mathbf{m}ij}} \\
&= -\tfrac{1}{4} \sum_{\mathbf{m}\in\mathbb{Z}^3}{}' \sum_j q_i \left(\boldsymbol{\mu}_j \cdot \mathbf{R}_{\mathbf{m}ij}\right) \left[\frac{2\mathrm{e}^{-\eta^2 R^2_{\mathbf{m}ij}} \eta R_{\mathbf{m}ij}}{\sqrt{\pi}} + \operatorname{erfc}(\eta R_{\mathbf{m}ij})\right] + \\
&\quad + \tfrac{1}{4} \sum_{\mathbf{m}\in\mathbb{Z}^3}{}' \sum_j q_j \left(\boldsymbol{\mu}_i \cdot \mathbf{R}_{\mathbf{m}ij}\right) \left[\frac{2\mathrm{e}^{-\eta^2 R^2_{\mathbf{m}ij}} \eta R_{\mathbf{m}ij}}{\sqrt{\pi}} + \operatorname{erfc}(\eta R_{\mathbf{m}ij})\right] \\
&= -\tfrac{1}{4} \sum_{\mathbf{m}\in\mathbb{Z}^3}{}' \sum_j \left[q_i(\boldsymbol{\mu}_j \cdot \mathbf{R}_{\mathbf{m}ij}) + \right. \\
&\quad \left. - q_j(\boldsymbol{\mu}_i \cdot \mathbf{R}_{\mathbf{m}ij})\right] \left(\frac{2\mathrm{e}^{-\eta^2 R^2_{\mathbf{m}ij}} \eta R_{\mathbf{m}ij}}{\sqrt{\pi}} + \operatorname{erfc}(\eta R_{\mathbf{m}ij})\right).
\end{aligned} \tag{4.59}$$

The force, calculated as in (4.54), is

$$\begin{aligned}
\mathbf{F}_i = \tfrac{1}{4} \sum_{\mathbf{m}\in\mathbb{Z}^3}{}' \sum_j (q_i \boldsymbol{\mu}_j - q_j \boldsymbol{\mu}_i) \left(\frac{2\mathrm{e}^{-\eta^2 R^2_{\mathbf{m}ij}} \eta R_{\mathbf{m}ij}}{\sqrt{\pi}} + \operatorname{erfc}(\eta R_{\mathbf{m}ij})\right) + \\
- \tfrac{1}{4} \sum_{\mathbf{m}\in\mathbb{Z}^3}{}' \sum_j \left[q_i(\boldsymbol{\mu}_i \cdot \mathbf{R}_{\mathbf{m}ij}) - q_j(\boldsymbol{\mu}_i \cdot \mathbf{R}_{\mathbf{m}ij})\right] \times \\
\times \left(\frac{2\eta R_{\mathbf{m}ij} \mathrm{e}^{-\eta^2 R^2_{\mathbf{m}ij}} (1 + \eta^2 R^2_{\mathbf{m}ij})}{\sqrt{\pi}} + \operatorname{erfc}(\eta R_{\mathbf{m}ij})\right) \frac{2\mathbf{R}_{\mathbf{m}ij}}{R^4_{\mathbf{m}ij}},
\end{aligned} \tag{4.60}$$

which is again possible to express as a sum of pairwise terms. The stress contribution will be

$$\begin{aligned}
W^{(\mathrm{CD})}_{\mathrm{dir,i},\alpha\beta} &= -\frac{1}{\Omega} \sum_{\mathbf{n}\in\mathbb{Z}^3}{}' \sum_j R_{\mathbf{n}ij,\alpha} F_{\mathbf{n}ij,\beta} \\
&= -\frac{1}{4\Omega} \sum_{\mathbf{m}\in\mathbb{Z}^3}{}' (q_i \mu_{j\beta} - q_j \mu_{i\beta}) \left(\frac{2\mathrm{e}^{-\eta^2 R^2_{\mathbf{m}ij}} \eta R_{\mathbf{m}ij}}{\sqrt{\pi}} + \right. \\
&\qquad \left. \operatorname{erfc}(\eta R_{\mathbf{m}ij})\right) R_{\mathbf{m}ij\alpha} + \\
&\quad - \tfrac{1}{4} \sum_{\mathbf{m}\in\mathbb{Z}^3}{}' \sum_j \left[q_i(\boldsymbol{\mu}_i \cdot \mathbf{R}_{\mathbf{m}ij}) - q_j(\boldsymbol{\mu}_i \cdot \mathbf{R}_{\mathbf{m}ij})\right] \times \\
&\quad \times \left(\frac{2\eta R_{\mathbf{m}ij} \mathrm{e}^{-\eta^2 R^2_{\mathbf{m}ij}} (1 + \eta^2 R^2_{\mathbf{m}ij})}{\sqrt{\pi}} + \right. \\
&\qquad \left. + \operatorname{erfc}(\eta R_{\mathbf{m}ij})\right) \frac{2 R_{\mathbf{m}ij\alpha} R_{\mathbf{m}ij\beta}}{R^4_{\mathbf{m}ij}}.
\end{aligned} \tag{4.61}$$

DD term

The dipole-dipole interaction energy is obtained from (4.52) by mapping both charges as in (4.58):

$$U^{(\mathrm{DD})}_{\mathrm{dir,i}} = \tfrac{1}{2} \sum_{\mathbf{m}\in\mathbb{Z}^3}{}' \sum_j \left(\boldsymbol{\mu}_i \cdot \frac{\partial}{\partial \mathbf{R}_{\mathbf{m}i}}\right) \left(\boldsymbol{\mu}_j \cdot \frac{\partial}{\partial \mathbf{R}_{\mathbf{m}j}}\right) \frac{\operatorname{erfc}(\eta R_{\mathbf{m}ij})}{R_{\mathbf{m}ij}}. \tag{4.62}$$

The calculation goes on similarly as before, and the result is:

$$\begin{aligned} U^{(\mathrm{DD})}_{\mathrm{dir,i}} = \tfrac{1}{2} \sum_{\mathbf{m}\in\mathbb{Z}^3}{}' \sum_j \Bigg\{ \Bigg[\frac{\boldsymbol{\mu}_i \cdot \boldsymbol{\mu}_j}{R^3_{\mathbf{m}ij}} - 3 \frac{(\boldsymbol{\mu}_i \cdot \mathbf{R}_{\mathbf{m}ij})(\boldsymbol{\mu}_j \cdot \mathbf{R}_{\mathbf{m}ij})}{R^5_{\mathbf{m}ij}} \Bigg] \times \\ \times \left(\frac{2\mathrm{e}^{-\eta^2 R^2_{\mathbf{m}ij}} \eta R_{\mathbf{m}ij}}{\sqrt{\pi}} + \operatorname{erfc}(\eta R_{\mathbf{m}ij}) \right) + \\ - \frac{(\boldsymbol{\mu}_i \cdot \mathbf{R}_{\mathbf{m}ij})(\boldsymbol{\mu}_j \cdot \mathbf{R}_{\mathbf{m}ij})}{R^3_{\mathbf{m}ij}} \frac{4\eta^3 \mathrm{e}^{-\eta^2 R^2_{\mathbf{m}ij}} R_{\mathbf{m}ij}}{\sqrt{\pi}} \Bigg\}. \end{aligned} \tag{4.63}$$

The computation of the associated stress is tedious, but straightforward, so only the result will be given:

$$\begin{aligned} W^{(\mathrm{DD})}_{\mathrm{dir,i},\alpha\beta} = -\frac{1}{2\Omega} \sum_{\mathbf{m}\in\mathbb{Z}^3}{}' \sum_j \Bigg\{ \Bigg[(\boldsymbol{\mu}_i \cdot \boldsymbol{\mu}_j) \frac{3 R_{\mathbf{m}ij\alpha} R_{\mathbf{m}ij\alpha}}{R^5_{\mathbf{m}ij}} + \\ - \Bigg(15 \frac{(\boldsymbol{\mu}_i \cdot \mathbf{R}_{\mathbf{m}ij})(\boldsymbol{\mu}_j \cdot \mathbf{R}_{\mathbf{m}ij})}{R^7_{\mathbf{m}ij}} R_{\mathbf{m}ij\alpha} R_{\mathbf{m}ij\beta} + \\ - 3 \frac{\boldsymbol{\mu}_j \cdot \mathbf{R}_{\mathbf{m}ij}}{R^5_{\mathbf{m}ij}} R_{\mathbf{m}ij\alpha} \mu_{i\beta} \Bigg) \Bigg] \left(\frac{2\mathrm{e}^{-\eta^2 R^2_{\mathbf{m}ij}} \eta R_{\mathbf{m}ij}}{\sqrt{\pi}} + \operatorname{erfc}(\eta R_{\mathbf{m}ij}) \right) \\ + \left[\frac{\boldsymbol{\mu}_i \cdot \boldsymbol{\mu}_j}{R^3_{\mathbf{m}ij}} - 3 \frac{(\boldsymbol{\mu}_i \cdot \mathbf{R}_{\mathbf{m}ij})(\boldsymbol{\mu}_j \cdot \mathbf{R}_{\mathbf{m}ij})}{R^5_{\mathbf{m}ij}} \right] \frac{4\mathrm{e}^{-\eta^2 R^2_{\mathbf{m}ij}} \eta^3 R_{\mathbf{m}ij}}{\sqrt{\pi}} R_{\mathbf{m}ij\alpha} R_{\mathbf{m}ij\beta} + \\ + \Bigg[\frac{3 R_{\mathbf{m}ij\alpha} R_{\mathbf{m}ij\beta} (\boldsymbol{\mu}_i \cdot \mathbf{R}_{\mathbf{m}ij})(\boldsymbol{\mu}_j \cdot \mathbf{R}_{\mathbf{m}ij})}{R^5_{\mathbf{m}ij}} + \\ + -\frac{R_{\mathbf{m}ij\alpha} \left(\mu_{i\beta} (\boldsymbol{\mu}_j \cdot \mathbf{R}_{\mathbf{m}ij}) + \mu_{j\beta} (\boldsymbol{\mu}_i \cdot \mathbf{R}_{\mathbf{m}ij}) \right)}{R^3_{\mathbf{m}ij}} \Bigg] \times \\ \times \frac{4\mathrm{e}^{-\eta^2 R^2_{\mathbf{m}ij}} \eta^3 R_{\mathbf{m}ij}}{\sqrt{\pi}} + \frac{(\boldsymbol{\mu}_i \cdot \mathbf{R}_{\mathbf{m}ij})(\boldsymbol{\mu}_j \cdot \mathbf{R}_{\mathbf{m}ij})}{R^3_{\mathbf{m}ij}} \times \\ \times \left(\frac{4\mathrm{e}^{-\eta^2 R^2_{\mathbf{m}ij}} \eta^3}{\sqrt{\pi} R_{\mathbf{m}ij}} - 8 \frac{\mathrm{e}^{-\eta^2 R^2_{\mathbf{m}ij}} \eta^5 R_{\mathbf{m}ij}}{\sqrt{\pi}} \right) R_{\mathbf{m}ij\alpha} R_{\mathbf{m}ij\beta} \Bigg\}. \end{aligned} \tag{4.64}$$

The total direct space atomic electrostatic stress tensor is the sum of the three contributions of eq. (4.57), (4.61) and (4.64):

$$\overleftrightarrow{\mathbf{W}}_{\mathrm{dir,i}} = \overleftrightarrow{\mathbf{W}}^{(\mathrm{CC})}_{\mathrm{dir,i}} + \overleftrightarrow{\mathbf{W}}^{(\mathrm{CD})}_{\mathrm{dir,i}} + \overleftrightarrow{\mathbf{W}}^{(\mathrm{DD})}_{\mathrm{dir,i}}. \tag{4.65}$$

The virial heat flux associated to the direct-space electrostatic interaction is

$$\mathbf{J}^{\mathrm{dir}}_{\mathrm{vir}} = \sum_{i=1}^{N} \overleftrightarrow{\mathbf{W}}_{\mathrm{dir,i}} \cdot \mathbf{V}_i. \tag{4.66}$$

4.6.2 Reciprocal-space term

The reciprocal space term is due to the Ewald summation method to handle the long-range part of the electrostatic interaction. As for the direct space part, there are three contributions.

The atomic stress tensor cannot be calculated as usual, because it is impossible to write the total force on an atom into a sum of pair terms and the interaction is long-ranged. To circumvent this problem, the thermodynamic definition of stress will be used, i.e.:

$$W_{\alpha\beta} = -\frac{1}{\Omega}\sum_{\gamma}\frac{\partial\Phi}{\partial h_{\alpha\gamma}}h_{\beta\gamma}, \tag{4.67}$$

where $h_{\alpha\beta}$ are the matrix elements of (4.53), i.e. the components of the simulation cell vectors.

In the code, the reciprocal space contribution to the stress tensor is calculated by the subroutine `ewald1p`. Before explicitly computing the Ewald contribution to the atomic stress tensor, some useful preliminary results will be obtained.

DERIVATIVE OF THE VOLUME. The simulation cell volume is calculated as

$$\Omega = (\mathbf{a}\times\mathbf{b})\cdot\mathbf{c} = \det(\mathbf{h}). \tag{4.68}$$

The derivative of the volume with respect to an element of $\mathbf{h}$ reads:

$$\frac{\partial\Omega}{\partial h_{\alpha\beta}} = \frac{\partial\det(\mathbf{h})}{\partial h_{\alpha\beta}}. \tag{4.69}$$

This can be computed via Jacobi's formula i.e., for a square matrix A of elements A_{ij}:

$$\frac{\partial\det(A)}{\partial A_{ij}} = \mathrm{C}_{ij}(A), \tag{4.70}$$

where $\mathrm{C}_{ij}(A)$ is the cofactor matrix of A. In the present case:

$$\begin{aligned}\frac{\partial\det(\mathbf{h})}{\partial h_{\alpha\beta}} &= \left[(\det(\mathbf{h})\mathbf{h}^{-1})^{\mathrm{T}}\right]_{\alpha\beta}\\ &= \det(\mathbf{h})\mathbf{h}^{-1}_{\beta\alpha}\\ &= \Omega(\mathbf{h}^{-1})_{\beta\alpha} \equiv \Omega h^{-1}_{\beta\alpha},\end{aligned} \tag{4.71}$$

where the formula for the inverse matrix $A^{-1} = \det(A)^{-1}\,\mathrm{C}^{\mathrm{T}}(A)$ has been used.

DERIVATIVE OF A RECIPROCAL SPACE VECTOR. The reciprocal space vectors are defined as to be orthogonal to the simulation cell vectors, the product being normalized to 2π:

$$\mathbf{k} = 2\pi(\mathbf{h}^{-1})^{\mathrm{T}}\begin{pmatrix} l\\ m\\ n\end{pmatrix}, \quad l, m, n \in \mathbb{Z}. \tag{4.72}$$

Then the derivative of a component of $\mathbf{k}$ is, with $\mathbf{K} = (l, m, n)$:

$$\begin{aligned}\frac{\partial k_\alpha}{\partial h_{\mu\nu}} =& 2\pi \frac{\partial}{\partial h_{\mu\nu}} \sum_\beta h^{-1}_{\beta\alpha} K_\beta \\ =& 2\pi \sum_\beta \frac{\partial h^{-1}_{\beta\alpha}}{\partial h_{\mu\nu}} K_\beta.\end{aligned} \tag{4.73}$$

To find the derivative of the inverse of $\mathbf{h}$ one can differentiate the identity, i.e.:

$$\begin{aligned}0 = \frac{\partial \delta_{\alpha\beta}}{\partial h_{\mu\nu}} &= \frac{\partial}{\partial h_{\mu\nu}} \sum_\gamma h_{\alpha\gamma} h^{-1}_{\gamma\beta} \\ &= \sum_\gamma \left(\frac{\partial h_{\alpha\beta}}{\partial h_{\mu\nu}} h^{-1}_{\gamma\beta} + h_{\alpha\gamma} \frac{\partial h^{-1}_{\gamma\beta}}{\partial h_{\mu\nu}} \right) \\ &= \sum_\gamma \left(\delta_{\alpha\mu}\delta_{\gamma\nu} h^{-1}_{\gamma\beta} + h_{\alpha\gamma} \frac{\partial h^{-1}_{\gamma\beta}}{\partial h_{\mu\nu}} \right) \\ &= \delta_{\alpha\mu} h^{-1}_{\nu\beta} + \sum_\gamma h_{\alpha\gamma} \frac{\partial h^{-1}_{\gamma\beta}}{\partial h_{\mu\nu}},\end{aligned} \tag{4.74}$$

so that

$$\sum_\gamma h_{\alpha\gamma} \frac{\partial h^{-1}_{\gamma\beta}}{\partial h_{\mu\nu}} = -\delta_{\alpha\mu} h^{-1}_{\nu\beta}. \tag{4.75}$$

By inspection it is evident that the tensor satisfying eq. (4.75) is:

$$\frac{\partial h^{-1}_{\gamma\beta}}{\partial h_{\mu\nu}} = -h^{-1}_{\gamma\mu} h^{-1}_{\nu\beta}. \tag{4.76}$$

The derivative in eq. (4.73) then becomes

$$\frac{\partial k_\alpha}{\partial h_{\mu\nu}} = -2\pi \sum_\beta h^{-1}_{\beta\mu} h^{-1}_{\nu\alpha} K_\beta. \tag{4.77}$$

INVARIANCE OF $\mathbf{k} \cdot \mathbf{R}$. Let us write a generic atomic position vector as

$$\mathbf{R} = \mathbf{h}\,\mathbf{s}, \tag{4.78}$$

where s is the scaled position in the simulation box, i.e. a quantity which is invariant under cell reshaping. The scalar product $\mathbf{k} \cdot \mathbf{R}$ can be written, using (4.72), as

$$\begin{aligned}\mathbf{k} \cdot \mathbf{R} &= \left(2\pi (\mathbf{h}^{-1})^{\mathrm{T}} \mathbf{K} \right) \cdot (\mathbf{h}\,\mathbf{s}) \\ &= 2\pi \sum_\alpha \left(\sum_\gamma h^{-1}_{\gamma\alpha} K_\gamma \right) \left(\sum_\lambda h_{\alpha\lambda} s_\lambda \right) \\ &= 2\pi \sum_{\gamma,\lambda} \left(\sum_\alpha h^{-1}_{\gamma\alpha} h_{\alpha\lambda} \right) K_\gamma s_\lambda \\ &= 2\pi \sum_{\gamma,\lambda} \delta_{\gamma\lambda} K_\gamma s_\lambda \\ &= 2\pi \mathbf{K} \cdot \mathbf{s}.\end{aligned} \tag{4.79}$$

The expression in (4.79) does not depend on the simulation cell matrix (4.53), so its derivatives with respect to the cell vectors components will be zero.

With the results (4.71), (4.77) and (4.79), we are ready to compute the atomic stress due to reciprocal space calculations.

CC term

The reciprocal space contribution to the charge-charge Coulombic energy per atom is:

$$U^{(\mathrm{CC})}_{\mathrm{rec,i}} = \frac{2\pi}{\Omega} \sum_{\mathbf{k}\neq\mathbf{0}} Q(k) q_i \sum_j q_j \cos(\mathbf{k}\cdot\mathbf{R}_{ij}), \tag{4.80}$$

where $Q(k)$ is

$$Q(k) = \frac{\mathrm{e}^{-k^2/4\eta^2}}{k^2}.$$

The CC stress tensor is, then:

$$\begin{aligned}
W^{(\mathrm{CC})}_{\mathrm{rec,i},\alpha\beta} &= -\frac{1}{\Omega}\sum_\gamma \frac{\partial U^{(\mathrm{CC})}_{\mathrm{rec,i}}}{\partial h_{\alpha\gamma}} h_{\beta\gamma} \\
&= \frac{2\pi}{\Omega^3}\sum_\gamma \frac{\partial \Omega}{\partial h_{\alpha\gamma}} h_{\beta\gamma} \sum_{\mathbf{k}\neq\mathbf{0}} Q(k) q_i \sum_j q_j \cos(\mathbf{k}\cdot\mathbf{R}_{ij}) + \\
&\qquad - \frac{2\pi}{\Omega}\sum_{\mathbf{k}\neq\mathbf{0}}\sum_\gamma \frac{\partial Q(k)}{\partial h_{\alpha\gamma}} h_{\beta\gamma} q_i \sum_j q_j \cos(\mathbf{k}\cdot\mathbf{R}_{ij}) \\
&= \frac{2\pi}{\Omega^2}\sum_\gamma h^{-1}_{\gamma\alpha} h_{\beta\gamma} \sum_{\mathbf{k}\neq\mathbf{0}} Q(k) q_i \sum_j q_j \cos(\mathbf{k}\cdot\mathbf{R}_{ij}) + \\
&\qquad - \frac{2\pi}{\Omega}\sum_{\mathbf{k}\neq\mathbf{0}}\sum_\gamma \frac{\partial Q(k)}{\partial h_{\alpha\gamma}} h_{\beta\gamma} q_i \sum_j q_j \cos(\mathbf{k}\cdot\mathbf{R}_{ij}) \\
&= \frac{2\pi}{\Omega^2}\delta_{\alpha\beta} \sum_{\mathbf{k}\neq\mathbf{0}} Q(k) q_i \sum_j q_j \cos(\mathbf{k}\cdot\mathbf{R}_{ij}) + \\
&\quad - \frac{2\pi}{\Omega}\sum_{\mathbf{k}\neq\mathbf{0}}\sum_\gamma \frac{\partial Q(k)}{\partial h_{\alpha\gamma}} h_{\beta\gamma} q_i \sum_j q_j \cos(\mathbf{k}\cdot\mathbf{R}_{ij}).
\end{aligned} \tag{4.81}$$

The derivative in (4.81) reads:

$$\begin{aligned}
\sum_\gamma \frac{\partial Q(k)}{\partial h_{\alpha\gamma}} h_{\beta\gamma} &= \frac{\partial Q(k)}{\partial (k^2)} \frac{\partial (k^2)}{\partial h_{\alpha\gamma}} h_{\beta\gamma} \\
&= -Q(k)\left(\frac{1}{k^2} + \frac{1}{4\eta^2}\right) \sum_{\lambda,\gamma} h_{\beta\gamma} \frac{\partial (k_\lambda^2)}{\partial h_{\alpha\gamma}} \\
&= -Q(k)\left(\frac{1}{k^2} + \frac{1}{4\eta^2}\right) \sum_{\lambda,\gamma} 2k_\lambda \frac{\partial k_\lambda}{\partial h_{\alpha\gamma}} h_{\beta\gamma},
\end{aligned} \tag{4.82}$$

where chain differentiation has been used. By using formula (4.77) we get:

$$\sum_\gamma \frac{\partial Q(k)}{\partial h_{\alpha\gamma}} h_{\beta\gamma} = -Q(k)\left(\frac{1}{k^2} + \frac{1}{4\eta^2}\right) \sum_{\lambda,\gamma} 2k_\lambda \left(-2\pi \sum_\mu h^{-1}_{\mu\alpha} h^{-1}_{\gamma\lambda} K_\mu\right) h_{\beta\gamma}. \tag{4.83}$$

The fact that the product of the cell matrix with its inverse is the identity yields:

$$\begin{aligned}\sum_{\gamma}\frac{\partial Q(k)}{\partial h_{\alpha\gamma}}h_{\beta\gamma} &= -Q(k)\left(\frac{1}{k^2}+\frac{1}{4\eta^2}\right)\sum_{\lambda,\mu}2k_{\lambda}\left(-2\pi h^{-1}_{\mu\alpha}\delta_{\beta\lambda}K_{\mu}\right)\\ &= -Q(k)\left(\frac{1}{k^2}+\frac{1}{4\eta^2}\right)\sum_{\mu}2k_{\beta}\left(-2\pi h^{-1}_{\mu\alpha}K_{\mu}\right)\\ &= -Q(k)\left(\frac{1}{k^2}+\frac{1}{4\eta^2}\right)2k_{\beta}\left(-k_{\alpha}\right)\\ &= 2Q(k)\left(\frac{1}{k^2}+\frac{1}{4\eta^2}\right)k_{\alpha}k_{\beta}.\end{aligned}\tag{4.84}$$

Putting things together we find

$$W^{\text{(CC)}}_{\text{rec,i},\alpha\beta} = \frac{2\pi}{\Omega^2}\sum_{\mathbf{k}\neq\mathbf{0}}\mathsf{B}_{\alpha\beta}(\mathbf{k})Q(k)q_i\sum_j q_j\cos(\mathbf{k}\cdot\mathbf{R}_{ij}),\tag{4.85}$$

where the auxiliary tensor B has components

$$\mathsf{B}_{\alpha\beta} = \delta_{\alpha\beta} - 2k_{\alpha}k_{\beta}\left(\frac{1}{k^2}+\frac{1}{4\eta^2}\right).\tag{4.86}$$

CD term

The reciprocal space contribution to the charge-dipole energy per atom is:

$$\begin{aligned}U^{\text{(CD)}}_{\text{rec,i}} =& \frac{2\pi}{\Omega}\sum_{\mathbf{k}\neq\mathbf{0}}Q(k)q_i\sum_j(\mathbf{k}\cdot\boldsymbol{\mu}_j)\cos(\mathbf{k}\cdot\mathbf{R}_{ij})+\\ &-\frac{2\pi}{\Omega}\sum_{\mathbf{k}\neq\mathbf{0}}Q(k)(\mathbf{k}\cdot\boldsymbol{\mu}_i)\sum_j q_j\cos(\mathbf{k}\cdot\mathbf{R}_{ij}).\end{aligned}\tag{4.87}$$

The associated stress tensor is, then:

$$\begin{aligned}W^{\text{(CD)}}_{\text{rec,i},\alpha\beta} &= -\frac{1}{\Omega}\sum_{\gamma}\frac{\partial U^{\text{(CD)}}_{\text{rec,i}}}{\partial h_{\alpha\gamma}}h_{\beta\gamma}\\ &= \frac{2\pi}{\Omega^2}\sum_{\mathbf{k}\neq\mathbf{0}}\mathsf{B}_{\alpha\beta}(\mathbf{k})Q(k)\left[q_i\sum_j(\mathbf{k}\cdot\boldsymbol{\mu}_j)\cos(\mathbf{k}\cdot\mathbf{R}_{ij})+\right.\\ &\left.-(\mathbf{k}\cdot\boldsymbol{\mu}_i)\sum_j q_j\cos(\mathbf{k}\cdot\mathbf{R}_{ij})\right]+\frac{2\pi}{\Omega^2}\sum_{\mathbf{k}\neq\mathbf{0}}\mathsf{B}_{\alpha\beta}(\mathbf{k})Q(k)\times\\ &\times\left[q_i\sum_j\sum_{\gamma}\frac{\partial(\mathbf{k}\cdot\boldsymbol{\mu}_j)}{\partial h_{\alpha\gamma}}h_{\beta\gamma}\cos(\mathbf{k}\cdot\mathbf{R}_{ij})+\right.\\ &\left.-\sum_{\gamma}\frac{\partial(\mathbf{k}\cdot\boldsymbol{\mu}_i)}{\partial h_{\alpha\gamma}}h_{\beta\gamma}\sum_j q_j\cos(\mathbf{k}\cdot\mathbf{R}_{ij})\right].\end{aligned}\tag{4.88}$$

The derivative of the scalar product in (4.88) reads:

$$\begin{aligned}\sum_{\gamma}\frac{\partial(\mathbf{k}\cdot\boldsymbol{\mu}_i)}{\partial h_{\alpha\gamma}}h_{\beta\gamma} =&\sum_{\gamma,\lambda}\frac{\partial(k_\lambda\mu_{i_\lambda})}{\partial h_{\alpha\gamma}}h_{\beta\gamma}\\ =&\sum_{\gamma,\lambda}\mu_{i_\lambda}\frac{\partial k_\lambda}{\partial h_{\alpha\gamma}}h_{\beta\gamma}\\ =&\sum_{\gamma,\lambda}\mu_{i_\lambda}\left(-2\pi\sum_{\rho}h^{-1}_{\rho\alpha}h^{-1}_{\gamma\lambda}K_\rho\right)h_{\beta\gamma}\\ =&\sum_{\lambda,\rho}\mu_{i_\lambda}\left(-2\pi\delta_{\beta\lambda}h^{-1}_{\rho\alpha}K_\rho\right)\\ =&\mu_{i_\beta}\sum_{\rho}\left(-2\pi h^{-1}_{\rho\alpha}K_\rho\right)\\ =&k_\alpha\mu_{i_\beta}.\end{aligned} \tag{4.89}$$

Plugging this result into (4.88) we obtain

$$\begin{aligned}W^{(\mathrm{CD})}_{\mathrm{rec,i},\alpha\beta} = \frac{2\pi}{\Omega^2}\sum_{\mathbf{k}\neq\mathbf{0}}\mathsf{B}_{\alpha\beta}(\mathbf{k})Q(k)\Bigg[q_i\sum_j(\mathbf{k}\cdot\boldsymbol{\mu}_j)\cos(\mathbf{k}\cdot\mathbf{R}_{ij})+\\ -(\mathbf{k}\cdot\boldsymbol{\mu}_i)\sum_j q_j\cos(\mathbf{k}\cdot\mathbf{R}_{ij})\Bigg]+\frac{2\pi}{\Omega^2}\sum_{\mathbf{k}\neq\mathbf{0}}Q(k)\times\\ \times\left[q_i\sum_j k_\alpha\mu_{j_\beta}\cos(\mathbf{k}\cdot\mathbf{R}_{ij})-k_\alpha\mu_{i_\beta}\sum_j q_j\cos(\mathbf{k}\cdot\mathbf{R}_{ij})\right].\end{aligned} \tag{4.90}$$

DD term

The reciprocal space contribution to the dipole-dipole energy per atom is:

$$U^{(\mathrm{DD})}_{\mathrm{rec,i}} = \frac{2\pi}{\Omega}\sum_{\mathbf{k}\neq\mathbf{0}}Q(k)(\mathbf{k}\cdot\boldsymbol{\mu}_i)\sum_j(\mathbf{k}\cdot\boldsymbol{\mu}_j)\cos(\mathbf{k}\cdot\mathbf{R}_{ij}). \tag{4.91}$$

Using the preliminary results calculated above we can readily compute the contribution to the stress tensor:

$$\begin{aligned}W^{(\mathrm{DD})}_{\mathrm{rec,i},\alpha\beta} = \frac{2\pi}{\Omega^2}\sum_{\mathbf{k}\neq\mathbf{0}}\mathsf{B}_{\alpha\beta}(\mathbf{k})Q(k)\left[(\mathbf{k}\cdot\boldsymbol{\mu}_i)\sum_j(\mathbf{k}\cdot\boldsymbol{\mu}_j)\cos(\mathbf{k}\cdot\mathbf{R}_{ij})\right]+\\ +\frac{2\pi}{\Omega^2}\sum_{\mathbf{k}\neq\mathbf{0}}Q(k)\sum_j\left[k_\alpha\mu_{i_\beta}(\mathbf{k}\cdot\boldsymbol{\mu}_j)+(\mathbf{k}\cdot\boldsymbol{\mu}_i)k_\alpha\mu_{j_\beta}\right]\cos(\mathbf{k}\cdot\mathbf{R}_{ij}).\end{aligned} \tag{4.92}$$

The total reciprocal space atomic electrostatic stress tensor is the sum of the three contributions of eq. (4.85), (4.90) and (4.92).

$$\overset{\leftrightarrow}{\mathbf{W}}_{\mathrm{rec,i}} = \overset{\leftrightarrow}{\mathbf{W}}{}^{(\mathrm{CC})}_{\mathrm{rec,i}}+\overset{\leftrightarrow}{\mathbf{W}}{}^{(\mathrm{CD})}_{\mathrm{rec,i}}+\overset{\leftrightarrow}{\mathbf{W}}{}^{(\mathrm{DD})}_{\mathrm{rec,i}}. \tag{4.93}$$

The virial heat flux associated to the reciprocal space electrostatic interaction is

$$\mathbf{J}^{\mathrm{rec}}_{\mathrm{vir}} = -\sum_{i=1}^{N}\overset{\leftrightarrow}{\mathbf{W}}_{\mathrm{rec,i}}\cdot\mathbf{V}_i. \tag{4.94}$$

4.6.3 Self-interaction term

The correction term due to double counting is a pairwise term in which the pair-forces are calculated from the analytic potential. This implies that the contribution to the atomic stress tensor $\overset{\leftrightarrow}{\mathbf{W}}_{\text{self,i}}$ will be the trivial one as in eq. (4.42). The virial heat flux due the self-interaction correction is

$$\mathbf{J}_{\text{vir}}^{\text{self}} = -\sum_{i=1}^{N} \overset{\leftrightarrow}{\mathbf{W}}_{\text{self,i}} \cdot \mathbf{V}_i. \tag{4.95}$$

4.6.4 TTM4-F model correction

In the MB-pol model the electrostatic interaction is actually implemented *à la* Thole, i.e. a damping function accompanies both charges and dipoles, as explained in 2.3.1 and in A.5.

The TTM contribution to the stress tensor contains terms of the form

$$\begin{aligned} \frac{\partial \lambda_n(u_{ij})}{\partial R_{\mathbf{m}i}} &= \frac{\partial \lambda_n(u)}{\partial u} \frac{\partial u_{ij}}{\partial R_{\mathbf{m}i}} \\ &= -\, n u_{ij} \lambda_{n+2}(u_{ij}) \frac{1}{A_{ij}} \frac{\partial \mathbf{R}_{\mathbf{m}ij}}{\partial R_{\mathbf{m}i}} \\ &= -\, n \frac{\lambda_{n+2}(u_{ij})}{A_{ij}^2} \mathbf{R}_{\mathbf{m}ij}, \end{aligned} \tag{4.96}$$

wherever charge-charge (λ_3), charge-dipole (λ_5) or dipole-dipole (λ_7) products appear. In the derivation of (4.96), the recursive definition (A.19) at page 76 has been used to express the derivative of the λ function with respect to u_{ij}.

The λ_n functions that appear in the formula of atomic stress are (with $m = 4$):

$$\lambda_1(u) = -\frac{\mathrm{e}^{-au^4}}{u} + \sqrt[4]{a}\,\Gamma\left(\frac{3}{4}, au^4\right) + \frac{1}{u}, \tag{4.97}$$

$$\lambda_3(u) = -4aue^{-au^4} - \frac{\mathrm{e}^{-au^4}}{u^3} + \frac{4\sqrt[4]{a}\mathrm{e}^{-au^4}\left(au^4\right)^{3/4}}{u^2} + \frac{1}{u^3}, \tag{4.98}$$

$$\begin{aligned} \lambda_5(u) = \frac{16}{3}a^{5/4}\mathrm{e}^{-au^4}\left(au^4\right)^{3/4} - \frac{16}{3}a^2u^3\mathrm{e}^{-au^4} - \frac{4\sqrt[4]{a}\mathrm{e}^{-au^4}\left(au^4\right)^{3/4}}{3u^4} + \\ - \frac{\mathrm{e}^{-au^4}}{u^5} + \frac{1}{u^5}, \end{aligned} \tag{4.99}$$

$$\begin{aligned} \lambda_7(u) = \frac{64}{15}a^{9/4}u^2\mathrm{e}^{-au^4}\left(au^4\right)^{3/4} - \frac{64a^{5/4}\mathrm{e}^{-au^4}\left(au^4\right)^{3/4}}{15u^2} - \frac{64}{15}a^3u^5\mathrm{e}^{-au^4} + \\ + \frac{16}{5}a^2u\mathrm{e}^{-au^4} - \frac{\mathrm{e}^{-au^4}}{u^7} - \frac{4\sqrt[4]{a}\mathrm{e}^{-au^4}\left(au^4\right)^{3/4}}{15u^6} - \frac{4a\mathrm{e}^{-au^4}}{5u^3} + \frac{1}{u^7}. \end{aligned} \tag{4.100}$$

The complete formula for the stress tensor is huge and not very eloquent, so it will not be shown here; the virial heat flux associated to the Thole corrections is

$$\mathbf{J}_{\text{vir}}^{\text{Thole}} = \sum_{i=1}^{N} \overset{\leftrightarrow}{\mathbf{W}}_i^{\text{Thole}} \cdot \mathbf{V}_i, \tag{4.101}$$

where $\overset{\leftrightarrow}{\mathbf{W}}_i^{\text{Thole}}$ is the atomic contribution to the stress tensor due to the Thole smeared charge densities. The Thole-corrections are calculated by the subroutine `qdforce`.

4.7 HEAT FLUX VECTOR IN THE MB-POL MODEL

Gathering all the pieces found in the sections above, the formula of the heat flux in the MB-pol model is finally obtained:

$$\begin{aligned}
\mathbf{J}_{\text{q}}{}^{\text{MB-pol}} = \sum_{i=1}^{N} \tfrac{1}{2} M_i V_i^2 \mathbf{V}_i + \mathbf{J}_{\text{conv}}^{\text{bond}} + \mathbf{J}_{\text{conv}}^{\text{ang}} + \\
+ \mathbf{J}_{\text{conv}}^{(2\text{B})} + \mathbf{J}_{\text{conv}}^{\text{VdW}} + \mathbf{J}_{\text{conv}}^{(3\text{B})} + \\
+ \mathbf{J}_{\text{conv}}^{\text{dir}} + \mathbf{J}_{\text{conv}}^{\text{rec}} + \mathbf{J}_{\text{conv}}^{\text{self}} + \mathbf{J}_{\text{conv}}^{\text{pol}} + \\
+ \mathbf{J}_{\text{vir}}^{\text{bond}} + \mathbf{J}_{\text{vir}}^{\text{ang}} + \\
+ \mathbf{J}_{\text{vir}}^{(2\text{B})} + \mathbf{J}_{\text{vir}}^{\text{VdW}} + \mathbf{J}_{\text{vir}}^{(3\text{B})} + \\
+ \mathbf{J}_{\text{vir}}^{\text{dir}} + \mathbf{J}_{\text{vir}}^{\text{rec}} + \mathbf{J}_{\text{vir}}^{\text{self}} + \mathbf{J}_{\text{vir}}^{\text{Thole}}.
\end{aligned} \tag{4.102}$$

5 SIMULATIONS

The computer simulations are conducted via the MD package `DL_POLY`, whose version 2 source code has been modified by the research group of Prof. Francesco Paesani at the University of California in San Diego to include the MB-pol potential for water. As explained in chapter 4, the author of this thesis has implemented the energy and stress decomposition to allow the computation of the heat flux. First, some preliminary results will be shown, to check that the equilibrium values of the thermodynamic observables are in agreement with the literature; then, the heat flux data obtained from the equilibrium simulations of MB-pol water will be analyzed.

5.1 PRELIMINARY RESULTS

In order to perform meaningful calculations, one should prepare the system in the correct thermodynamic state. In the present case, the quantity of interest is the thermal conductivity of liquid water at atmospheric pressure, so a set of configurations with temperatures ranging from ≈ 270K to ≈ 370K have been prepared. The simulation box is cubic and contains 256 water molecules. To be sure that the system is in the liquid state, the equilibrium density ρ will be calculated, alongside with a dynamical property, the self-diffusion coefficient D, and some structural properties, the radial distribution functions (RDF).

The quantities hereby mentioned are already accessible from simulations done with the original `DL_POLY` software modified to include the MB-pol potential; since the heat flux calculations increase considerably the computational cost of the MD run, they have not been carried out in this initial stage.

5.1.1 Density

The equilibrium density ρ has been computed as a function of temperature T. The calculations have been carried out in the NPT ensemble with a 4-chain Nosé-Hoover barostat/thermostat. A single initial configuration of MB-pol water at ≈ 300K has been used as starting point to sample twelve different water configurations at atmospheric pressure and temperatures ranging from 264K to 374K with steps of $10K$. The simulation has been carried out for more than 1ns. The first tens of picoseconds has been discarded as an equilibration part, while the remaining 1000ps have been used for the computation. In a NPT run, the cell volume is allowed to change with time. After some equilibration time, its value will fluctuate around its mean in a controlled way. The time-series of the cell volume Ω has been block-averaged

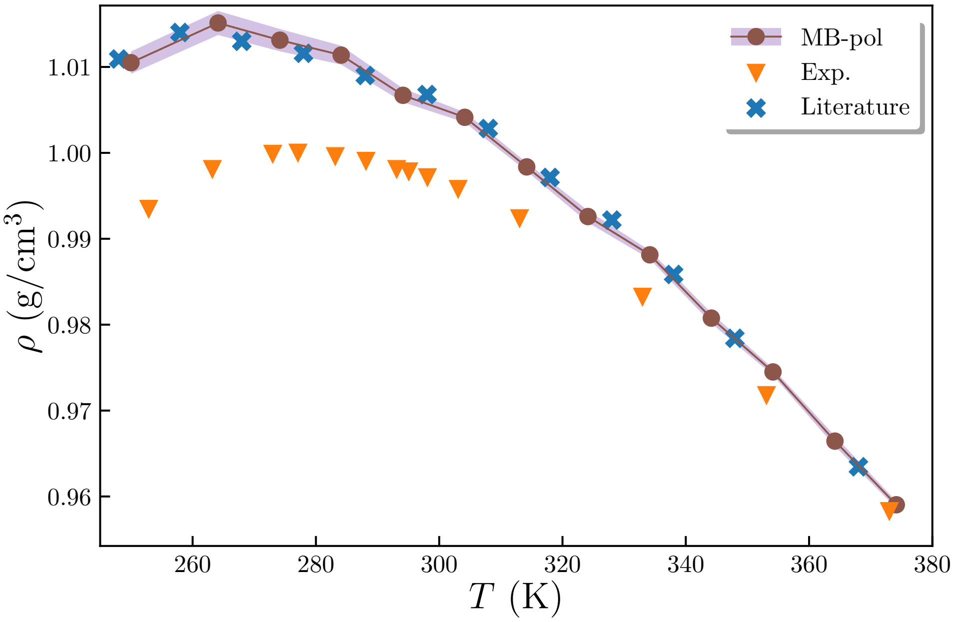

Figure 5.1: Density as a function of temperature for the MB-pol model at the atmospheric pressure. The results are compared to the experimental values. The circles represent the densities computed via MD with the error bands obtained via block analysis. The triangles are the experimental data [Wagner and Pruß, 2002].

in 10 blocks of 100ps to obtain an estimate of the standard error of the mean. The density has been calculated as:

$$\rho = \frac{N_{\text{mol}} m_{\text{mol}}}{N_{\text{A}} \Omega}, \tag{5.1}$$

$$m_{\text{mol}} = 18.0107\text{g/mol}, \tag{5.2}$$

where m_{mol} is the value of the molar mass of water in the MB-pol model and N_{A} is the Avogadro constant.

In figure 5.1 the results are compared to the experimental values available in the literature [Wagner and Pruß, 2002]. The accuracy is very good at high temperature, while it worsens at lower temperatures; however, the overall accuracy of the MB-pol density is higher than other common force-fields for water and, most importantly, it accounts for the presence of a density maximum. This feature of the MB-pol model was already noticed in the literature [Reddy et al., 2016]; better results should be achieved via more sofisticated techniques like Path-Integral-Molecular-Dynamics (PIMD), that take into account the presence of nuclear quantum effects. The correct values of the density ensures that the packing of the system is compatible with that of liquid water.

5.1.2 Diffusivity

The computation of the self-diffusion coefficient is useful to check if the system is in a fluid state; in fact, the diffusivity of a solid is very small, while for a liquid or a gas it is finite. The self-diffusion coefficient D, or diffusiv-

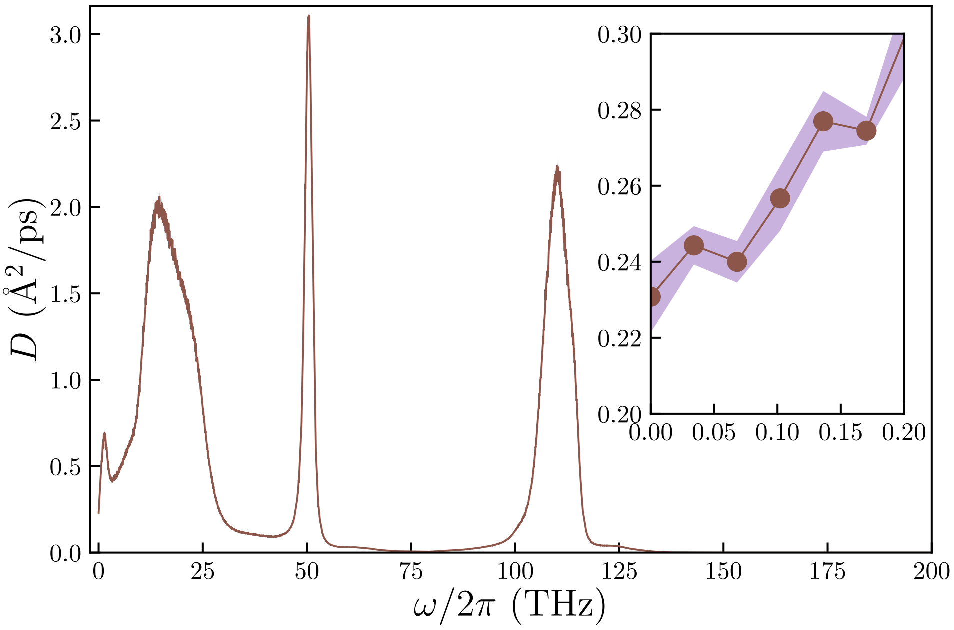

Figure 5.2: Vibrational spectrum of MB-pol water at ≈ 295K. The zoomed region shows the zero-frequency value of the spectrum, i.e. the diffusion coefficient D.

ity, is expressed as the time-integral of the velocity-velocity autocorrelation function [Allen and Tildesley, 1987]:

$$D = \frac{1}{3N}\sum_{i=1}^{N}\int_0^\infty \left\langle \mathbf{V}_i(0)\cdot\mathbf{V}_i(t)\right\rangle_{\mathrm{eq}}\,\mathrm{d}t. \tag{5.3}$$

The integral above is a Green-Kubo integral that can be recast into the zero-frequency value of the so called *vibrational spectrum*, i.e. the power spectrum of the velocity, via the Wiener-Kintchine theorem (see theorem 1 at page 22).

Differently from the heat flux case, the velocity time-series does not need to be analyzed via the sophisticated cepstral analysis: each MD simulation yields $3N$ independent time-series, i.e. each of the three Cartesian components of the N atomic velocities[1]. A simple block-average of the periodogram provides a good estimate of the velocity power spectrum. Figure 5.2 displays the vibrational spectrum computed in this way. The same procedure has been carried out for every temperature at disposal. For each vibrational spectrum, the zero frequency value has been collected and plotted versus the temperature (fig. 5.3). The agreement with experimental data [Holz et al., 2000] of water at the same condition is very good: yet another evidence of the accuracy of the MB-pol model.

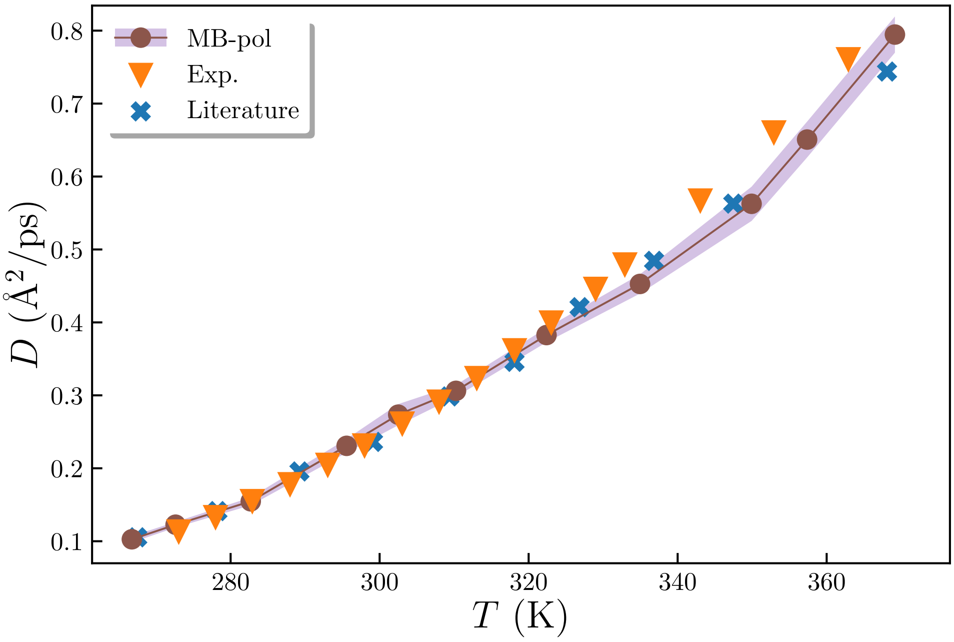

Figure 5.3: Diffusivity of MB-pol water as a function of temperature. The agreement with the experimental values [Holz et al., 2000] is very good.

5.1.3 Radial distribution functions

While the density as computed in section 5.1.1 is a global property of the system, a the radial distribution functions describe the local density variations in the liquid. For an isotropic system it is defined as

$$g(x) = \frac{1}{4\pi x^2} \frac{\Omega}{N^2} \sum_{i=1}^{N} \sum_{j=1}^{N} \langle \delta(x - |\mathbf{R}_i - \mathbf{R}_j|) \rangle \, . \tag{5.4}$$

In water there are two atomic species, oxygen and hydrogen, so there will be three different radial pair distribution functions: one involving distances among oxygens, one among oxygens and hydrogens, and one among hydrogens only. Numerically, the computation is done by analysing the instantaneous configurations written by `DL_POLY`: for each atom in the configuration, a routine counts the number of atoms of the selected species that are enclosed in a spherical shell of given width (the resolution of the RDF) and normalizes the result with respect to the volume the shell. The other normalization constants are such that the asymptotic value of the RDF is 1. This is done for every configuration: the results are then averaged to suppress the fluctuations and obtain a better estimate of $g(x)$. The visualization tool `VMD` [Humphrey et al., 1996] includes a `Tcl` function to accomplish the calculation described above for a simulation snapshot; with another simple `Tcl` script such function has been used to compute the RDFs of water for each temperature available.

---

[1] Actually, the conservation of total momentum imposes three linear constraints on the possible values of the atomic velocities, so the independent time-series are $3N - 3$. However, this does not affect the validity of the argument.

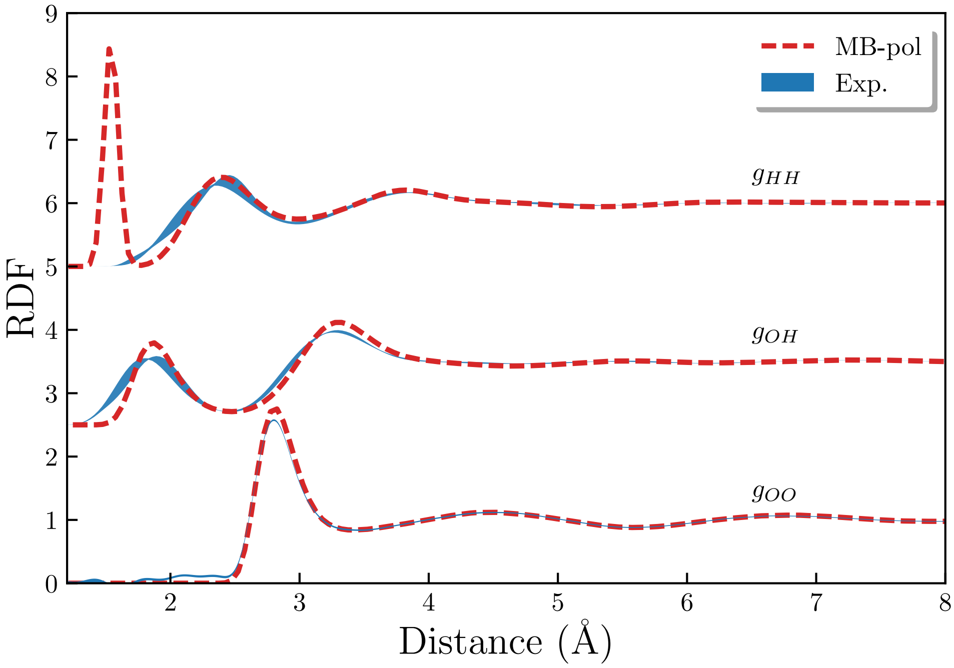

Figure 5.4: O-O, O-H and H-H radial distribution functions of MB-pol water at $\approx 295K$ compared to joint neutron and X-ray scattering experimental values at ambient pressure. The first peak in the H-H radial distribution function, due to the two hydrogen atoms within the same molecule, is not resolved with the experimental techniques used in the paper from which the data are taken.

Figures 5.4 compare the simulation results with experimental data. The O-O radial distribution function agrees well with data, while for the O-H and H-H distribution functions a better agreement can be achieved via PIMD [Medders et al., 2014]. In is important to notice that the worst agreement with the experimental data is for the second peak in the O-H RDF: the position and intensity of this peak describe the spatial correlation between oxygens and hydrogens in adjacent molecules, i.e. atoms that are directly involved in hydrogen bonds. This property is notoriously difficult to measure.

5.2 HEAT TRANSPORT SIMULATIONS

After having shown the preliminary results in section 5.1, let us now outline how the computation of the thermal conductivity has been performed. The molecular dynamics simulations to compute the heat flux time series have been carried out in the NVE (microcanonical) ensemble; this is a common choice when it comes to compute dynamical properties, since it allows better control on the simulation than other statistical ensembles.

5.2.1 Equilibration

The equilibration phase coincides with the long NVE run that has allowed to compute the diffusion coefficient and the radial distribution functions.

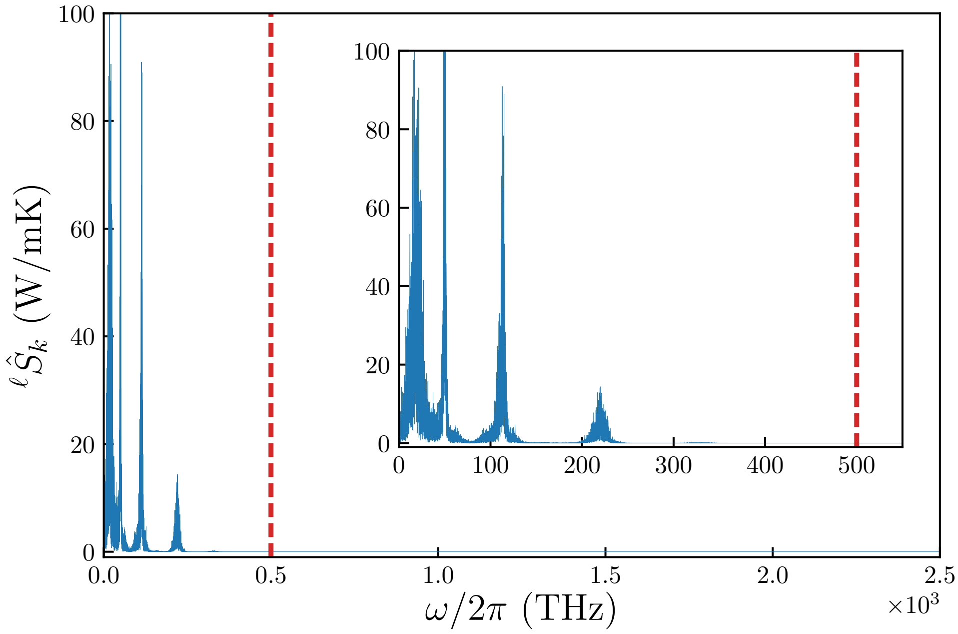

Figure 5.5: Periodogram of the heat flux at 300K after 60ps of MD simulation. At 500THz the magnitude of the periodogram is zero: the Nyquist frequency can be safely reduced from 2500THz to 500THz.

The calculation of the above properties proves that the system is in the correct configuration and is ready for the production phase.

5.2.2 Production

The production runs have been carried out in the microcanonical ensemble starting from the final configurations produced by the equilibration phase. The simulation time-step has been set to 0.2fs; at the beginning of the computation the program has been instructed to print the heat flux at each time-step. This requires many resources; however, the optimum sampling rate is the maximum time interval that satisfies the *Nyquist–Shannon sampling theorem*, which states that a signal that contains no frequency higher than B hertz is completely determined by sampling its values with a discrete time-series spaced $1/2B$ seconds apart. This prevents from coming across unwanted aliasing effect. To collect the value of B, after a few tens of picoseconds the periodogram has been computed and plotted (fig. 5.5). Since after $\approx 500\text{THz}$ the value of the periodogram is zero, a good value for the sampling rate is

$$\varepsilon = \frac{1}{2 \cdot 500\text{THz}} = 1\text{fs},$$

i.e. the program will print the data to a file once every 5 simulation steps, while keeping the simulation-time step to 0.2fs.

The total length of each simulation (one trajectory per temperature) is of $\approx 1.5\text{ns}$. This value is considerably high, taking into account the fairly high computational cost of MB-pol forces together with the heat flux computation. This conservative approach has been chosen because the complex nature of the interaction in MB-pol water may require long convergence times;

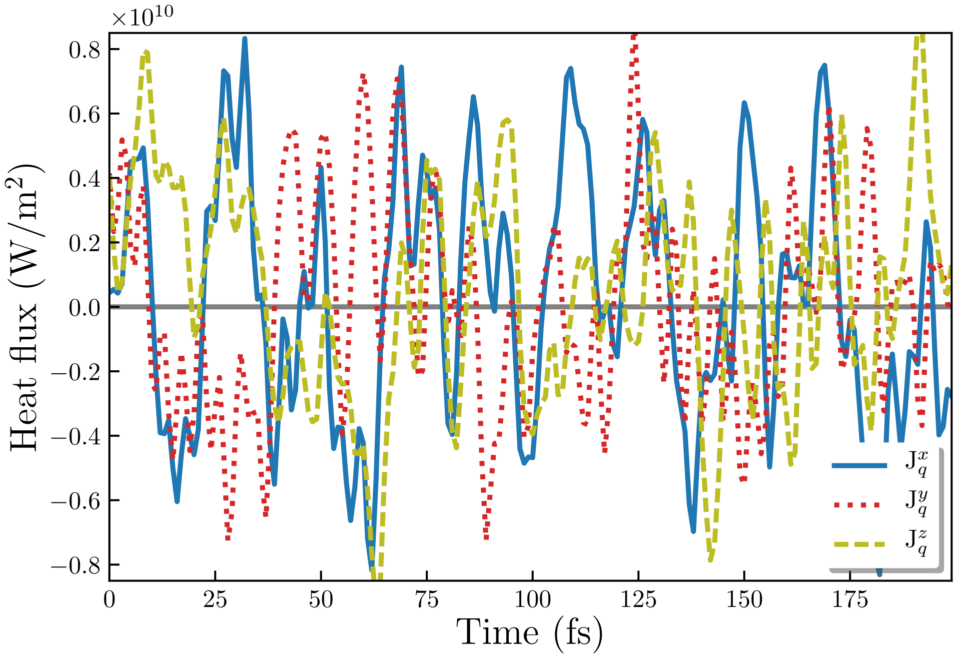

Figure 5.6: Sample of a few hundred femtoseconds of the energy flux time series. The energy flux fluctuates around zero, its equilibrium value.

nevertheless, this incidental necessity provides a useful benchmark to the still experimental technique of multi-component cepstral analysis applied to molecular fluids.

5.2.3 Results and data analysis

The collected data useful to the calculation of the thermal conductivity consist, for each configuration, of the three Cartesian components of the energy flux, $\mathbf{J}_{\text{q}}$, the three Cartesian components of the non-diffusive flux $\mathbf{J}_{\text{OH}}$ (see section 1.6.1 at page 12) and all the thermodynamic quantities such as temperature, pressure, and volume. The data acquisition procedure and the subsequent analysis can be summarized as:

- Compute the energy flux $\mathbf{J}_{\text{q}}$ and the Oxygen-Hydrogen mass flux $\mathbf{J}_{\text{OH}}$;
- Compute the cross-periodograms via discrete-Fourier transforms of the time-series of the fluxes;
- From the discrete Fourier transforms of the fluxes, calculate the cross-periodograms ${}^{\ell M}\hat{S}_k^{ij}$ (see eq. (3.55));
- Compute the multi-component periodogram (eq. (3.68)), estimator of the multi-component power spectrum, ${}^{\ell M}\hat{S}'_k$: this is the time-series whose zero-frequency value is proportional to the thermal conductivity;
- Compute the cepstrum ${}^{\ell M}\hat{C}_n$ of the resampled time-series;
- Apply Akaike Information Criterion (AIC), eq. (3.49), to estimate the number of cepstral coefficients P^* to retain;

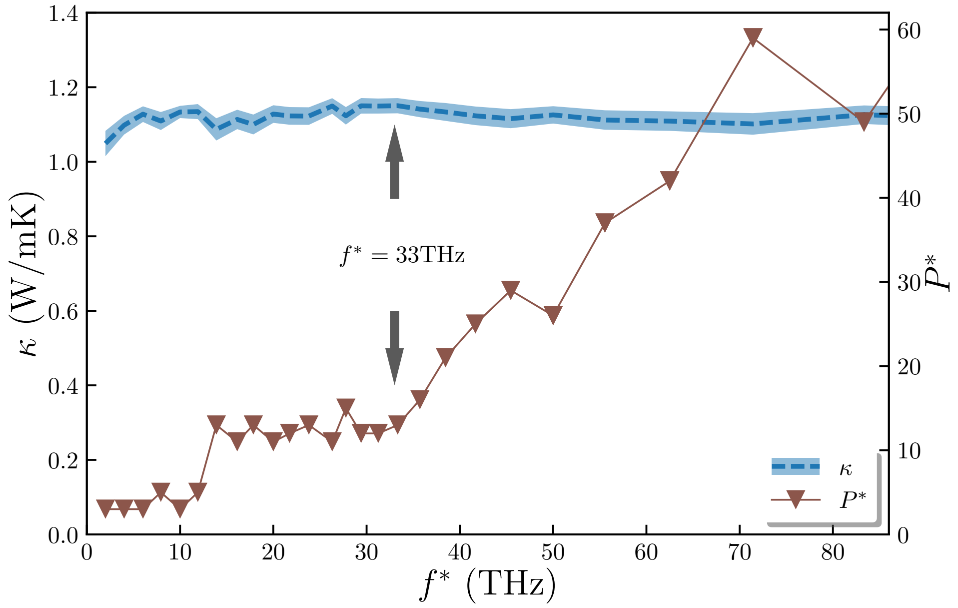

Figure 5.7: Conductivity κ (scale on the left) and number of cepstral coefficients P^* (scale on the right) as functions of the resampling frequency f^*. After a saturation region, where P^* is constant with respect to f^*, the relationship between P^* and f^* becomes linear. The arrow points at the frontier of these two regions, where the error on κ is at its minimum.

- Evaluate the thermal conductivity and its statistical error as explained in eq. (3.73) and (3.74):

$$\kappa = \frac{\Omega}{2k_{\mathrm{B}}T^2} \exp\left[\sum_{n=-P^*+1}^{P^*-1} {}^{\ell M}\hat{C}_n - \psi(\ell - M + 1) - \log(\ell - M + 1)\right] \tag{5.5}$$

$$\varepsilon_\kappa = \kappa\sqrt{\psi'(\ell - M + 1)\frac{4P^* - 2}{N}}. \tag{5.6}$$

Let us now take as an example a particular set of data, say the results of the simulation performed at ≈ 300K, and go through each of the steps above to get to the estimate of the conductivity of MB-pol water. The software `thermocepstrum` [Ercole and Bertossa, 2018] already mentioned above, is a python module designed specifically to handle the computation of thermal conductivities via cepstral analysis. The original software, available as an open source project on GitHub, has been forked and slightly extended by the author of this thesis.

The heat flux and the non-diffusive mass flux as written by the MD package `DL_POLY` modified as described in section 4 have been computed in a long simulation run. Figure 5.6 presents a sample of the $\mathbf{J}_{\mathrm{q}}$ trajectory. The fluxes have been fed to `thermocepstrum`, where the discrete Fourier transforms have been calculated and rearranged to get the cross-periodograms and, in the end, the multi-component periodogram.

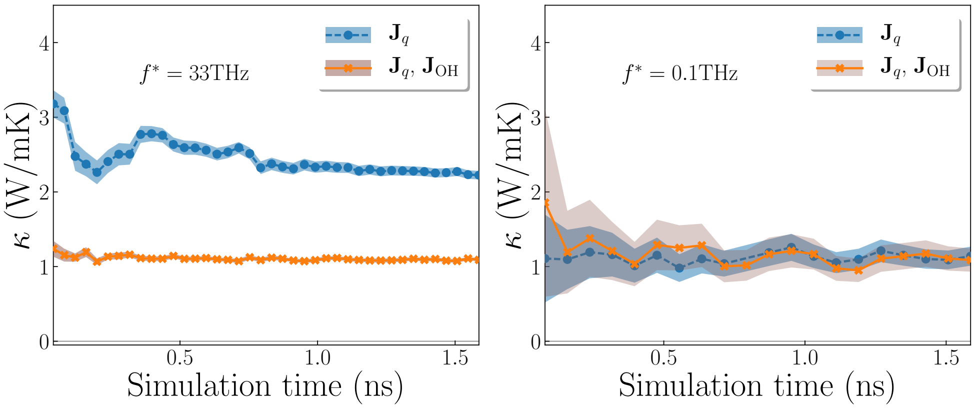

Figure 5.8: Thermal conductivity versus simulation time computed with the heat flux alone (one-component analysis) and with both the heat flux and the non-convective $\mathbf{J}_{\mathrm{OH}}$ (two-component analysis). On the left, the resampling frequencies for the cepstral analysis have been chosen adopting the method of figure 5.11. On the right, the same parameter is set to 0.1THz: this is the value for which the spectrum in figure 5.9 abruptly drops.

Convergence with respect to the resampling frequency

The spectrum whose logarithm we want to analyze goes to zero above the Nyquist frequency; moreover, it often happens that the spectrum is gapped, i.e. it features frequency regions where its value is almost negligible with respect to the value of the peaks. This implies that the logarithm of the periodogram, i.e. the time-series that is analyzed via the cepstral technique, in these regions would tend to diverge, since $\lim_{x\to 0}\log(x) = -\infty$. To avoid this drawback, one can resample the time-series of the heat flux to lower its Nyquist frequency to a safer value. The procedure of resampling goes like this:

1. Choose a tentative value f^* for the new Nyquist frequency. One should aim to move the Nyquist frequency to a region right after a peak: usually the lowest frequency peak is a good choice, if the gap between the first two peaks is sufficiently large;
2. Find the new sampling rate as $\varepsilon^* = 1/2f^*$ and, if necessary, round it to the nearest multiple of the actual sampling rate of the original heat flux time-series;
3. Apply a low-pass filter of the heat flux time-series with a window as large as ε^*, e.g. with a moving average. This helps to avoid aliasing effects on the resulting signal, being the initial time-series very noisy;
4. Resample the time-series with the desired sampling rate.

The output signal is then analyzed as discussed above. To understand if resampling the multi-component periodogram is useful to get a better result from the available data, `thermocepstrum` has been instructed to perform a sequence of conductivity computations with resampling frequencies ranging from 0.1THz to 80THz. From equation (3.74) at page 32 it is clear that if

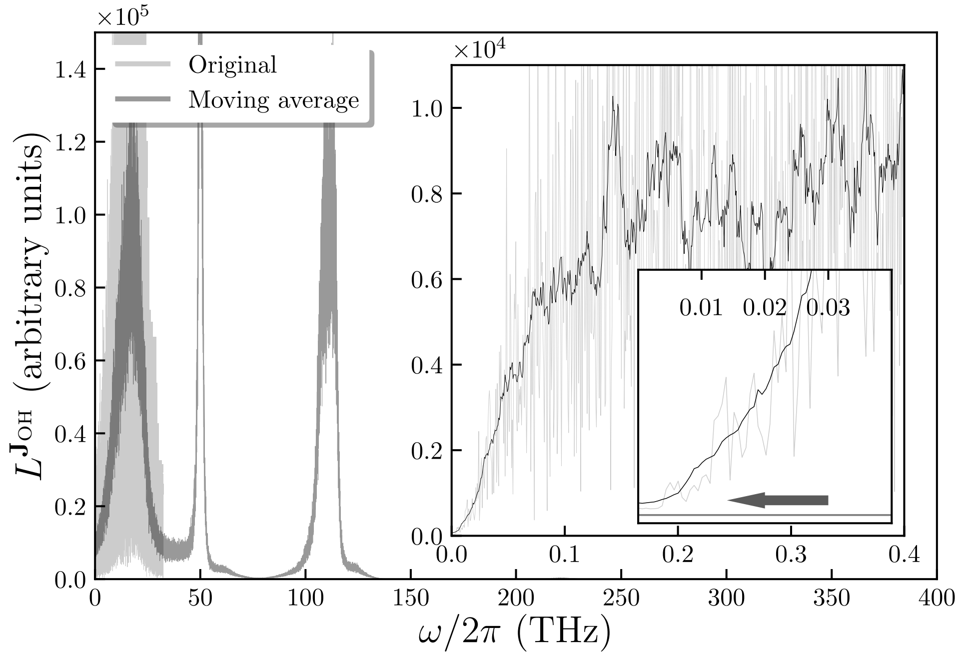

Figure 5.9: Periodogram of the non-convective flux $\mathbf{J}_{\mathrm{OH}}$. The magnified picture exhibits the very-low-frequency part of the spectrum: the zero-frequency value is the Onsager's coefficient $L^{\mathbf{J}_{\mathrm{OH}}}$ related to this flux. Being $\mathbf{J}_{\mathrm{OH}}$ non-convective, $L^{\mathbf{J}_{\mathrm{OH}}}$ must be equal to zero. Despite being not exactly zero due to the finite length of the MD trajectory, the zero-frequency value of the periodogram seems to approach zero. However, the change is abrupt at very low frequency. This behavior is found in the periodogram of the heat flux as well.

P^* and N, the latter being proportional to the resampling frequency[2], are linearly related, the error on κ is constant. On the other hand, when P^* is constant with respect to f^*, the error decreases.

In figure 5.7, after an initial region, where the number of retained cepstral coefficients is too low to be meaningful, there is a plateau in the graph of P^*: the end of the plateau is where the error on the conductivity is at its lowest value. The resampling frequency corresponding to that value should be the selected one. In the case of $T \approx 350$K, the best resampling frequency happens to be $f^* = 33.0$THz. The same policy has been applied to each available temperature.

Convergence with respect to simulation time

For benchmarking purposes, it is useful to know after how many simulation steps the value of the conductivity calculated via cepstral analysis stabilizes around some value. For this reason, the computed conductivity has been studied as a function of the simulation time.

---

[2] The value of f^* is the chosen Nyquist frequency, i.e.

$$f^* = 1/2\varepsilon = N/2\mathcal{T},$$

where $\mathcal{T}$ is the simulation time and ε is the sampling rate. That means $f^* \propto N$.

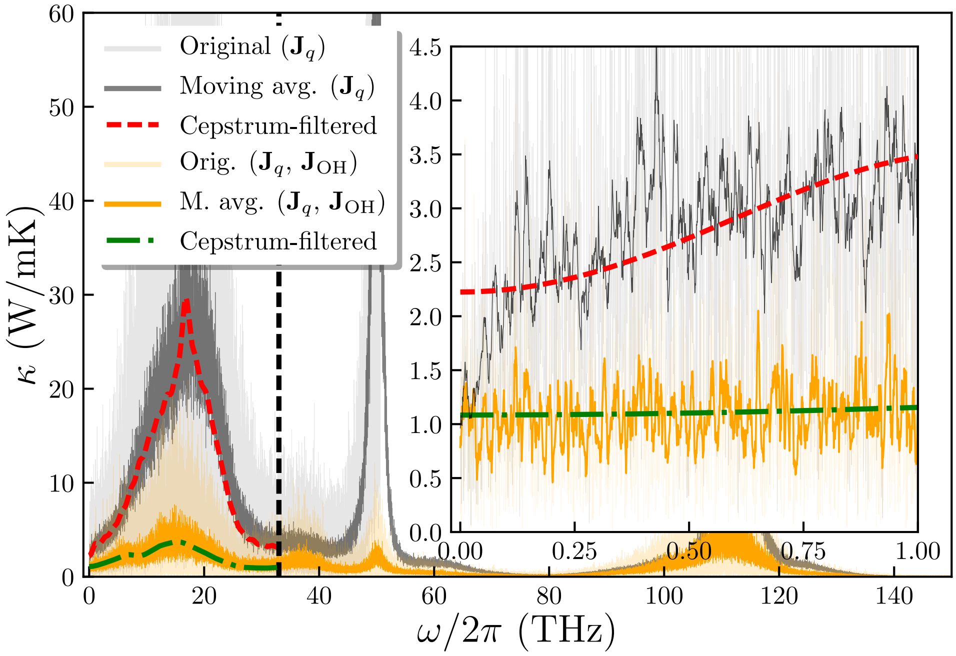

Figure 5.10: Comparison between the low-frequency periodograms obtained with the energy flux alone and with the multi-component analysis of the energy flux and $\mathbf{J}_{\mathrm{OH}}$. The intermediate filtering is done via a moving average with a window of $0.01\mathrm{THz}$ to visualize the qualitative behavior of the spectra: they have not been used to obtain any quantitative value. The trend near zero of the one-component spectrum is not matched by the cepstral filter: the drop is too abrupt. Instead, the qualitative behavior is correct, with the two periodograms assuming similar values near the origin.

Figure 5.9 displays the behavior of the periodogram of the non-diffusive flux $\mathbf{J}_{\mathrm{OH}}$ at low frequencies. The periodogram behaves as expected near $\omega{=}0$: despite being not exactly zero, due to the finite length of the MD simulation, the filtered periodogram seems to approach zero for very low frequencies. However, the change is abrupt in the very narrow window under $\approx 0.1\mathrm{THz}$. As one can see in figure 5.10, this behavior is found in the periodogram of the heat flux, too; in the latter case, the value in zero is positive, as it must be. To investigate the possible correlations between the two fluxes, two-component analysis has been performed on the heat flux and the non-diffusive mass flux. The result is shown in figure 5.10, together with the heat flux periodogram. In the very low frequency region, the two values tend to be the same; still, the two-component periodogram is flatter than the heat flux periodogram. Cepstral analysis works better with smooth periodograms: an abrupt change in the spectrum is not easy to match as it requires a large number of cepstral coefficients for a small portion of signal. Moreover, the value of the conductivity computed via one-component analysis on the heat flux depends strongly on the resampling frequency: this suggests that there are some problems in the filtering of the signal near zero. The value of κ has been computed as a function of the simulation time at two different resampling frequencies, using both the simple one-component analysis and the two-component analysis (fig. 5.8).

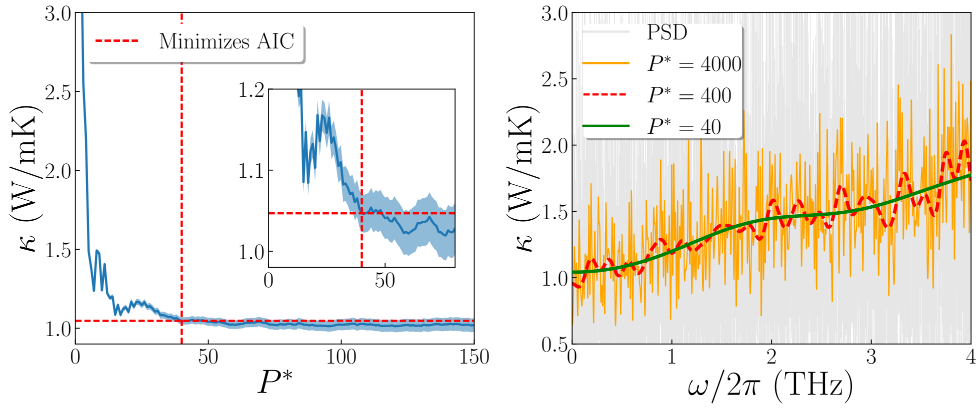

Figure 5.11: Conductivity computed via cepstral analysis as a function of the number of retained cepstral coefficient. The crossing dashed lines identify the value of κ given by the P^* that minimizes the Akaike Information Criterion of eq. (3.49).

While the two-component conductivity computed with a resampling frequency of 33THz is compatible with the same quantity computed with a resampling frequency of 0.1THz, this is not true for the thermal conductivity calculated from the periodogram of the heat flux alone. With f^*=0.1THz, the one component and two-components conductivities are compatible. This is symptomatic of the pathological behavior of the periodogram of the heat flux: the resampling frequency is so low that the only portion of the periodogram that is being analyzed is the badly behaved part. There is a small number of data points, so the error is large; however, the value of κ is correct within the errorbars, since the cepstral filter has to recover the low-lying behavior of an almost linear signal. With f^*=33.0THz, the conductivity of obtained from the cepstral analysis of the periodogram of the heat flux is larger than the one obtained with two-components analysis. The low-frequency behavior of the periodogram of $\mathbf{J}_{\mathrm{OH}}$ and of $\mathbf{J}_{\mathrm{q}}$ compared with the smoother low-frequency behavior of the two-component spectrum strongly suggests to always perform a two-component analysis, even when the system under exam is not genuinely a two-component fluid, but simply a molecular fluid, such as in our case. This is the route we will follow in the next sections.

To investigate a possible reason behind the sudden drop of the value of the periodogram at low frequency, it could be insightful to investigate size effects. Green-Kubo theory is built upon the hypothesis of thermodynamic limit, where volumes and number of particles are taken to be infinite. In particular, the fact that the non-diffusive flux exhibits non-zero transport coefficient could be a symptom of spurious correlations due to the imposed periodicity of the cell boundary conditions. However, these effects should not be preponderant, since we are dealing with a liquid system.

The choice of P^*

As discussed in section 3.3 when talking about the cepstral technique, the computed value of the conductivity depends on the number P^* of cepstral coefficients that one keeps when Fourier-transforming back the log-spectrum of the fluxes.

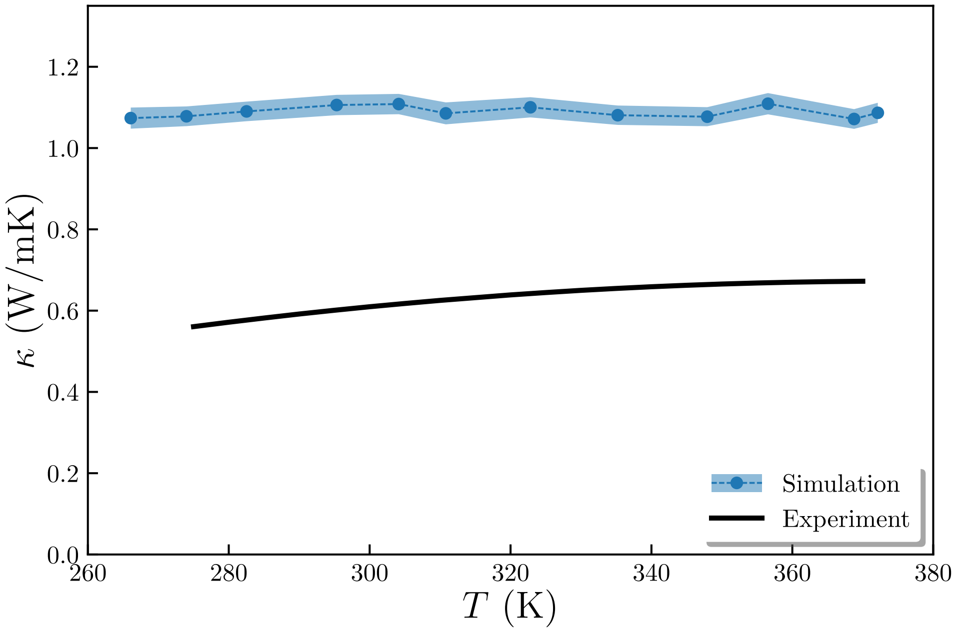

Figure 5.12: Conductivity of the MB-pol model obtained via the cepstral analysis of the heat flux time series. The dashed line is a quadratic fit on the data. The solid line is obtained from the experimental referece data at ampient pressure. The computed values of κ are not compatible with the experimental data [Ramires et al., 1995].

Figure 5.11 (left) shows the plot of the conductivity as a function of the number of retained cepstral coefficients. The intersection of the dashed lines locates the value of κ that minimizes the function $\mathrm{AIC}(P)$ of equation (3.49). The plot on the right shows the filtering power of the cepstral analysis: the higher the value of P^*, the noisier the signal.

Of course, a further reduction of P^* would yields a cleaner spectrum, since it means to discard a larger number of high-frequency terms: the role of the Akaike Information Criterion is to decide when to stop throwing away high-frequency components and leave only those components necessary to reconstruct the large-scale behavior of the spectrum.

Thermal conductivity

After the preliminary analysis, let us finally present the results of the calculations of the thermal conductivity as a function of temperature. Figure 5.12 displays the values of κ obtained with the methodology exposed above. The values are not compatible with the experimental results, but larger. This is not uncommon for flexible models, that tend to overestimate the magnitude of the thermal conductivity.

A comprehensive account for what concern the thermal conductivity of various models is given by Sirk et al., 2013, both for equilibrium (G. K.) and non-equilibrium molecular dynamics (NEMD) in the Müller-Plathe flavor [Müller-Plathe, 1997]. The values of κ at ambient conditions ($\approx 300\mathrm{K}$ and $\approx 1\mathrm{atm}$) for different models are:

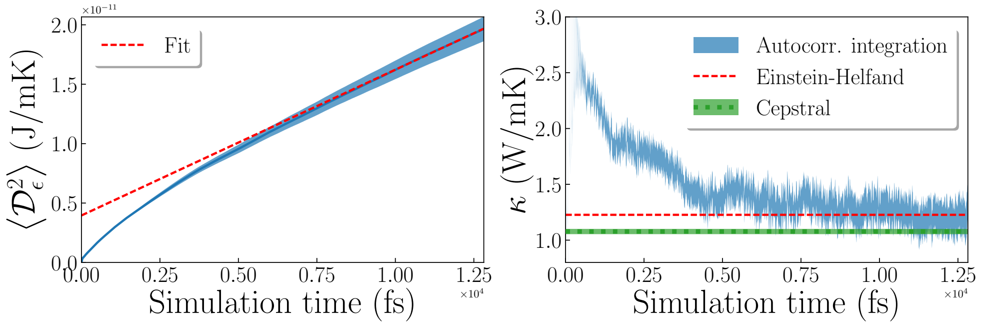

Figure 5.13: On the left, the so-called *energy displacement* as a function of the simulation time. A linear fit of the terminal part of the graph provides an estimate of the thermal conductivity. On the right, the comparison of the actual Green-Kubo integral as a function of the simulation time with the Einstein-Helfand estimate and with the cepstral estimate.

	Rigid models	
Model	NEMD (W/mK)	G.K. (W/mK)
SPC	0.802	0.776
SPC/E	0.821	0.806
TIP3P-Ew	0.814	0.797
TIP4P-Ew	0.766	0.816
	Flexible models	
Model	NEMD (W/mK)	G.K. (W/mK)
SPC/Fw	1.011	0.854
SPC/Fd	0.997	0.793
TIP3P/Fs	1.063	0.851

It is important to notice that the thermal conductivities listed above are computed via direct trapezoidal integration of the autocorrelation function of a 1ns long heat flux time-series. Although the models above are simpler than MB-pol, i.e. they present a less complex form of interaction, we are apt to think that such a relatively short trajectory may not be sufficient to obtain an accurate estimate of the value of κ, *a fortiori* for the fact that the Einstein-Helfand method is not mentioned in the original paper. Moreover, there is no clarity on the method used to obtain an estimate on the error bar.

Comparison with the Green-Kubo integral

In conclusion, let us compare the cepstral analysis technique with the standard Green-Kubo integral approach via the Einstein-Helfand approximation. Fig. 5.13 (left) shows the mean value of the square of the energy displacement for MB-pol water at $\approx$ 347K. The thermal conductivity is the asymptotic slope of the graph. The error bars are obtained via block analysis on the heat flux time-series with 100 blocks. On the right, the integral of the time autocorrelation function is plotted together with the values of κ as given by the linear fit of $\langle \mathcal{D}_\epsilon^2 \rangle$, and by the cepstral analysis.

The values are not compatible, but this is not surprising: the Einstein-Helfand approach requires very long trajectories to achieve convergence, and this is not affordable with the MB-pol potential. As proved in the literature [Ercole, Marcolongo, et al., 2017], for sufficiently long trajectories the Einstein-Helfand method yields results compatible with cepstral analysis, and that is what is expected in this case.

6 CONCLUSIONS

In this study we have applied the Green-Kubo linear response theory to compute the thermal conductivity κ to the MB-pol model of water. To determine the heat flux, we have written the computer code that enables the separation of the total energy and the virial stress into atomic contributions in a version of the molecular dynamics package `DL_POLY` that already contained an implementation of MB-pol.

Our aim was to compute the thermal conductivity of MB-pol water in the temperature range for which water is liquid at ambient pressure. After an equilibration phase, where the system has been prepared at the desired values of temperature and pressure via thermostats and barostats, some thermodynamic and structural properties have been calculated. This phase has served to validate of the physical state of the simulated system. Computed density, diffusivity and radial distribution functions are consistent with the results found in the literature and accurate with respect to experiments.

The simulations of the equilibrated systems have been carried out for more than $1\mathrm{ns}$ in the microcanonical ensemble to acquire the heat flux time-series. This quantity has been analyzed together with the non-diffusive particle flux $\mathbf{J}_{\mathrm{OH}}$ using the *cepstral* technique, a recently developed statistical method to filter out the non-Gaussian noise from the log-periodogram of the heat flux. The cepstral technique has proven to reproduce the results of the well known integration of the heat flux time-autocorrelation function, with the advantage of requiring shorter trajectories. This approach, together with the *gauge invariance* of thermal conductivity, makes the Green-Kubo approach to thermal transport affordable in an *ab initio* framework.

Given the great accuracy demonstrated by the MB-pol model for a wide range of properties of water, we expected to retrieve a similar degree of veracity in the computation of the thermal conductivity. That has not revealed to be the case: in fact, the collected results are of the order of $1.0\mathrm{W/mK}$ in the whole temperature range, while the experimental value is of the order of $0.6\mathrm{W/mK}$, at the same thermodynamic conditions. The overestimation is of about 60%, while other water models usually overestimate the quantity of approximately 30%. There could multiple reasons behind this discrepancy:

- MB-pol mimics the hydrogen bonding of pairs and triplets of water molecules via an elaborate fitting polynomial that involves the positions of many atoms at the same time. The many-body nature of the interaction introduces correlations that fatten the tail of the heat flux time-autocorrelation function: this may enlarge the convergence time of its integral and consequently complicates the estimation of the thermal conductivity;

- The electrostatic contribution to the energy and the forces takes into account the polarizable nature of water, with the self-consistent computation of the induced dipoles at every step. This feature, albeit providing excellent results for other properties of water, may introduce correlations that affect the computation. Moreover, Römer et al., 2012 showed that the explicit polarizability and molecular flexibility are not needed to achieve results that are in good agreement with experiments, including the existence of an anomalous maximum value of κ.

- Finite size effects might alter the value of the conductivity derived from the spectrum of the heat flux. An analogous effect exists for diffusivity and shear viscosity [Yeh and Hummer, 2004], that are transport coefficients as well. However, in the case of diffusivity, size-effects do not seem to be relevant for 256 molecules, i.e. the number of molecules used in our simulations.

To better understand the obtained results, a possible route is the systematic analysis of the various contributions to the heat flux coming from the different forms of interactions that constitute MB-pol. This would help to interpret how the value of κ arises from the heat fluxes related to the different interaction terms, and to troubleshoot possible localized problems in the implementation.

Direct comparison of MB-pol and other implementations of water models that yield results in better agreement with experiments could be useful to spot what the most slowly converging terms are and how to improve their computation. A more in-depth study of the possible presence of non-diffusive fluxes that hinder the convergence of the value of κ may shed light on how to efficiently decorrelate the heat flux from all the other fluxes, and achieve accurate results with shorter simulations. A systematic size-effects study should highlight the presence of convergence problems related to the finite size of the simulated system, or at least it would let us single out this hypothesis. In conclusion, to validate or discard the values computed in this work, it could be useful to compute the conductivity with other methods, such as the non-equilibrium technique introduced by Müller-Plathe.

From the data analysis perspective, the use of two-component cepstral analysis in the case of a molecular fluid, aimed at the decorrelation of the heat flux from the non-diffusive fluxes, has been validated and proven to yield better and faster convergence on the computed value of κ. This has been shown to be essential to achieve a robust estimate of the thermal conductivity, with low dependence on the choice of parameters such as the resampling frequency and the number of cepstral coefficients to retain in the filtering process. We suggest this to become the standard prescription for molecular fluids and, in general, multi-component fluids for whom non-diffusive fluxes can be defined.

A ELECTROSTATIC ENERGY OF A CONFIGURATION

THE TOTAL electrostatic energy of a configuration of charges and dipoles can be expressed as:

$$U_{\text{elec,tot}} = U^{(\text{CC})} + U^{(\text{CD})} + U^{(\text{DD})} + U_{\text{pol}}, \tag{A.1}$$

where CC stands for charge-charge interaction, CD for charge-dipole, DD for dipole-dipole and *pol* stands for polarization.

A.1 CHARGE-CHARGE INTERACTION

The interaction energy $U_{ab}^{(\text{CC})}$ of two point charges q_a placed in $\mathbf{R}_a$ and q_b placed in $\mathbf{R}_b$ is given by the product of one of the charges (e.g. q_a) and the Coulomb potential ϕ_{C} generated by the other (q_b):

$$\phi_{\text{C}}(|\mathbf{r} - \mathbf{R}_b|) = \frac{q_b}{|\mathbf{r} - \mathbf{R}_b|}, \tag{A.2}$$

$$\begin{aligned} U_{ab}^{(\text{CC})} =& q_a \phi_{\text{C}}(|\mathbf{R}_a - \mathbf{R}_b|) \\ =& \frac{q_a q_b}{|\mathbf{R}_a - \mathbf{R}_b|} \\ \equiv& \frac{q_a q_b}{R_{ab}}. \end{aligned} \tag{A.3}$$

When there are many particles, the total charge-charge contribution to the energy is:

$$U^{(\text{CC})} = \tfrac{1}{2} \sum_{a \neq b} \frac{q_a q_b}{R_{ab}}. \tag{A.4}$$

A.2 CHARGE-DIPOLE INTERACTION

The interaction energy U_{ab}^{CD} of a point charge q_a placed in $\mathbf{R}_a$ and a dipole $\boldsymbol{\mu}_b = q_b \mathbf{l}_b$ made of a pair of charges $\pm q_b$ placed in $\mathbf{R}_b$ and $\mathbf{R}_b + \mathbf{l}_b$, where

$l_b \ll R_{ab}$ can be obtained as a first order expansion of the Coulomb interaction between the charge q_a and the two charges $\pm q_b$:

$$\begin{aligned} U_{ab}^{(\text{CD})} =& \frac{q_a(-q_b)}{R_{ab}} + \frac{q_a q_b}{|\mathbf{R}_a - \mathbf{R}_b - \mathbf{l}_b|} \\ =& -\frac{q_a q_b}{R_{ab}} \left[1 - \frac{1}{\sqrt{1 + l_b^2/R_{ab}^2 - 2\mathbf{R}_{ab} \cdot \mathbf{l}_b / R_{ab}^2}} \right] \\ =& -\frac{q_a q_b}{R_{ab}} \left[1 - \left(1 + \frac{\mathbf{R}_{ab} \cdot \mathbf{l}_b}{R_{ab}^2} + \mathcal{O}\left(\frac{\mathbf{l}_b^2}{R_{ab}^2} \right) \right) \right] \\ \simeq& \frac{q_a \mathbf{R}_{ab} \cdot (q_b \mathbf{l}_b)}{R_{ab}^3} \\ =& \frac{q_a \mathbf{R}_{ab} \cdot \boldsymbol{\mu}_b}{R_{ab}^3}. \end{aligned} \tag{A.5}$$

When there are many particles, the total charge-dipole contribution to the energy is:

$$U^{(\text{CD})} = \tfrac{1}{2} \sum_{a \neq b} \frac{q_a \mathbf{R}_{ab} \cdot \boldsymbol{\mu}_b}{R_{ab}^3}. \tag{A.6}$$

A.3 DIPOLE-DIPOLE INTERACTION

In analogy with what done before, the dipole-dipole interaction will be obtained from the second order expansion of the Coulomb interaction between a pair of dipoles $\boldsymbol{\mu}_a$ in $\mathbf{R}_a$ and $\boldsymbol{\mu}_b$ in $\mathbf{R}_b$:

$$\begin{aligned} U_{ab}^{(\text{DD})} =& \frac{(-q_a)(-q_b)}{R_{ab}} + \frac{(-q_a)q_b}{|\mathbf{R}_a - \mathbf{R}_b - \mathbf{l}_b|} + \frac{q_a(-q_b)}{|\mathbf{R}_a + \mathbf{l}_a - \mathbf{R}_b|} + \frac{q_a q_b}{|\mathbf{R}_a + \mathbf{l}_a - \mathbf{R}_b - \mathbf{l}_b|} \\ =& q_a q_b \left[\frac{1}{R_{ab}} - \frac{1}{\sqrt{R_{ab}^2 + l_b^2 - 2\mathbf{R}_{ab} \cdot \mathbf{l}_b}} - \frac{1}{\sqrt{R_{ab}^2 + l_a^2 + 2\mathbf{R}_{ab} \cdot \mathbf{l}_a}} + \right. \\ & \left. + \frac{1}{\sqrt{R_{ab}^2 + l_a^2 + l_b^2 - 2\mathbf{R}_{ab} \cdot \mathbf{l}_b + 2\mathbf{R}_{ab} \cdot \mathbf{l}_a - 2\mathbf{l}_a \cdot \mathbf{l}_b}} \right]. \end{aligned} \tag{A.7}$$

At the first order in the expansion of the inverse square roots in the above equation, the only term who does not cancel due to sign differences is the $\mathbf{l}_a \cdot \mathbf{l}_b$ part coming from the last term. At the second order, only the cross terms between $2\mathbf{R}_{ab} \cdot \mathbf{l}_a$ and $-2\mathbf{R}_{ab} \cdot \mathbf{l}_b$ survive, for the same reason. So what remains is:

$$\begin{aligned} U_{ab}^{(\text{DD})} =& \frac{q_a q_b}{R_{ab}} \left[\frac{\mathbf{l}_a \cdot \mathbf{l}_b}{R_{ab}^2} + \tfrac{3}{8} \left(\frac{-8(\mathbf{R}_{ab} \cdot \mathbf{l}_a)(\mathbf{R}_{ab} \cdot \mathbf{l}_b)}{R_{ab}^4} \right) \right] \\ =& \frac{q_a q_b}{R_{ab}} \left[\frac{\mathbf{l}_a \cdot \mathbf{l}_b}{R_{ab}^2} - 3 \frac{(\mathbf{R}_{ab} \cdot \mathbf{l}_a)(\mathbf{R}_{ab} \cdot \mathbf{l}_b)}{R_{ab}^4} \right] \\ =& \frac{\boldsymbol{\mu}_a \boldsymbol{\mu}_b}{R_{ab}^3} - 3 \frac{(\mathbf{R}_{ab} \cdot \boldsymbol{\mu}_a)(\mathbf{R}_{ab} \cdot \boldsymbol{\mu}_b)}{R_{ab}^5}. \end{aligned} \tag{A.8}$$

When there are many particles, the total dipole-dipole contribution to the energy is:

$$U^{(\mathrm{DD})} = \tfrac{1}{2}\sum_{a\neq b}\left[\frac{\boldsymbol{\mu}_a\boldsymbol{\mu}_b}{R_{ab}^3} - 3\frac{(\mathbf{R}_{ab}\cdot\boldsymbol{\mu}_a)(\mathbf{R}_{ab}\cdot\boldsymbol{\mu}_b)}{R_{ab}^5}\right]. \tag{A.9}$$

A.4 POLARIZATION ENERGY

The polarization contribution is the difference between the total electrostatic energy and the sum of the terms found up to now:

$$\begin{aligned}
U_{\text{pol}} =& U_{\text{elec,tot}} - (U^{(\mathrm{CC})} + U^{(\mathrm{CD})} + U^{(\mathrm{DD})}) \\
=& U_{\text{elec,tot}} - \tfrac{1}{2}\sum_{a\neq b}\frac{q_a q_b}{R_{ab}} - \tfrac{1}{2}\sum_{a\neq b}\left\{\frac{q_a\mathbf{R}_{ab}\cdot\boldsymbol{\mu}_b}{R_{ab}^3} + \left[\frac{\boldsymbol{\mu}_a\boldsymbol{\mu}_b}{R_{ab}^3} + \right.\right. \\
& \left.\left. -3\frac{(\mathbf{R}_{ab}\cdot\boldsymbol{\mu}_a)(\mathbf{R}_{ab}\cdot\boldsymbol{\mu}_b)}{R_{ab}^5}\right]\right\} \\
=& U_{\text{tot}} - \tfrac{1}{2}\sum_{a\neq b}\frac{q_a q_b}{R_{ab}} + \\
& -\sum_b \boldsymbol{\mu}_b\cdot\tfrac{1}{2}\sum_{a(\neq b)}\left[\frac{q_a(-\mathbf{R}_{ba})}{R_{ba}^3} + \left(\frac{\boldsymbol{\mu}_a}{R_{ba}^3} - 3\frac{(\mathbf{R}_{ba}\cdot\boldsymbol{\mu}_a)\mathbf{R}_{ba}}{R_{ba}^5}\right)\right] \\
=& U_{\text{tot}} - \left\{\tfrac{1}{2}\sum_{a\neq b}\frac{q_a q_b}{R_{ab}} + \right. \\
& \left. -\sum_b \boldsymbol{\mu}_b\cdot\underbrace{\tfrac{1}{2}\sum_{a(\neq b)}\left[\frac{q_a\mathbf{R}_{ba}}{R_{ba}^3} + \left(3\frac{(\mathbf{R}_{ba}\cdot\boldsymbol{\mu}_a)\mathbf{R}_{ba}}{R_{ba}^5} - \frac{\boldsymbol{\mu}_a}{R_{ba}^3}\right)\right]}_{\mathbf{E}(\mathbf{R}_b)\text{ generated by the rest of the sources}}\right\} \\
=& U_{\text{tot}} - \left[\tfrac{1}{2}\sum_{a\neq b}\frac{q_a q_b}{R_{ab}} - \sum_b \boldsymbol{\mu}_b\cdot\mathbf{E}(\mathbf{R}_b)\right].
\end{aligned} \tag{A.10}$$

In equilibrium, the total energy is invariant under small variations $\mathrm{d}\boldsymbol{\mu}$ of the induced dipoles; thus:

$$\begin{aligned}
\mathrm{d}U_{\text{pol}} =& \mathrm{d}U_{\text{elec,tot}} + \sum_b \mathrm{d}\boldsymbol{\mu}_b\cdot\mathbf{E}(\mathbf{R}_b) \\
=& \sum_b \mathrm{d}\boldsymbol{\mu}_b\cdot\mathbf{E}(\mathbf{R}_b);
\end{aligned} \tag{A.11}$$

since the molecules are globally neutral, only the dipole contribution to the electric field will be relevant. Hence, the electric field at site b will be, in equilibrium:

$$\mathbf{E}(\mathbf{R}_b) = \tfrac{1}{\alpha_b}\boldsymbol{\mu}_b. \tag{A.12}$$

The variation in polarization energy becomes:

$$\begin{aligned} \mathrm{d}U_{\mathrm{pol}} &= \sum_b \tfrac{1}{\alpha_b} \mathrm{d}\boldsymbol{\mu}_b \cdot \boldsymbol{\mu}_b \\ &= \sum_b \tfrac{1}{2\alpha_b} \mathrm{d}(\boldsymbol{\mu}_b \cdot \boldsymbol{\mu}_b). \end{aligned} \tag{A.13}$$

If the process of polarizing the molecules is reversible, then the above expression is the differential of an analytic function and one can integrate it to get:

$$U_{\mathrm{pol}} = \sum_b \tfrac{1}{2\alpha_b} \boldsymbol{\mu}_b \cdot \boldsymbol{\mu}_b. \tag{A.14}$$

Finally, the total energy of a configuration of charges and dipoles is:

$$\begin{aligned} U_{\text{elec,tot}} =& \tfrac{1}{2} \sum_{a \neq b} \frac{q_a q_b}{R_{ab}} + \tfrac{1}{2} \sum_{a \neq b} \frac{q_a \mathbf{R}_{ab} \cdot \boldsymbol{\mu}_b}{R_{ab}^3} + \\ &+ \tfrac{1}{2} \sum_{a \neq b} \left[\frac{\boldsymbol{\mu}_a \boldsymbol{\mu}_b}{R_{ab}^3} - 3 \frac{(\mathbf{R}_{ab} \cdot \boldsymbol{\mu}_a)(\mathbf{R}_{ab} \cdot \boldsymbol{\mu}_b)}{R_{ab}^5} \right] + \sum_b \tfrac{1}{2\alpha_b} \boldsymbol{\mu}_b \cdot \boldsymbol{\mu}_b \end{aligned} \tag{A.15}$$

In equilibrium, when the induced dipoles are such that the total electrostatic energy is minimized, i.e.:

$$\forall \boldsymbol{\mu}_a \quad \frac{\partial U_{\text{elec,tot}}}{\partial \boldsymbol{\mu}_a} = 0, \tag{A.16}$$

the total energy can be written as:

$$U_{\text{elec,tot}} = \tfrac{1}{2} \sum_a \sum_{b(\neq a)} \frac{q_a q_b}{R_{ab}} - \tfrac{1}{2} \sum_a \boldsymbol{\mu}_a \cdot \mathbf{E}_a(\mathbf{R}_a), \tag{A.17}$$

where $\{\boldsymbol{\mu}_a\}$ are the dipoles which minimize the $U_{\text{elec,tot}}$ and $\mathbf{E}_a(\mathbf{R}_a)$ is the electric field at site a due to the other charges and dipoles.

A.5 THOLE-TYPE MODEL (TTM)

In a TTM framework, the point charges and the dipoles in the interaction terms are smeared on a volume around their position, to overcome the problem of divergent polarizability at short distances [Thole, 1981]. The prescription is to equip the inverse power law behavior of the interaction with functions λ_n in such way:

$$\frac{1}{R_{ab}^n} \mapsto \frac{\lambda_n(u_{ab})}{A_{ab}^n}, \tag{A.18}$$

where $u_{ab} = R_{ab}/A_{ab}$, $A_{ab} = (\alpha_a \alpha_b)^{1/6}$ and the λ functions are defined recursively as:

$$\lambda_{n+2}(u) = -\frac{1}{un} \frac{\partial \lambda_n(u)}{\partial u} \tag{A.19}$$

$$\lambda_1(u) = \frac{1 - \mathrm{e}^{-au^m}}{u} + a^{1/m} \Gamma\left(1 - \tfrac{1}{m}, au^m\right) \tag{A.20}$$

$$\Gamma(c, x) = \int_x^\infty \mathrm{d}t\, t^{c-1} \mathrm{e}^{-t} \tag{A.21}$$

The value of m is set to 4 in the TTM4-F model, which is the one implemented in the MB-pol potential for water; a is a fitting parameter, and Γ is the upper incomplete gamma function.

The electrostatic energy within this framework becomes:

$$\begin{aligned} U_{\text{tot}} =& \tfrac{1}{2}\sum_{a\neq b}\frac{q_a q_b \lambda_1(u_{ab})}{A_{ab}} + \tfrac{1}{2}\sum_{a\neq b}\frac{q_a \mathbf{R}_{ab}\cdot\boldsymbol{\mu}_b \lambda_3(u_{ab})}{A_{ab}^3} + \\ &+ \tfrac{1}{2}\sum_{a\neq b}\left[\frac{\boldsymbol{\mu}_a\boldsymbol{\mu}_b\lambda_3(u_{ab})}{A_{ab}^3} - 3\frac{(\mathbf{R}_{ab}\cdot\boldsymbol{\mu}_a)(\mathbf{R}_{ab}\cdot\boldsymbol{\mu}_b)\lambda_5(u_{ab})}{A_{ab}^5}\right] + \\ &+ \sum_b \tfrac{1}{2\alpha_b}\boldsymbol{\mu}_b\cdot\boldsymbol{\mu}_b \end{aligned} \tag{A.22}$$

The equilibrium expression for the interaction takes the form:

$$\begin{aligned} U_{\text{tot}} =& \tfrac{1}{2}\sum_a \sum_{b(\neq a)}\frac{q_a q_b \lambda_1(u_{ab})}{A_{ab}} - \tfrac{1}{2}\sum_a \boldsymbol{\mu}_a\cdot\mathbf{E}_a(\mathbf{R}_a) \\ \overset{\text{def}}{=}& \sum_a V_a^{\text{TTM,elec}} + V_a^{\text{TTM,ind}}. \end{aligned} \tag{A.23}$$

BIBLIOGRAPHY

Akaike, H.

1974 "A new look at the statistical model identification", *IEEE Transactions on Automatic Control*, 19, 6 [Dec. 1974], pp. 716-723, ISSN: 0018-9286, DOI: 10.1109/TAC.1974.1100705.

Allen, M.P. and D.J. Tildesley

1987 *Computer Simulation of Liquids*, Oxford science publications, Clarendon Press, ISBN: 9780198553755, https://books.google.com.tr/books?id=ibURAQAAIAAJ.

Babin, V., C. Leforestier, and F. Paesani

2013 "Development of a "First Principles" Water Potential with Flexible Monomers: Dimer Potential Energy Surface, VRT Spectrum, and Second Virial Coefficient", *J Chem Theory Comput*, 9, 12.

Babin, V., R. Medders G., and F. Paesani

2014 "Development of a "First Principles" Water Potential with Flexible Monomers. II: Trimer Potential Energy Surface, Third Virial Coefficient, and Small Clusters", *J Chem Theory Comput*, 10, 4.

Bertossa, Riccardo, Loris Ercole, and Stefano Baroni

2018 "Transport coefficients in multi-component fluids from equilibrium molecular dynamics" [Aug. 2018].

De Leeuw, S. W., J. W. Perram, and E. R. Smith

1980 "Simulation of electrostatic systems in periodic boundary conditions. I. Lattice sums and dielectric constants", *Proceedings of the Royal Society of London A: Mathematical, Physical and Engineering Sciences*, 373, 1752, pp. 27-56, ISSN: 0080-4630, DOI: 10.1098/rspa.1980.0135.

Einstein, A.

1905 "Über die von der molekularkinetischen Theorie der Wärme geforderte Bewegung von in ruhenden Flüssigkeiten suspendierten Teilchen", German, *Annalen der Physik*, 322, 8, pp. 549-560, DOI: 10.1002/andp.19053220806.

Ercole, Loris and Riccardo Bertossa

2018 *ThermoCepstrum. a code to estimate transport coefficients from the cepstral analysis of a multi-variate current stationary time series*, https://github.com/lorisercole/thermocepstrum.

Ercole, Loris, Aris Marcolongo, and Stefano Baroni

2017 "Accurate thermal conductivities from optimally short molecular dynamics simulations", *Scientific reports*, 7, 1, p. 15835.

Fourier, Jean Baptiste Joseph

1822 *Théorie Analytique de la Chaleur*, Cambridge Library Collection – Mathematics, Cambridge University Press, DOI: 10.1017/CBO9780511693229.

Green, Melville S.

1952 "Markoff Random Processes and the Statistical Mechanics of Time-Dependent Phenomena", *The Journal of Chemical Physics*, 20, 8, pp. 1281-1295, DOI: 10.1063/1.1700722, eprint: https://doi.org/10.1063/1.1700722, https://doi.org/10.1063/1.1700722.

1954 "Markoff Random Processes and the Statistical Mechanics of Time-Dependent Phenomena. II. Irreversible Processes in Fluids", *The Journal of Chemical Physics*, 22, 3, pp. 398-413, DOI: 10.1063/1.1740082.

Helfand, Eugene

1960 "Transport Coefficients from Dissipation in a Canonical Ensemble", *Phys. Rev.* 119 [1 July 1960], pp. 1-9, DOI: 10.1103/PhysRev.119.1.

Holz, Manfred, Stefan R. Heil, and Antonio Sacco

2000 "Temperature-dependent self-diffusion coefficients of water and six selected molecular liquids for calibration in accurate 1H NMR PFG measurements", *Phys. Chem. Chem. Phys.* 2 [20 2000], pp. 4740-4742, DOI: 10.1039/B005319H.

Humphrey, William, Andrew Dalke, and Klaus Schulten

1996 "VMD: visual molecular dynamics", *Journal of molecular graphics*, 14, 1, pp. 33-38.

Kadanoff, Leo P. and Paul C. Martin

1963 "Hydrodynamic equations and correlation functions", *Annals of Physics*, 24, pp. 419-469, ISSN: 0003-4916, DOI: https://doi.org/10.1016/0003-4916(63)90078-2.

Kubo, Ryogo

1957 "Statistical-Mechanical Theory of Irreversible Processes. I. General Theory and Simple Applications to Magnetic and Conduction Problems", *Journal of the Physical Society of Japan*, 12, 6, pp. 570-586, DOI: 10.1143/JPSJ.12.570.

Kubo, Ryogo, Mario Yokota, and Sadao Nakajima

1957 "Statistical-Mechanical Theory of Irreversible Processes. II. Response to Thermal Disturbance", *Journal of the Physical Society of Japan*, 12, 11, pp. 1203-1211, DOI: 10.1143/JPSJ.12.1203, eprint: https://doi.org/10.1143/JPSJ.12.1203, https://doi.org/10.1143/JPSJ.12.1203.

Marcolongo, Aris, Paolo Umari, and Stefano Baroni

2015 "Microscopic theory and quantum simulation of atomic heat transport", 12 [Mar. 2015].

Medders G., R., V. Babin, and F. Paesani

2014 "Development of a "First-Principles" Water Potential with Flexible Monomers. III. Liquid Phase Properties", *J Chem Theory Comput*, 8, 10.

Millot, Marius, Sebastien Hamel, J Ryan Rygg, Peter M. Celliers, Gilbert W. Collins, Federica Coppari, Dayne E. Fratanduono, Raymond Jeanloz, Damian Swift, and J Eggert

2018 "Experimental evidence for superionic water ice using shock compression", 14 [Feb. 2018].

Müller-Plathe, Florian

1997 "A simple nonequilibrium molecular dynamics method for calculating the thermal conductivity", *The Journal of Chemical Physics*, 106, 14, pp. 6082-6085, DOI: `10.1063/1.473271`.

Onsager, Lars

1931a "Reciprocal Relations in Irreversible Processes. I." *Phys. Rev.* 37 [4 Feb. 1931], pp. 405-426, DOI: `10.1103/PhysRev.37.405`, `https://link.aps.org/doi/10.1103/PhysRev.37.405`.

1931b "Reciprocal Relations in Irreversible Processes. II." *Phys. Rev.* 38 [12 Dec. 1931], pp. 2265-2279, DOI: `10.1103/PhysRev.38.2265`, `https://link.aps.org/doi/10.1103/PhysRev.38.2265`.

Paesani, F.

2016 "Getting the Right Answers for the Right Reasons: Toward Predictive Molecular Simulations of Water with Many-Body Potential Energy Functions", *Accounts of Chemical Research*, 49, 9, pp. 1844-1851.

Partridge, H. and D. W. Schwenke

1997 "The determination of an accurate isotope dependent potential energy surface for water from extensive ab initio calculations and experimental data", *J Chem Phys*, 106, 11, pp. 4618-4639, DOI: `10.1063/1.473987`.

Peligrad, Magda and Wei Biao Wu

2010 "Central limit theorem for Fourier transforms of stationary processes", *Ann. Probab.* 38, 5 [Sept. 2010], pp. 2009-2022, DOI: `10.1214/10-AOP530`, `https://doi.org/10.1214/10-AOP530`.

Ramires, Maria L. V., Carlos Nieto de Castro, Yuchi Nagasaka, Akira Nagashima, Marc Assael, and William Wakeham

1995 "Standard Reference Data for the Thermal Conductivity of Water", 24 [May 1995], p. 1377.

Reddy, Sandeep K., Shelby C. Straight, Pushp Bajaj, C. Huy Pham, Marc Riera, Daniel R. Moberg, Miguel A. Morales, Chris Knight, Andreas W. Götz, and Francesco Paesani

2016 "On the accuracy of the MB-pol many-body potential for water: Interaction energies, vibrational frequencies, and classical thermodynamic and dynamical properties from clusters to liquid water and ice", *The Journal of Chemical Physics*, 145, 19, p. 194504, DOI: `10.1063/1.4967719`.

Römer, Frank, Anders Lervik, and Fernando Bresme

2012 "Nonequilibrium molecular dynamics simulations of the thermal conductivity of water: A systematic investigation of the SPC/E and TIP4P/2005 models", *The Journal of Chemical Physics*, 137, 7, p. 074503, DOI: `10.1063/1.4739855`.

Sirk, Timothy W., Stan Moore, and Eugene F. Brown

2013 "Characteristics of thermal conductivity in classical water models", *The Journal of Chemical Physics*, 138, 6, p. 064505, DOI: `10.1063/1.4789961`.

Thole, B. T.

1981 "Molecular polarizabilities calculated with a modified dipole interaction", *Chemical Physics*, 59 [Aug. 1981], pp. 341-350, DOI: `10.1016/0301-0104(81)85176-2`.

Wagner, W. and A. Pruß

2002 "The IAPWS Formulation 1995 for the Thermodynamic Properties of Ordinary Water Substance for General and Scientific Use", *Journal of Physical and Chemical Reference Data*, 31, 2, pp. 387-535, DOI: `10.1063/1.1461829`.

Yeh, In-Chul and Gerhard Hummer

2004 "System-Size Dependence of Diffusion Coefficients and Viscosities from Molecular Dynamics Simulations with Periodic Boundary Conditions", *The Journal of Physical Chemistry B*, 108, 40, pp. 15873-15879, DOI: `10.1021/jp0477147`.